Universidad Autónoma de Madrid

Facultad de Ciencias

Departamento de Biología Molecular

Role of proteases implicated in the lysosomal pathway on APP processing in a cellular model of neurodegeneration

Patricia Llorente Ginés

Octubre 2018

Universidad Autónoma de Madrid

Thesis director

Dr. María Jesús Bullido Gómez-Heras

Centro de Biología Molecular Severo Ochoa

Universidad Autónoma de Madrid

Institute for Stem Cell Research and Regenerative Medicine (ISRM)

Heinrich Heine - University of Düsseldorf

AGRADECIMIENTOS

Esta tesis no podría haberse realizado sin el apoyo emocional, espiritual y económico de Antonio Ginés. Sé que yayo, estés donde estés, has sido y serás la fuerza que guía mi camino.

Gracias mamá, por las palabras de apoyo y la tranquilidad que me has transmitido en los momentos de más estrés, por estar ahí cada día de esta tesis y por confiar ciegamente en mí.

Gracias aita, por preocuparte de esta tesis como si fuera tuya, por las largas llamadas contándote todo el proceso en la distancia y por los buenos consejos recibidos a cambio.

Gracias yaya, por todo el cariño que me has mandado Zaragoza-Madrid, por preguntar en casa todos los días por mí y por cómo iba mi trabajo, incluso sin entender muy bien de que va esto de la ciencia.

Gracias al resto de mi familia por el apoyo constante vía whatsapp, en España o en Alemania, interesándoos por como evolucionaba este trabajo.

Gracias a la gente del labo 410; Mariaje, Meri, Isabel y Jesús por el apoyo de estos años y por todo lo que me habéis enseñado. Pero sobre todo por los buenos momentos y risas dentro y fuera del laboratorio, que es lo que me llevo para siempre. Gracias Marta, por tu ayuda incondicional en esta última etapa y por la compañia en las comidas.

Gracias a toda la gente que ha pasado por el labo; Julia, Ana, Dani, Víctor y Sara, porque en algún punto de este trabajo habéis sido un pilar fundamental, gracias por las horas de charla compartiendo problemas y apoyo, y los martes de pizza :) Sobre todo, Ana y Víctor, que os ha tocado soportarme más de cerca y sois parte directa de esta tesis. Estoy muy orgullosa de poderos llamar amigos.

Gracias Heni, por ser mi gran apoyo tanto dentro como fuera del labo, incluso a miles de kilómetros de distancia. Por las tardes de vinos y cervezas, y porque espero que siempre sigas estando ahí.

Gracias a mis labos de acogida, el 122 y el 202, y a toda su gente; los Adris, Bea, Daniel, Guada (aunque te hayas mudado), Álvaro, Irene y Silvia, por los descansos para el café que me han dado un chute de energía en los momentos bajos y por los buenos consejos.

Gracias a Mauro, Dani, Elena, Raquel, Gonzalo y Andrés por las risas en las comidas y el aire fresco de los cafés en la pérgola que me han hecho desconectar en los días duros.

Gracias a la gente del labo del profesor Adjaye en Düsseldorf: Nina, Audrey, Lucas, Lisa por acogerme como a una más y por tratarme tan bien. A Martina por la ayuda técnica. Al Dr. Adjaye por permitirme participar y aprender en su laboratorio. Y sobre todo a Robert y Soraia, por enseñarme el mundo de las iPSC y porque habéis hecho mi estancia más sencilla con tardes de risas, Altbier, barbacoa y clases de español ;)

Gracias al servicio de microscopía, al de proteómica y al de instrumentación por su ayuda.

Gracias a todo el que me he cruzado en el CBM y en algún momento me ha echado un cable.

CONTENTS

SUMMARY

Alzheimer's disease (AD), the most common cause of dementia, is characterized by massive neuronal damage leading to cerebral atrophy and the loss of cognitive function. Most AD cases (>95%) are sporadic. Sporadic AD is a highly complex disease for which neither the causal agents nor the molecular mechanisms behind are well known. Among the environmental risk factors, oxidative stress (OS) is intimately linked to aging and thought to be crucial to the onset and development of the disease. In addition, persistent brain infections, particularly those induced by Herpes Simplex virus type 1 (HSV-1), seem to play a key role in AD pathogenesis. Our group works with both factors to simulate the sporadic form of AD *in vitro*.

AD is characterized by the accumulation of senile plaques, which are predominantly composed of β-amyloid peptide (Aβ). Two pathways of proteolytic processing have been characterized in detail: amyloidogenic and non-amyloidogenic (currently called canonical pathways) that promote or prevent the generation of Aβ peptide from its APP precursor, acting in a coordinated and competitive manner. Recent studies describe additional pathways of proteolytic processing of APP (non-canonical) that seem to be at least partly executed by enzymes of the lysosomal pathway (cysteine proteases, metalloproteinases), and generate proteolytic fragments capable of inhibiting neuronal activity in the hippocampus. Based on data from our experimental model demonstrating that OS alters the lysosomal degradation pathway and the processing / metabolism of APP, we postulate that these non-canonical pathways of APP proteolytic processing could, as canonical secretases, be altered in the aging induced OS and take part in the mechanisms of neurodegeneration of the model. Thus, proteases of the lysosomal pathway modulated by OS and capable of acting as APP secretases, would be potential targets to inhibit neurodegeneration.

The objective of the present study was the identification of proteases that were part of the non-canonical processing of APP and were related to lysosomal function. After a whole human genome expression microarray study of the cell model, we selected two proteins, cathepsin B (CTSB) and matrix metalloproteinase 14 (MMP-14), and we studied their role on proteolysis of APP and lysosomal function changes induced by OS and HSV-1. For this, we used pharmacological inhibitors and generated human neuroblastoma SK-N-MC cell lines with CTSB or MMP-14 silenced. The results indicated that, in cells subjected to OS, CTSB participates in the accumulation of APP and a 56 kDa peptide likely corresponding to

oligomeric forms of Aβ, while MMP-14 mediates the accumulation of an 85 kDa APP fragment. In addition, both proteases modify the levels of lysosomal markers induced by OS. The HSV-1 virus affects the proteolysis of APP, increasing the amyloid oligomers levels and reducing the APP levels when combined with CTSB inhibition. Moreover, we observed that the deficiency of MMP-14 significantly inhibited the infection. In addition, we generated neurons and neural progenitors derived from iPSCs of patients with sporadic Alzheimer's disease carrying the R47H variant in TREM2. The study of the role of these proteases in the processing of APP and in the lysosomal dysfunction induced by OS were analyzed and confirmed the results obtained in the neuroblastoma model.

RESUMEN

La enfermedad de Alzheimer (EA) es la causa más común de demencia y se caracteriza por un masivo daño neuronal que conduce a la atrofia cerebral y a la pérdida de funciones cognitivas. En la gran mayoría de los casos (>95%), la EA constituye una enfermedad compleja cuya causa y mecanismos moleculares aún se desconocen. Entre los factores de riesgo ambientales, el estrés oxidativo (EO) asociado al envejecimiento desempeña un papel clave en el desarrollo de la enfermedad. Otro factor son las infecciones cerebrales, y en particular la infección por el virus herpes simplex 1 (HSV-1). Nuestro grupo trabaja con ambos factores para simular la forma esporádica de la EA *in vitro*.

La EA se caracteriza por la acumulación de placas seniles, que están compuestas predominantemente por péptido β-amiloide (Aβ). Se han caracterizado en detalle dos vías de procesamiento proteolítico: amiloidogénica y no amiloidogénica (actualmente denominadas vías canónicas) que promueven o previenen la generación del péptido Aβ a partir de su precursor APP, actuando de una manera coordinada y competitiva. Estudios recientes describen vías adicionales de procesamiento proteolítico del APP (vías no canónicas) que parecen ser, al menos en parte, ejecutadas por enzimas de la vía lisosomal (cisteín proteasas, metaloproteinasas), y generan fragmentos proteolíticos capaces de inhibir la actividad neuronal en el hipocampo. Basándonos en datos de nuestro modelo experimental que demuestran que el EO altera la vía de degradación lisosomal y el procesamiento/metabolismo de APP, postulamos que estas vías no canónicas de procesamiento proteolítico la APP podrían, igual que ocurre con las canónicas, estar alteradas en el EO inducido por envejecimiento y ser parte de los mecanismos de neurodegeneración del modelo. Así, las proteasas de la vía lisosomal moduladas por EO y capaces de actuar como APP secretasas serían potenciales dianas para inhibir la neurodegeneración.

El objetivo del presente estudio era la identificación de proteasas que formaran parte del procesamiento no canónico de APP y estuvieran relacionados con la función lisosomal. Tras un estudio microarrays de expresión de genoma humano completo del modelo celular, seleccionamos dos proteínas, Catepsina B (CTSB) y Metaloproteinasa de matriz 14 (MMP-14), y estudiamos su papel en los cambios en la proteolisis de APP y en la función lisosomal inducidos por EO y HSV-1. Para ello, utilizamos inhibidores farmacológicos y generamos líneas celulares del neuroblastoma humano SK-N-MC con CTSB o MMP-14 silenciadas.

Los resultados indicaron que, en células sometidas a EO, CTSB participa en la acumulación de APP y de un péptido de 56 kDa probablemente correspondiente a formas oligoméricas de Aβ, mientras que MMP-14 media la acumulación de un fragmento de APP de 85 kDa. Además, ambas proteasas modifican los niveles de marcadores lisosomales inducidos por EO. El virus HSV-1 afecta la proteolisis de APP, aumentando los niveles de oligómeros amiloides y disminuyendo los niveles de APP cuando se combina con la inhibición de CTSB. Además, observamos que la deficiencia de MMP-14 inhibía significativamente la infección. Por último, generamos neuronas y progenitores neurales derivados de iPSCs de pacientes con Alzheimer esporádico portadores de la variación R47H en TREM2. El análisis del papel de estas proteasas en el procesamiento de APP y en la disfunción lisosomal inducidas por EO en estas células confirmó los resultados obtenidos en el modelo de neuroblastoma.

ABBREVIATIONS

AD - Alzheimer’s disease

ADAM10 - Disintegrin and metalloproteinase domain-containing protein 10

AICD - Amyloid precursor protein intracellular domain

AMC - 7-amino-4-methylcoumarin

APLP - APP-like protein

APOE - Apolipoprotein E

APP - Amyloid precursor protein

ATCC - American Type Culture Collection

ATP - Adenosine triphosphate

Aβ - Beta amyloid

BACE-1 - Beta-site amyloid precursor protein cleaving enzyme 1

BCA - Bicinchoninic acid

BDNF - Brain-derived neurotrophic factor

BSA - Bovine serum albumin

C - Control

cDNA - Complementary deoxyribonucleic acid

CMA - Chaperone-mediated autophagy

CMV - Cytomegalovirus

CNS - Central nervous system

Co-IP - Co-immunoprecipitation

CSF - Cerebrospinal fluid

CTF - C-terminal fragment

CTS - Cathepsin

CTSB - Cathepsin B

Cyt - Cytosolic fraction

Dapi - 4',6-diamidino-2-phenylindole

DMEM - Dulbecco’s modified Eagle médium

DMSO - Dimethyl sulfoxide

DNA - Deoxyribonucleic acid

DSHB - Developmental Studies Hybridoma Bank

EADI - European Alzheimer’s Disease Initiative

EBV - Epstein Barr Virus

ECM - Extracellular matrix

EEA1 - Early endosome antigen 1

ER - Endoplasmic reticulum

ESC - Embryonic stem cell

FAD - Familial Alzheimer’s disease

FBS - Fetal bovine serum

FCS - Fetal calf serum

FGF2 - Fibroblast growth factor 2

GDNF - Glial-derived neurotrophic factor

GSK3 - Glycogen synthase kinase 3

GWAS - Genome-wide association studies

H - Hours

H_2O_2 - Hydrogen peroxide

HHV6 - Human herpes virus 6

HRP - Horseradish peroxidase

HSV-1 - Herpes simplex virus type 1

Ig - Immunoglobulin

IGF1 - Insulin-like growth factor 1

ILVs - Intraluminal vesicles

iNOS - Induced nitric oxide synthase

iPSC - Induced pluripotent stem cell

KEGG - Kyoto encyclopedia of genes and genomes

KPI - Kunitz-type protease inhibitor

L/LE - Lysosomal and endosomal fraction

LAMP - Lysosome-associated membrane protein

LIMP - Lysosomal integral membrane protein

LC3 - Microtubule-associated protein light chain 3

LSD - Lysosomal storage diseases

LT - LysoTracker® Red DND-99

M6P - Mannose 6-phosphate

MAPT - Microtubule-associated protein tau

MEF - Mouse embryonic fibroblast

MEM - Minimal Eagle’s medium

Min - Minutes

MMP - Matrix metalloproteinase

Moi - Multiplicity of infection

MT-MMP - Membrane type matrix metalloproteinase

MTT - 3-(4,5-dimethyl-thiazol-2-yl)-2,5-diphenyl tetrazolium bromide

MVBs - Multivesicular bodies

NaCl - Sodium chloride

NADPH - Nicotinamide adenine dinucleotide phosphate

NEAA - Non-essential amino acid

NFT - Neurofibrillary tangle

NMDA - N-methyl-D-aspartate

NPC1 - Niemann-Pick type C disease

NPC - Neural progenitor cell

ON - Overnight

OS – Oxidative stress

P-tau - Hyperphosphorylated tau

PBS - Phosphate-buffered saline

PCR - Polymerase chain reaction

PFU - Plaque forming units

PGlu-Aβ - Pyroglutamylated beta amyloid

PHF - Paired helical filament

PLD3 - Phospholipase D3

PM - Plasma membrane

PNS - Peripheral nervous system

PSEN - Presenilin

RNA - Ribonucleic acid

ROS - Reactive oxygen species

RQ - Relative quantity

RT - Room temperature

RT-PCR - Reverse transcription polymerase chain reaction

SAD - Sporadic Alzheimer’s disease

sAPP - Soluble amyloid precursor protein

SD - Standard deviation

SDS - Sodium deoxycholate sulphate

SEM - Standard error of the mean

shRNA - Short hairpin ribonucleic acid

SNP - Single nucleotide polymorphism

SP - Senile plaque

TGN - Trans-Golgi-network

TNFα - Tumor necrosis factor alpha

TREM2 - Triggering receptor expressed on myeloid cells 2

X-XOD - Xanthine-xanthine oxidase

β-ME - Beta-mercaptoethanol

INTRODUCTION

Alzheimer's disease (AD) is an age-related progressive neurodegenerative disorder, the most common cause of dementia, and it is clinically characterized by cognitive and memory dysfunction caused by an irreversible progression of neuronal death. The disease is divided into two subtypes based on the genetic background: familial AD (FAD) and sporadic AD (SAD). About 99% of the cases correspond to the sporadic form, which result from a complex interaction of genetic and environmental factors. Aging is the most important risk factor: AD incidence increases exponentially with age from 65 to 90 years and doubles approximately every 5 years (Jorm et al., 1998).

In 1906, the clinical psychiatrist and neuroanatomist Alois Alzheimer described for the first time the case of a 50-year-old woman whom he had followed from her admission for paranoia, progressive sleep and memory disturbance, aggression, and confusion, until her death 5 years later. The neuropathological lesions he observed in the brain autopsy of this patient with early-onset dementia were the presence of "striking changes in neurofibrils" and the distribution of "minute military foci caused by the deposition of a special substance", which are considered until today the two pathological hallmarks of AD. Currently, these features are known as neurofibrillary tangles (NFTs) and senile plaques (SPs), respectively. NFTs are intracellular aggregates of hyperphosphorylated microtubule-associated protein tau (MAPT). SPs are extracellular aggregates primarily composed of β-amyloid peptides (Aβ), a proteolytic product of the amyloid precursor protein (APP).

1. The Amyloid Precursor Protein. Metabolism and proteolytic proccessing

It is widely accepted that the physiopathological functions of APP are far beyond its role as the "carrier" of the Aβ peptides (Zheng et al., 2006). Although, not surprinsingly, research in AD has focused mostly to the biology of Aβ, increasing evidence continue shifting the attention towards the physiological role of APP as key to understand neurodegeneration, and it is becoming apparent that APP plays a central role in the mechanisms that guarantee the accuracy and the robustness of brain wiring (Soldano et al., 2014). Roles of APP in transmembrane transduction, cell adhesion, calcium metabolism, neurite outgrowth, and synaptogenesis have been reported (Muller et al., 2017).

The human APP gene was first identified in 1987 by the isolation and sequencing of a full-length complementary DNA clone coding for the Aβ peptide (Kang et al., 1987) and belongs, together with the APP-like protein 1 (APLP1) and 2 (APLP2), to the APP protein

family identified in mammals. All three are type I transmembrane proteins and share a single membrane-spanning domain, a large extracellular N-terminal region and a short cytoplasmic C-terminal tail (De Strooper et al., 2000). Although they undergo similar processing, only APP contains the sequence encoding the Aβ domain. The APP gene (ENSG00000142192) is localized on chromosome 21 (21q21.3) and alternative splicing of exons 7 and 8 gives rise to three major isoforms: APP695, APP751 and APP770 (containing 695, 751, and 770 amino acids, respectively) (Kitaguchi et al., 1988). APP751 and APP770 are ubiquitously expressed (Schmechel et al., 1988) and contain a protease inhibitor KPI domain, whereas APP695, devoid of this domain, is predominantly expressed in neurons (Tanaka et al., 1988).

APP is localized at the plasma membrane (PM), in membranes of the endoplasmic reticulum (ER), Golgi, trans-Golgi network (TGN), lysosomes, endosomes, and mitochondria (Zhang et al., 2011). Figure 1 shows the intracellular trafficking of APP, which is synthesized in the endoplasmic reticulum (ER) and transported through the TGN. During its transit from the ER to the PM following the constitutive secretory pathway, nascent APP is posttranslationally modified by N- and O-linked glycosylation, phosphorylation, and tyrosine sulphation. Only a small fraction of nascent APP molecules reaches the PM, whereas the majority of APP at steady-state localizes to the Golgi and TGN (Jiang et al., 2014). APP which is not shed from the cell surface is re-internalized within minutes because of the presence of its “YENPTY” internalization motif near the carboxyl terminus (residues 682–687 of the APP695 isoform) (Lai et al., 1995; Marquez-Sterling et al., 1997). Following endocytosis, APP is delivered to endosomes, and a fraction of endocytosed molecules is recycled to the cell surface.

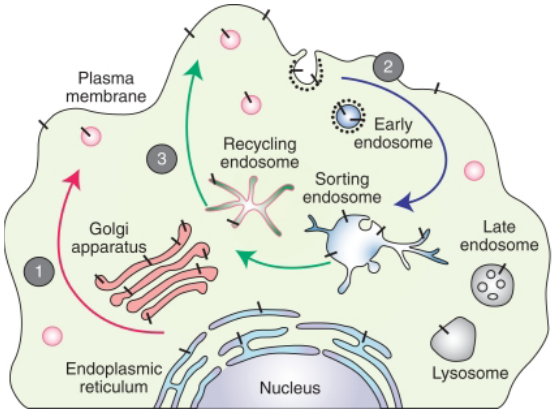

Figure 1. Intracellular trafficking of APP. APP molecules (black bars) mature through the constitutive secretory pathway (1). Once APP reaches the cell surface, it is rapidly internalized (2) and subsequently trafficked through endocytic and recycling organelles to the TGN or the cell surface (3). A small fraction is also degraded in the lysosome (image from Haas et al., 2012).

1.1. APP proteolytic processing: Canonical pathways

The most studied modification of APP is probably its proteolytic processing, which is intimately linked with its intracellular trafficking and generates, appart from Aβ peptides, multiple fragments with either neuroprotective or neurotoxic capabilities (Nhan et al., 2015). APP is mainly processed via the canonical pathways, which includes the amyloidogenic and the non-amyloidogenic routes (Figure 2) (Zhang et al., 2011). The latter is more prevalent and excludes the generation of Aβ. Here, APP is first cleaved by the α-secretase within the Aβ-domain, which results in a large N-terminal ectodomain (sAPPα) and the membrane-remaining C-terminal fragment (α-CTF), which is subsequently cleaved by the γ-secretase. This second cleavage produces the short peptide P3 and the APP intracellular domain fragment (AICD or γ-CTF). In contrast, the amyloidogenic pathway leads to the production of Aβ because of the sequential cleavage by the β- and γ-secretases. In a first step, the β-secretase cleaves APP at the N-terminal end of the Aβ domain (carried out by β-site APP-cleaving enzyme 1 — BACE1) to generate sAPPβ and the 99 amino acid long membrane-bound C-terminal fragment (β-CTF). Further processing of β-CTF causes Aβ and γ-CTF-formation. This final step can produce Aβ peptides of different length, between 39 and 42 amino acids. Non amyloidogenic processing mainly occurs at the cell surface where α-secretases are present. Amyloidogenic processing involves transit through the endocytic organelles where APP encounters β- and γ-secretases (Haas et al., 2012). As the amyloidogenic and non amyloidogenic proteolytic pathways likely occur in different cell

compartments (Soldano et al., 2014), any factor perturbing APP intracellular location could alter its proteolytic processing, and this could finally result in neuronal damage and disease.

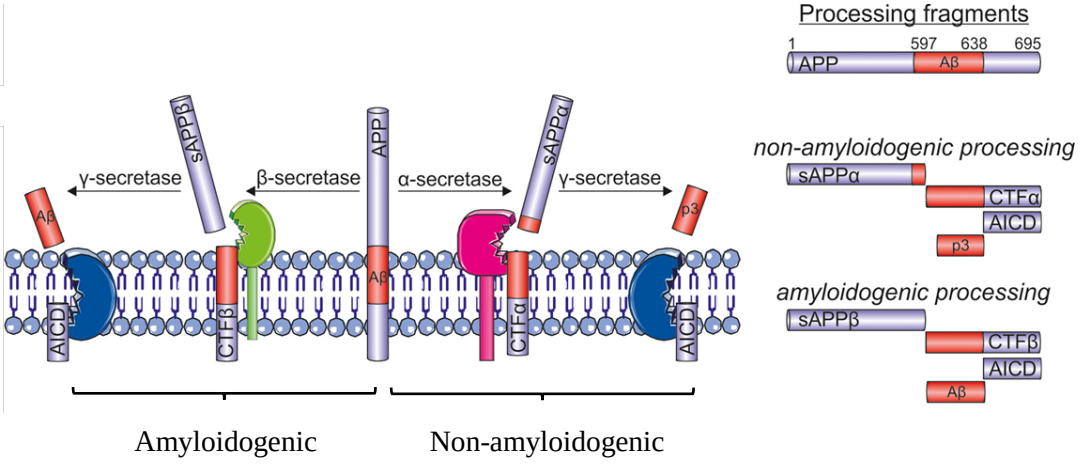

Figure 2. APP canonical processing. It includes the amyloidogenic, formation of Aβ by the sequential cleavage of β- and γ-secretase, and non-amyloidogenic pathways, cleavage of α- and γ-secretase that prevent the formation of Aβ (image from Andrew et al., 2016).

In this scenario, a shift toward amyloidogenic processing would not only increase the production of Aβ but would also deplete the pool of APP undergoing non-amyloidogenic processing.

1.2. APP proteolytic processing: Non-canonical pathways

Recent studies have revealed the complexity in the proteolytic processing of APP, with new secretases and the corresponding proteolytic fragments being identified (Andrew et al., 2016; Muller et al., 2017). These fragments include APP metabolites that accumulate in the brains of AD patients and may contribute to the synaptic dysfunction observed in the disease. In addition, numerous proteins that interact with APP, modulating its proteolysis and Aβ production are being identified (Andrew et al., 2016). These new APP secretases and metabolites, along with the APP interactors, may represent novel therapeutic targets that are alternative to direct modulation of the levels of Aβ or of the canonical secretases. The most relevant of these new pathways are the δ and η secretases pathways (Zhang et al., 2015 and Willem et al., 2015). These new secretases can increase Aβ production by initially cleaving the full-length APP molecule, making it a better substrate for BACE1 cleavage by

reducing the steric hindrance of the large N-terminal ectodomain, as well as generating additional neurotoxic fragments.

Among these non-canonical proteases, cathepsin B, proposed as an alternative β secretase, and members of the matrix metalloproteinase family were specially interesting for us, since they were modulated in our *in vitro* models of OS and HSV 1 infection (Kristen et al., 2018), and they could therefore be good candidates to mediate the alterations in APP proteolysis found in these cell models.

1.2.1. Cathepsin B

The lysosomal cysteine protease cathepsin B (CTSB) has also been proposed as a putative β-secretase (Hook et al., 2014). CTSB belongs to the superfamily of papain-like cysteine proteases. The CTSB gene encodes a member of the C1 family of peptidases and is localized to chromosome 8p23.1. Alternative splicing of this gene results in multiple transcript variants. At least one of these variants encodes a protein that is synthesized as a proenzyme of 339 amino acid residues. Activation occurs by cleaving and dissociation of a 62 residues region. The final proteolytic event is the cleavage between residues 47 and 50 to yield a two-chain form of the enzyme, CTSB light and heavy chains, with the excision of a dipeptide. This enzyme has both endopeptidase and exopeptidase activities that play a role in protein turnover and intracellular degradation. Processing to the mature enzyme form occurs in the acidic environment of the trans-Golgi and the lysosome. The presence of a signal sequence and N-glycosylation sites indicates that CTSB is targeted to the endosomal/lysosomal compartment via the mannose-6-phosphate receptor pathway. Moreover, mature and proenzyme forms of CTSB have been identified at early endosomes in most cases of AD patients, but only a small proportion at endosomes of normal brains (Cataldo et al., 1995).

The role of CTSB as a β-secretase remains controversial, with conflicting evidence indicating that genetic deletion or inhibition of CTSB in APP transgenic mice can either enhance or reduce Aβ pathology. Cysteine protease activity was demonstrated as the major β-secretase activity in regulated secretory vesicles of neuronal chromaffin cells (Hook et al., 2005). The cysteine protease activity in these secretory vesicles was identified as CTSB and shown to colocalize with Aβ in these vesicles (Hook et al., 2005). Furthermore, the inhibition of CTSB in APP transgenic mice resulted in significant improvement in memory

deficit, reduced amyloid plaque load in brain and reduced levels of Aβ40, Aβ42 and β-CTF when compared with untreated control animals (Hook et al., 2008).

CTSB cleavage of APP may enhance the production of N-terminally truncated pyroglutamylated forms of Aβ (pGlu-Aβ) in which the N-terminal glutamate is cyclized by glutaminyl cyclase (Hook et al., 2014). pGlu-Aβ exhibits increased aggregation propensity and increased cellular toxicity and disrupts long term potentiation to a greater extent than Aβ non-pyroglutamylated species. In addition, recent work has proposed pGlu-Aβ as the predominant Aβ species within the brains of AD patients (Portelius et al., 2015), and the design of therapeutics specifically targeting this Aβ species have been successful in mouse models (Frost et al., 2015). However, evidence for direct proteolysis of APP between Ala598-Glu599 (APP695 isoform) by CTSB remains to be provided.

1.2.2. Matrix Metalloproteinases

Matrix metalloproteinases (MMPs) are members of the metzincin group of proteases which share the conserved zinc-binding motif in their catalytic active site. MMP family can be divided into six groups: collagenases, gelatinases, stromelysins, matrilysins, membrane-type MMPs, and other non-classified MMPs. MMPs are responsible for collagen and other proteins degradation in the extracellular matrix (ECM) (Brinckerhoff et al., 2002).

Soluble and membrane-bound matrix metalloproteinases (MT-MMPs) have been of interest to the AD field due to their capacity to proteolytically cleave APP and Aβ *in vitro* and *in vivo* (Hernandez-Guillamon et al., 2015). MT-MMPs were also observed in the vicinity of Aβ deposits, even co-localizing with senile plaques (Brzdak et al., 2017).

The matrix metalloproteinase-24 (MMP-24, also named MT5-MMP), postulated to be η-secretase, was shown to cleave APP between Asn504-Met505 (APP695 isoform). This cleavage results in the shedding of an 80–95 kDa soluble fragment (sAPPη) and leaves the novel membrane-bound CTF, CTFη (Figure 3), which contributes to the production of Aβ and the induction of synaptic dysfunction (Willem et al., 2015). Using a suite of antibodies and extensive mass spectrometry analyses, further processing of CTFη by both α- and β-secretases to produce fragments termed Aη-α and Aη-β was elucidated (Figure 3). η-secretase cleavage of APP exceded β-secretase cleavage by almost 10-fold in human neurons, and accumulation of ηCTFs was also observed in dystrophic neurites surrounding

amyloid plaques in the brains of AD patients (Willem et al., 2015). Moreover, genetic and pharmacological inhibition of BACE1 activity resulted in the accumulation of CTFη and Aη-α. This highlights that therapeutic inhibition of BACE1, as currently underway in multiple clinical trials, needs to be carefully monitored to ensure that accumulation of alternative neurotoxic APP fragments, such as Aη-α, does not occur under such therapeutic intervention (Willem et al., 2015).

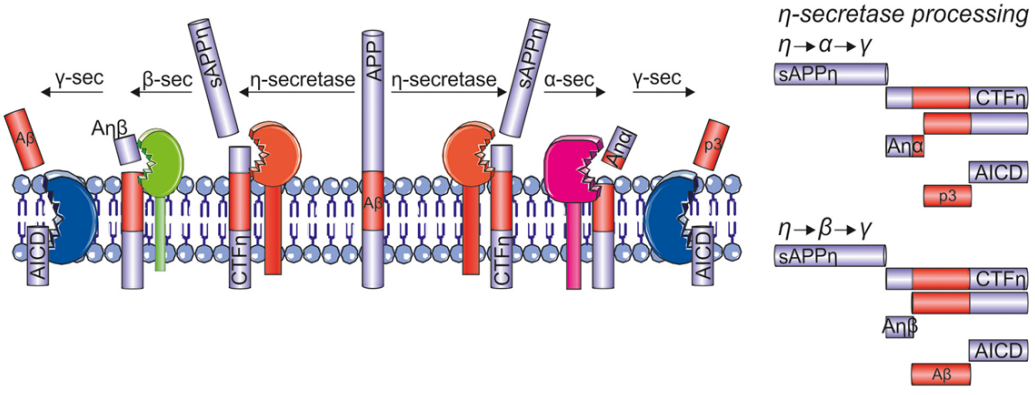

Figure 3. η-secretase, a non-canonical APP processing pathway. It generates sAPPη and CTFη, that can be then processed by α- or β-secretase to yield Aη-α and Aη-β fragments (image from Andrew et al., 2016).

The membrane-type matrix metalloproteinase-1, also known as MMP-14 or MT1-MMP is another membrane-bound metalloproteinase, phylogenetically close to MMP-24 in relation to their catalytic domains that shows cross reaction in substrate recognition (Ratnikov et al., 2014). Moreover, MMP-14 cleaves the APP at the same site than MMP-24 (Higashi et al., 2003). The MMP-14 encoding gene (MMP-14, ENSG00000157227) is localized to chromosome 14q11.2. The protein consists of 582 amino acids. The 62 kDa active form of MMP-14 is processed to 40–44 kDa lacking the catalytic domain through autolytic action.

MMP-14 appears to be highly expressed in brain regions exhibiting amyloid pathology and neuroinflammation. Under non-pathological conditions MMP-14 likely has a secondary role in regulation of brain Aβ levels compared with other Aβ-degrading enzymes that are constitutively expressed. However, when amyloid deposition and neuroinflammation occur, as in AD, reactive astrocytes and vascular smooth muscle cells markedly increase their expression of MMP-14 which may then play a significant role degrading soluble and deposited Aβ peptides (Liao et al., 2010).

The upregulation of the active form of MMP-14 in the hippocampus of the AD mouse model 5xFAD at 6 months was uncovered, along with strong accumulation of β-CTF and Aβ trimers (Py et al., 2014). MMP-14 overexpression in HEK cells increased the production of both Aβ and its precursor β-CTF, suggesting a possible link between increased MMP-14 activity *in vivo* and amyloidosis (Py et al., 2014). One possible consequence of APP cleavage by MMP-14 would be to stimulate the generation of β-CTF, described as an early neurotoxic metabolite of APP that accumulates much earlier than Aβ species (Lauritzen et al., 2012). β-CTF can be then processed by γ-secretase resulting in Aβ production.

Moreover, it has been described that CTSB may change the balance between metalloproteinases (MMP) and their inhibitors, and directly activates some of the MMPs (Porter et al., 2013). The interaction of these proteses would be of interest in the pathology of AD.

1.3. The "amyloid" and the "amyloid oligomer" hypotheses

The amyloid hypothesis, which has been the predominant framework for AD research, postulates that the accumulation of Aβ acts as the root cause of AD and initiates its pathogenesis (Frackowiak et al., 1994; Selkoe et al., 2016). For a long time, it has been assumed that insoluble extracellular fibrils (main constituents of amyloid plaques) were the most neurotoxic species. However, they are also present in the brain of non-demented individuals and the SP density do not correlate with deterioration of cognitive function (Aizenstein et al., 2008). Clinical trials that removed SP failed to reverse the damage or stop disease progression (Cappai et al., 2008; Hardy, 2009). Focus switched then to soluble Aβ aggregates, also called Aβ oligomers, as the primary toxic species. Indeed, the levels of Aβ oligomers are better correlated with disease severity than the insoluble fibrils or SP (Tomic et al., 2009; Cline et al., 2018). How exactly Aβ oligomers mediate neurotoxicity is still unknown.

The generation of Aβ takes place in different cellular organelles including PM, ER, Golgi/TGN, lysosomes, and endosomes. Aβ exists as two major peptide isoforms depending on its amino acid length, Aβ40 and Aβ42; the Aβ40 isoform is the most abundant (80-90%), whereas Aβ42 is more hydrophobic and fibrillogenic (LaFerla et al., 2007), markedly more prone to accumulation and aggregation (Jan et al., 2008). Aβ peptides not only differ in length, additional heterogeneity is added by modifications through aminopeptidases,

glutaminylcyclases, and other modifications that might contribute to Aβ neurotoxicity (Kuperstein, 2010). Monomeric Aβ peptides form low molecular weight oligomers (dimer/trimer) and then high molecular weight soluble aggregates. Those finally build spherical oligomers composed of 12-24 monomers, which prolong to form protofibrils and become insoluble fibrils that form senile plaques (Glabe, 2008) (Figure 4A). Soluble Aβ oligomers formed during the first stages of AD are believed to be particularly toxic and responsible for early memory failure. Recently, intermediate and large oligomeric Aβ assembly states have been associated with both aging and AD (Baker-Nigh et al., 2015).

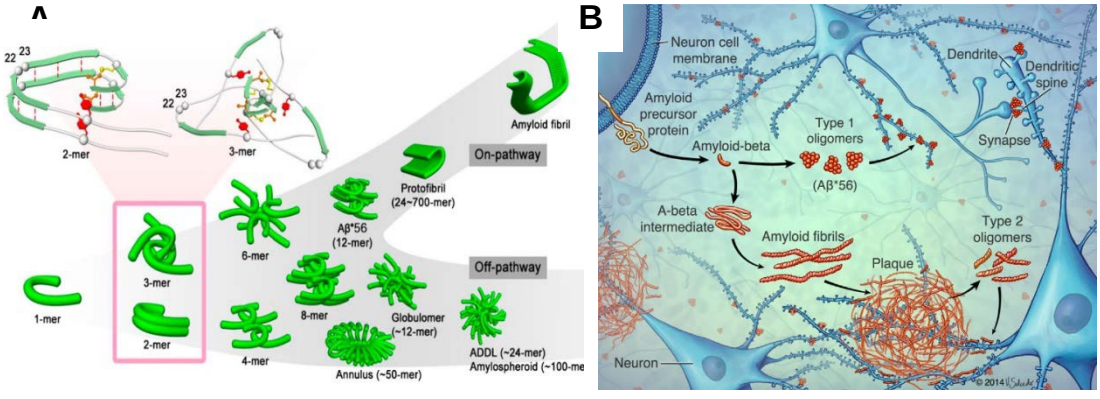

Figure 4. Classification of brain-derived Aβ oligomers. A. Schematic aggregation pathway of Aβ, based on the dimer and trimer as a minimum unit for oligomerization, previous to amyloid fibrils and senile plaques formation (image from Murakami, 2014). B. Type 2, but not type 1, oligomers have a spatiotemporal and structural relationship with amyloid plaques but do not impair cognition, possibly due to spatial sequestration around plaques (image from Liu et al., 2015).

There are numerous types of potentially toxic oligomers, and little is known about their effects when generated in the living brain, although recent work by Liu and colleagues has helped to refine the understanding of the pathogenicity of Aβ oligomers *in vivo*. These authors showed that Aβ oligomers can be assigned to two classes (type 1 and type 2) based on their temporal, spatial, and structural relationships to amyloid fibrils (Figure 4B). The type 2 oligomers are related to amyloid fibrils and represent the majority of oligomers generated *in vivo*, but they remain confined to the vicinity of amyloid plaques and do not impair cognition at relevant levels. By contrast, type 1 oligomers are unrelated to amyloid fibrils and may have greater potential to cause global neural dysfunction in AD because they are dispersed (Liu et al., 2015).

The debate on the pathogenic mechanisms induced by either monomeric or oligomeric Aβ is still open, as it is the pathogenic potential of the extracellular and intracellular pools. Several studies propose the interaction of soluble extracellular Aβ with receptors of the cell surface as causative for neuronal dysfunction and neurodegeneration. Aβ oligomers caused functional disruption of the N-methyl-D-aspartate (NMDA) receptor by inducing its endocytosis and repressing NMDA-evoked currents in neurons (Snyder et al., 2005). Interaction of Aβ with nerve growth factor receptor induces neuronal death (Yamamoto et al., 2007) through the p75 neurothrophin receptor, a member of the tumor necrosis factor receptor superfamily (Sotthibundhu et al., 2008). Another mechanism by which Aβ might induce neurodegeneration is the ability of this peptide to integrate into membranes to form membrane channels. These channels permit influx of some ions -including calcium- leading to the disruption of calcium homeostasis (Kawahara et al., 2000), increased reactive oxygen species (ROS) formation (Yatin et al., 1998) and tau phosphorylation (Takashima et al., 1993). In addition, it has been reported that amyloid oligomers cause membrane permeabilization by affecting the lipid bilayer conductance (Kayed et al., 2004).

Numerous authors suggest that intracellular accumulation of Aβ is an event preceding the formation of extracellular deposits of Aβ (LaFerla et al., 2007). In this sense, intracellular Aβ may contribute to AD pathology through the inhibition of mitochondrial enzymes causing a reduction in oxygen consumption (Caspersen et al., 2005), as well as mediating the inhibition of proteasome function (Almeida et al., 2006). Furthermore, intraneuronal Aβ peptides cause synaptic dysfunction and memory impairment (Billings et al., 2005; Oddo et al., 2003). Other studies report Aβ toxicity through the inhibition of cell redox activity (Shearman et al., 1994), induction of apoptosis and activation of caspases (Lustbader et al., 2004), as well as the possible contribution to tau phosphorylation and paired helical filament formation (Lewis et al., 2001; Zheng et al., 2002).

2. Risk factors for Alzheimer's disease

AD is divided according to the genetic background into familial and sporadic cases. The FAD form is due to autosomal dominant transmitted mutations. In contrast, most of AD cases (99%) manifest as a late onset sporadic form. Many genetic and environmental factors may contribute to determining the SAD form, being aging the main risk factor. Further, other non-genetic factors for AD are female gender (Vina et al., 2010), oxidative stress

(Markesbery et al., 1999; Smith et al., 2000) and lipid alterations (Bjorkhem, 2006; Grimm et al., 2013). Growing evidence also points to chronic or latent infections of the central nervous system (CNS) as a major player in the pathogenesis of AD (Harris et al., 2015; Itzhaki et al., 2016).

2.1. Genetic predisposition

Genetic researchers could first identify the 3 genes associated with FAD: Amyloid precursor protein (APP), Presenilin 1 (PSEN1) and Presenilin 2 (PSEN2). PSEN1 and PSEN2 are catalytic subunits of γ-secretase. Mutations of these genes cause autosomal dominant FAD with a penetrance of almost 100% (Tanzi et al., 1996). PSEN1 is the most commonly involved gene (221 pathogenic mutations reported), accounting for about 80% of autosomal dominant FAD cases, mutations in APP for about 15% and PSEN2 for 5%. All these mutations are able to increase the aggregation of the Aβ peptide by increasing total production or increasing aggregation-prone form of the peptide (Rogaeva, 2002). Although mutations in these genes are known to cause FAD, there are additional variants in APP, PSEN1, PSEN2 and ADAM10 (the major α-secretase involved in proteolysis of the APP ectodomain) that alter the risk in SAD cases (Cruchaga et al., 2012).

After the discovery of APP, PSEN1 and PSEN2, genetic studies aimed to identify genes associated with the more frequent late-onset form of the disease. In this way, twenty-five years ago allele 4 of Apolipoprotein E (APOE) was discovered as a genetic risk factor for SAD (Corder et al., 1993). The APOE gene is located at chromosome 19q13.2 and encodes a highly pleiotropic glycoprotein (Siest et al., 1995). There are three alleles (ε2, ε3, and ε4) for the APOE gene, and higher risk and earlier age of onset of AD is associated with APOE-ε4, whereas the ε2 allele is associated with lower risk of AD and delayed age of onset (Corder et al., 1994). Still, the combinations of these four genes (APP, PSEN1, PSEN2 and APOE) might explain 30-50% of AD heritability (Cuyvers et al., 2016). Advances in genomic technologies and the advent of genome-wide association studies (GWAS) have allowed the identification of novel genetic associations. Consortia like the Genetic and Environmental Risk in Alzheimer's Disease (GERAD) and the European Alzheimer's Disease Initiative (EADI) were able to identify genome-wide significant associations with single nucleotide polymorphisms (SNPs) in more than twenty loci besides APOE (Lambert et al., 2009; Lambert et al., 2011; Lambert et al., 2013). Most of these loci present common

variants with a small individual effect on risk (Figure 5), but still have helped to create a broader picture of the processes and pathways involved in AD. It has been estimated that these variants only modify disease risk by 0.10 to 0.15-fold, whereas the presence of APOE-ε4 results in an almost 4-fold increase (Bertram et al., 2010). Interestingly, these variants can be clustered into a few pathways, being the most prominent lipid metabolism, immune response, and endocytosis (International Genomics of Alzheimer's Project, 2015; Karch et al., 2015).

New approaches are currently underway in order to identify new candidates with higher risk. Whole-exome and whole-genome chips and sequencing strategies are revealing rare coding variants associated with AD (Guerreiro et al., 2013, Cruchaga et al., 2014; Sims et al., 2017). Among them, the variant p.R47H in triggering receptor expressed on myeloid cells 2 (TREM2) is consistently reported as conferring a higher risk for AD than the common variants identified by GWAS.

TREM2 is differentially expressed by microglia among different brain regions (Schmid et al., 2002). Two independent groups found a rare missense variant (db SNP rs75932628), in exon 2 of TREM2 (Guerreiro et al., 2013; Jonsson et al., 2013) producing a substitution of histidine for arginine at residue 47 (R47H) that increases SAD risk at a magnitude similar to that of APOE4. Other groups have found similar associations in Caucasian populations from both Europe and North America (Benitez et al., 2013; Giraldo et al., 2013; Gonzalez Murcia et al., 2013; Ruiz et al., 2014 and Roussos et al., 2015). This variant has also been associated with FAD in a case/control study of Caucasian individuals of French descent (Pottier et al., 2013). Given the reported anti-inflammatory role of TREM2 in the brain, the R47H substitution may lead to an increased predisposition to AD through impaired containment of inflammatory processes.

Despite all efforts, they are still under pressure to explain the missing inheritability, which in part might be explained by epistasis, rare variants, and somatic mutations (Karch et al., 2015; Naj et al., 2016).

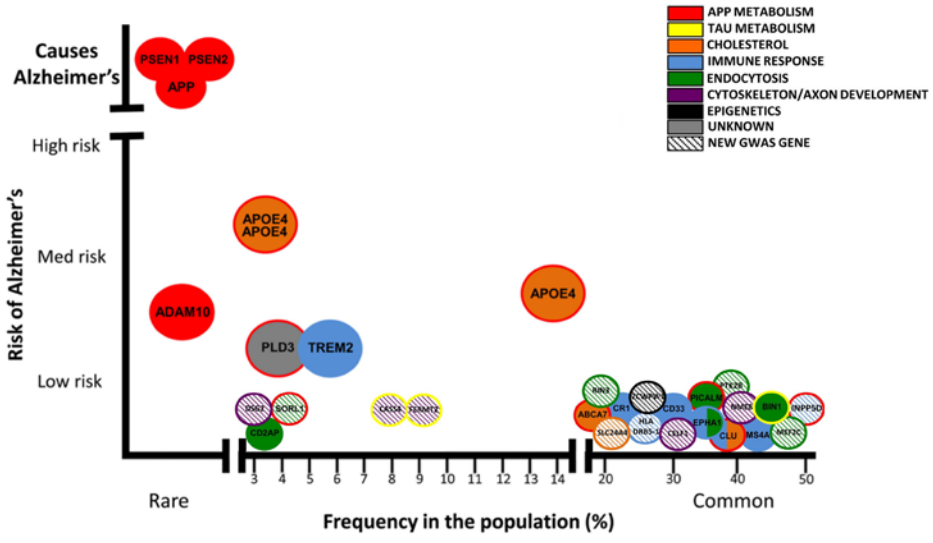

Figure 5. Genetics of Alzheimer's disease. Rare and common variants contribute to AD risk. The majority of the variants are common in the population and have a very low risk. The ones with higher risk are related to FAD and are very rare in the population. The new variants in TREM2 and PLD3 are more frequent in the population and have higher risk than common variants (image from Karch et al., 2015).

2.2. Oxidative stress

Oxidative stress (OS) contributes to neuronal damage and has been associated with neuronal cell death in several neurodegenerative diseases (Andersen, 2004; Nunomura et al., 2006). Since aging is associated with increased reactive oxygen species (ROS) production and decreased ROS clearance in age-related neurodegenerative diseases, like AD, OS is not only an early event but also would play an important role in initiating the disease. This is performed through activation of cell signalling pathways leading to apoptosis and neuroinflammation (Cai et al., 2011). The mechanisms behind the onset of AD are not fully known, but there is clear evidence that OS is important in the initiation and development of neuronal damage (Nunomura et al., 2001; Gibson et al., 2005; Masters et al., 2015). The high oxygen consumption of the human brain makes this organ especially susceptible to OS (Shulman et al., 2004). A possible explanation of the disease mechanism has emerged from the observations linking mitochondrial dysfunction and increased production of ROS to the development of AD.

The mitochondrial cascade hypothesis states that in sporadic, late-onset AD, loss of mitochondrial function associated with age affects the expression and processing of APP

initiating Aβ accumulation (Swerdlow et al., 2014). A theory currently gaining favor suggests that the SP and NFT represent responses to try to counteract the effects of toxic molecules derived from OS. OS results from an imbalance in prooxidant/antioxidant homeostasis leading to the generation of toxic ROS. Increased production of ROS associated with age, disease-dependent loss of mitochondrial function, altered metal homeostasis, and reduced antioxidant defense directly affect synaptic activity and neurotransmission in neurons leading to cognitive dysfunction. In the mitochondria, it is estimated that 2-4% of oxygen consumption during electron transport is not reduced to water by cytochrome C oxidase but that the semiquinone anion is formed and can transfer one or two electrons to molecular oxygen with the subsequent formation of the superoxide anion (O_2^-). The O_2^- is converted into hydrogen peroxide (H_2O_2) through the Fenton reaction with low molecular weight complexes of Fe (II) such as citrate Fe (II) or ATP Fe (II) generating hydroxyl radicals (OH^-). Other sources of O_2^- and H_2O_2 are oxidative enzymes, such as xanthine oxidase, NADPH / NADH oxidases, acyl CoA oxidase and cytochromes P-450, and small autooxidable molecules such as cotecholamines and the quinones (Dalton et al., 1999; Gamaley and Klyubin, 1999). Some exogenous sources generating ROS in organisms are antibiotics, drugs (e.g. paracetamol), pollutants (cigarette smoke), chemotherapy and exposure to ultraviolet and ionizing radiation (Finkel and Holbrook, 2000).

Molecular targets of ROS include nuclear and mitochondrial DNA, lipids and proteins, affecting seminal cellular functions like calcium homeostasis, mitochondrial dynamics and function, cellular architecture, receptor trafficking and endocytosis, and energy homeostasis. Abnormal cellular metabolism could therefore influence the production and accumulation of Aβ and hyperphosphorylated tau protein by different mechanisms (Cai et al., 2011), which in turn could exacerbate mitochondrial dysfunction and ROS production, thereby contributing to a vicious cycle.

Under normal conditions, the amount of ROS produced as a consequence of different cellular processes is controlled by antioxidants such as glutathione peroxidase and catalase and by non-enzymatic antioxidant molecules such as glutathione, vitamin E, ascorbic acid and carotenoids (Bunker, 1992). In relation with AD, an increase of OS markers, including RNA/DNA damage and lipid peroxidation, have been reported in AD brains and animal models of the disease (Gabbita et al., 1998; Nunomura et al., 1999; Williams et al., 2006).

Several studies reported increased activity of the major antioxidant enzymes in cortex and hippocampus of AD patients (Pappolla et al., 1992; Zemlan et al., 1989). To study the involvement of OS in AD, our group developed a human neuronal cell model of mild OS induced by the xanthine/xanthine oxidase (X-XOD) free radical generating system that allows the analysis of the events preceding cell death (Recuero et al., 2009). In this model, we also showed that OS affects APP proteolytic processing, trafficking and catabolism and these effects are mediated by the two main protein degradative pathways: the ubiquitin-proteasome system (UPS) and the autophagy-lysosomal pathway (Recuero et al., 2010 and 2013).

2.3. Infectious hypothesis. Herpes simplex 1 virus in Alzheimer's disease

Growing evidence supports that chronic or latent infection of the CNS might be implicated in the etiology of AD (see recent reviews in Harris et al., 2015; Itzhaki et al., 2016; Fullop et al., 2018; Haas et al., 2018). The idea of the so-called pathogen/infectious hypothesis came up in the 1960s and has gained support since then. First evidence came from the fact that several microbes can access the CNS, remain there in latent form by evading the host immune response, and that they are highly prevalent in the AD brain (Readhead et al., 2018). Among them, bacteria like Chlamydia pneumonia (Gerard et al., 2006), Helicobacter pylori (Kountouras et al., 2007) and several types of spirochaete (Miklossy, 2011), funghi (Alonso et al., 2014; Pisa et al., 2015) and herpes viruses such as Herpes simplex virus type 1 (HSV-1), Epstein Barr Virus (EBV), Cytomegalovirus (CMV), and Human herpes virus 6 (HHV6) have been associated with AD (Harris et al., 2015 and 2018). The hypothesis states that in combination with genetic risk factors, these pathogens participate in the generation of the Aβ peptide, tau hyperphosphorylation and inflammation. From the numerous evidences provided in the last years, two very recent ones demonstrated that herpesviruses are common in human brain and some of them appear to be part of a late-onset Alzheimer's disease associated virome (Readhead et al., 2018). The binding of Aβ to HSV-1 and HHV-6 surface causes fibrillar Aβ agglutination that can protect against viral challenge (Eimer et al., 2018). These findings have refuelled the field leading some researchers to claim for a change in the current paradigms relating the causes and mechanisms of AD (Fullop et al., 2018; Haas et al., 2018).

Of all pathogens studied in relation with AD, HSV-1 has emerged as a major factor in the etiology of the disease (Itzhaki, 2014 and 2016, Eimer et al., 2018, Harris et al., 2018). HSV-1 belongs to the alphaherpesvirus subfamily. Other members of this group are the closely related HSV-2 and Varicella zoster virus (Steiner et al., 2007). HSV-1 is a ubiquitous neurotropic virus, with a worldwide seroprevalence of more than 80% in adults. The virion of all alphaherpesviruses consists of four components: (1) an electron-dense core containing lineal viral DNA of approximately 152 kDa, (2) the capsid, an icosadeltahedral structure that surrounds the core composed of 6 structural proteins, (3) the surrounding tegument, a protein layer composed of 22 viral proteins and (4) an envelope (Owen et al., 2015). The envelope is derived from cellular membranes and includes viral glycoproteins, which are important for the virus adsorption to the cell surface, receptor recognition and membrane fusion to enable viral entry into the host cell (Fields et al., 1996).

HSV-1 usually enters orofacial mucosal epithelia cells where productive infection takes place (Figure 6). From there, the virus can spread to neurons of the trigeminal ganglia innervating the epithelium where it can establish lifelong latency (Kennedy et al., 2015; Nicoll et al., 2012). After primary infection, the virus can replicate or stay latent in the neuron cell body until reactivation by diverse stimuli (like stress and immunosuppression). When reactivated, the virus travels back to the primary site of infection where it causes the so-called cold sores (herpes labialis). Infected peripheral nervous system (PNS) neurons are in direct synaptic contact with CNS neurons providing a direct route of spread from the periphery (Koyuncu et al., 2013). Once in the CNS, the virus can stay latent until periodical reactivation, which could cause neuronal damage. Acute HSV-1 infection is known to cause different neurological diseases, like herpes keratitis (Rowe et al., 2013) or encephalitis (Bradshaw et al., 2016), and mounting evidence links it to AD.

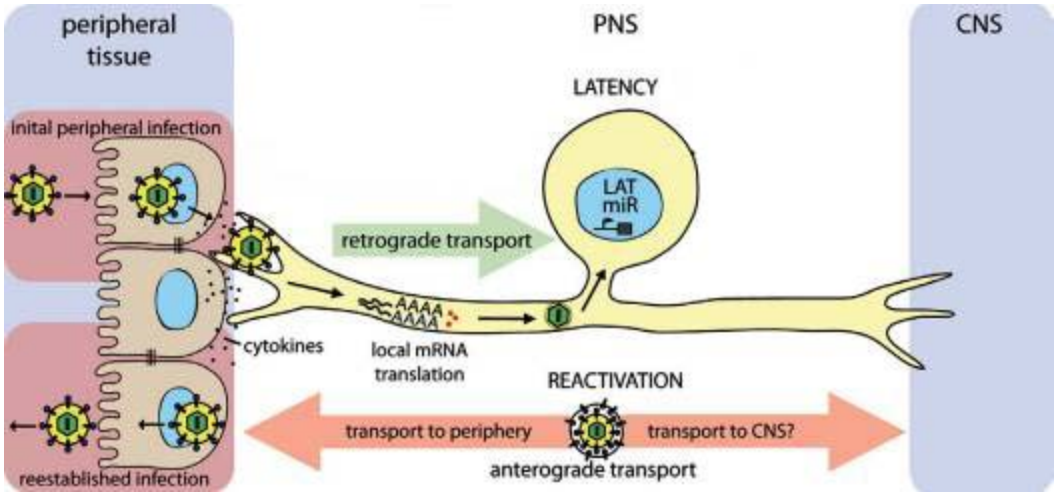

Figure 6. HSV-1 access route to the CNS. Epithelial cells of the orofacial mucosa are initially infected with HSV-1. The virus enters sensory neurons by fusion with the plasma membrane or via endocytosis. Once inside the sensory process, viral particles undergo long-distance retrograde transport to the neuronal cell body, where the virus replicates or becomes latent. When the HSV-1 genome reactivates, newly synthesized virions travel anterograde back to the primary site of infection causing recurrent herpes labialis and/or access the CNS. Image modified from Koyuncu et al., 2013.

Brain autopsies showed that latent HSV-1 is present in a high proportion of SAD and normal elderly individuals, and that it was found in the areas most affected by AD, namely temporal and frontal cortices and hippocampus (Jamieson et al., 1991). Furthermore, the viral DNA seems to colocalize with SPs suggesting an active role of the virus in their generation (Wozniak et al., 2009). In contrast, no viral DNA has been found in younger brains (Wozniak et al., 2005), suggesting that HSV-1 reaches the CNS at older age when the immune system declines. Evidence from epidemiological studies postulate that in synergy with the possession of the APOE-ε4 allele, HSV-1 infection represents a risk factor for AD (Itzhaki et al., 1997), even though neither of the two factors alone is necessary nor sufficient for the development of the disease. In this sense, using mice models, our group previously showed that the ApoE dose and genotype determine the viral load in the CNS. The viral neuroinvasion was reduced in animals lacking the ApoE gene compared to wildtype animals and a direct correlation between HSV-1 concentration and ApoE allelic dose was detected (Burgos et al., 2002). In posterior reports, we then showed that during both acute and latent infection, ApoE-ε4 was more efficient than ApoE-ε3 in promoting viral colonisation of the brain (Burgos et al., 2003; Burgos et al., 2006). Besides APOE, many genes are thought to interact with some aspect of HSV-1 infection. Indeed, GWAS identified a set of genes associated with SAD which may affect the individual susceptibility to HSV-1 infection

(Porcellini et al., 2010). These genes could constitute a genetic fingerprint modulating the individual's susceptibility to HSV-1 infection thereby causing neuronal loss, inflammation and Aβ deposition (Licastro et al., 2011; Porcellini et al., 2010). Letenneur and colleagues studied the presence of HSV IgG (immunoglobulin of primary infection) and IgM antibodies (immunoglobulin of reactivation) in the serum of AD patients and controls. They found out that the reactivation of HSV might be highly correlated with the progression of the disease (Letenneur et al., 2008). These results were confirmed by Lövheim's group in an independent study (Lovheim et al., 2014). Finally, several researchers, including our group, linked HSV-1 to the main neuropathological hallmarks of AD in neuronal and animal models of HSV-1 infection: infection leads to an accumulation of intracellular Aβ (Santana et al., 2012; Wozniak et al., 2007), autophagic vesicles (Itzhaki et al., 2008; Santana et al., 2012) and hyperphosphorylated tau protein (Alvarez et al., 2012; Wozniak et al., 2009).

Despite the evidences and the hundreds of publications indicating the involvement of infectious agents in AD pathology, the infectious hypothesis is still not fully accepted, and little effort has been made to initiate antiviral/antimicrobial clinical studies in relation to AD (Itzhaki et al., 2016).

2.4. Interaction between oxidative stress and HSV-1

Several studies also demonstrate an association between acute and latent HSV-1 infection of the CNS and oxidative damage (Milatovic et al., 2002; Valyi-Nagy et al., 2000). HSV-1 has been described to induce the peroxidation of lipids (Palu et al., 1994). During acute infection, HSV-1 provokes encephalitis in mice accompanied by severe inflammation and elevated levels of F2-isoprostanes and F4-neuroprostanes, two markers of oxidative damage (Milatovic et al., 2002). Latent HSV-1 infection induces oxidative damage of RNA and DNA molecules in infected areas of the murine brain (Valyi-Nagy et al., 2000). On the other hand, latent infection of HSV-1 in murine models is also associated with persistent and chronic inflammation in the brain, and with high levels of proinflammatory cytokines such as the tumor necrosis factor α (TNFα) and increased activity of induced nitric oxide synthase. These factors may play an important role in preventing the reactivation of HSV-1 (Koprowski et al., 1993; Marques et al., 2008; Meyding-Lamade et al., 1998). Both TNFα and nitric oxide have antiviral activities but can directly generate potent free radicals or ROS-mediated oxidative damage through different cell signalling pathways. Therefore,

immune system and inflammatory response plays an important role in the generation of oxidative damage in the brain during HSV-1 infection (Valyi-Nagy et al., 2005). In conclusion, although few reports exist on the interplay of OS and HSV-1 infection, the results suggest that OS may promote the neurodegenerative events associated to HSV-1 infection.

Our group has been studying the relationships among OS, HSV-1 and neurodegeneration for several years. We showed that OS enhances the intracellular accumulation of Aβ mediated by HSV-1 infection, and further decreased its secretion to the extracellular medium. Furthermore, OS potentiates the accumulation of immature autophagic compartments and the inhibition of the autophagic flux induced by HSV-1. At the same time, OS reduced the efficiency of HSV-1 infection (Santana et al., 2013). When we studied the molecular pathways regulated by OS by means of whole human genome expression microarrys, we found a very specific and prominent induction of the KEGG pathway “Lysosome” in human neuroblastoma cells infected by HSV 1 or carrying an APP mutation causing FAD. These results suggest that the lysosome pathway could account for the molecular mechanisms mediating the neurodegeneration process initiated by OS in sensitized neurons (Kristen et al., 2018).

3. The lysosomal system

The cellular homeostasis requires a highly regulated equilibrium between the synthesis and degradation of proteins. Alterations in this balance cause numerous pathological processes. There are two main systems involved in the degradation of proteins in mammals: proteasome and lysosome. In eukaryotic cells, short-lived proteins are mainly degraded by the proteasome, whereas long-lived proteins and protein aggregates are mostly degraded by autophagy, the main degradative pathway linked to the lysosome system. This degradative process recycles cellular waste and eliminates potentially toxic damaged organelles and protein aggregates, like the ones formed during OS.

Lysosomes were first described in 1955 by Christian de Duve and thought to be just the cellular waste bags. They are the major digestive compartments within cells and are involved in multiple functions like the degradation and recycling of intra- and extracellular material, cholesterol homeostasis and cell death signalling (Appelqvist et al., 2013). Lysosomes have an acidic lumen, limited by a 7-10 nm thick phospholipid bilayer

membrane, and contain several types of hydrolases for the degradation of substrates. There are 25 lysosomal membrane proteins (Lubke et al., 2009) being the lysosome-associated membrane proteins (LAMPs) and the lysosomal integral membrane proteins (LIMPs) the most abundant ones (Eskelinen et al., 2003). Since the low lysosomal pH provides optimal conditions for hydrolase activity, those proteins are protected from cleavage by dense glycosylation. Besides being a mechanical border, the lysosomal membrane has many other functions, like the maintenance of the pH gradient between lysosomal lumen and cytoplasm, the mediation of fusion with endosomes or other organelles, and the selective transport of material into or out of the lysosome (Eskelinen et al., 2003; Saftig et al., 2009).

A constant lysosomal pH between 4.8-5.2 is guaranteed by the action of an ATP-dependent proton pump—the vacuolar (V)-ATPase (Toei et al., 2010). V-ATPases are multi-subunit protein complexes consisting of a membrane-associated V0 complex that serves as a transmembrane pore for protons, and a soluble cytosolic V1 complex. Beside the maintenance of lysosomal pH, the V-ATPase also regulates vesicle fusion and is located to several membranes including lysosomes, endosomes, Golgi-derived vesicles and sometimes even to the PM (Yamamoto et al., 1998; Yoshimori et al., 1991). Several potent and selective inhibitors have been identified over the years to interfere with this tightly regulated network. Ammonium chloride or chloroquine are lysosomotropic weak bases, which elevate the pH by entering the acidic compartment in their unprotonated form and titrating the pH upward (Ohkuma et al., 1978). Bafilomycin A1, in contrast, is a specific V-ATPase inhibitor (Bowman et al., 1988).

Inside the lysosome reside more than 60 different soluble hydrolases, including sulphatases, glycosidases, peptidases, phosphatases, lipases and nucleases, most of them only active at acidic pH. The best-studied hydrolases are the cathepsins (CTSs) which activity is widely used as an indicator of functionality of the lysosomes. The CTSs are categorised in three groups based on the amino acid at their active site: serine (CTS A and G), cysteine (CTS B, C, F, H, K, L, O, S, V, X and W) and aspartic (CTS D and E) (Turk et al., 2012).

Lysosomal hydrolases are synthesized in the ER as immature and enzymatically inactive precursors. They are then transported in vesicles from the ER through the Golgi to the TGN and from there to the lysosome. To be targeted to lysosomes, a mannose 6-phosphate (M6P) tag is added in the Golgi complex (Rohrer et al., 2001). This signal is recognised by diverse

M6P receptors in the TGN (Braulke et al., 2009; Ghosh et al., 2003). There, clathrin-coated vesicles are formed containing the receptor-ligand complexes. These vesicles move towards the cell periphery and fuse with endosomes. Inside the endosome, the hydrolases are dissociated from the receptors because of the low pH (around pH 6) and the receptors will be transported back to the TGN (Braulke et al., 2009). The constant trafficking of material from the TGN to the endosomes and back is an important feature for the maintenance of lysosomal intactness, acidity, and perinuclear localization (Bucci et al., 2000). The decreasing intraluminal pH during endosomal maturation initiates hydrolase activity and digestion of endocytosed material. However, only after fusion with lysosomes, the hydrolases have reached their final destination with maximal proteolytic activity. As depicted in Figure 7, the lysosome is the destiny organelle, and there are two routes by which material for degradation reaches the lysosome: extracellular material and parts of the PM reach the lysosome by endocytosis, whereas intracellular material is transported to the lysosome through autophagy.

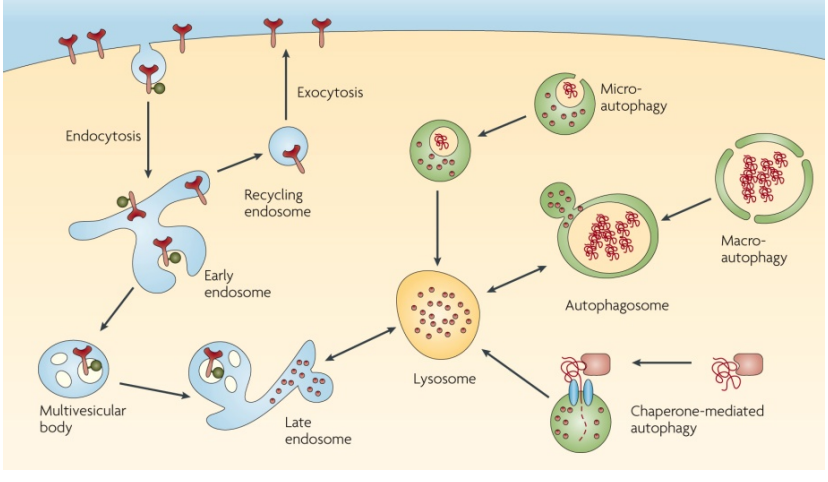

Figure 7. Schematic representation of the lysosomal pathway. Primary endocytic vesicles were formed at the plasma membrane and deliver their cargo to early endosomes where some material will be recycled back to the plasma membrane. Maturation from early endosomes (EE) to late endosomes (LE) takes place. Fusion with lysosomes forms hybrid organelles, endolysosomes, where degradation of the cargo takes place. The lysosome is the destiny organelle of the endocytic and of the autophagic pathways. Image from Tai et al., 2008.

3.1. Endocytic pathway

Endocytosis is a process by which cells internalize the PM along with cell surface receptors and soluble molecules (Maxfield et al., 2004). As a first step, the material to be ingested is

progressively enclosed by parts of the PM, which invaginates and then pinches off to form an endocytic vesicle. These vesicles then fuse with early endosomes, the first sorting station of endocytosis. From there, the majority of the cargo is recycled back to the PM via recycling endosomes (Steinman et al., 1983). Otherwise, cargo will be retained in the early endosomes, which mature into late endosomes, the second sorting station. During maturation several events take place, amongst other things the formation of intraluminal vesicles (ILVs) from the limiting membrane. The presence of many ILVs inside the late endosomes (often up to >30) got them the name of multivesicular bodies (MVBs) (Piper et al., 2007). Further, the decrease in luminal pH is taking place during this transformation from early (pH 6.8-5.9) to late endosomes (pH 6.0-4.9). The continuous transformation, fusion and fission of these organelles make their identification with molecular markers difficult. Late endosomes differ from lysosomes by the presence or absence of M6P receptors, respectively (Brown et al., 1986).

3.2. Autophagy

Autophagy is the process by which cells digest their own cytoplasm to provide material for new synthesis. There exist three forms of autophagy in the cell: chaperone-mediated autophagy (CMA), microautophagy, and macroautophagy. CMA, as indicated by its name, includes the recognition of the substrates via the action of chaperones and the lysosomal receptor LAMP2A (Kaushik et al., 2012). The direct engulfment of small cytoplasmic material by the lysosomal membrane is called microautophagy (Li et al., 2012). The principal form of autophagy, though, is macroautophagy, herein referred to as autophagy.

Autophagy begins with the formation of a double-layered isolation membrane (also called phagophore) that engulfs and sequesters cytoplasmic material in its interior. The elongation of this phagophore assures the formation of a double-membraned structure, the so-called autophagosome (Nakamura et al., 2017). The most characterized protein associated with autophagosomes is the lipidated form of microtubule-associated protein light chain 3 (LC3-II). The conversion of LC3-I (the non-lipidated form) to LC3-II is the main marker for monitoring autophagic flux (Klionsky et al., 2016). The autophagosome subsequently might fuse with endosomes or directly with lysosomes for the degradation and recycling of their cargo. In this way, the degraded products are released into the cytoplasm to newly synthesize macromolecules or serve as energy source. There is always a basal activity of

autophagy present to maintain cellular homeostasis acting as an essential mechanism of quality control for cellular structures. However, autophagy can be activated through diverse stimuli, like stress, low nutrient levels or viral infections, participating in multiple processes such as cell differentiation, innate and adaptive immunity and anti-tumoral and anti-aging mechanisms (Yin et al., 2016).

3.3. Lysosomal alterations and neurodegeneration

Neurons especially rely on functional lysosomal degradation (endocytic and autophagic pathways) since they live extremely long without cell division. It is therefore not surprising that defects in autophagy and endocytosis are relevant to neurodegenerative diseases, in particular to AD (Whyte et al., 2017). Indeed, altered endocytosis is one of the earliest neuropathologic features observed in AD preceding Aβ accumulation (Cataldo et al., 2000). The presence of autophagic vesicles was detected in dystrophic neurites of cortex and hippocampus in brains of transgenic mice expressing human APP (Yu et al., 2005). These vesicles contained APP, different Aβ peptides, and β- and γ-secretases necessary for their generation (Yu et al., 2004). In this sense, autophagic activation significantly increases Aβ production in mouse fibroblasts (Yu et al., 2005) and in rat neurons (LeBlanc et al., 1996). The generated Aβ is targeted to the lysosome for degradation by cathepsins. Thus, efficient autophagy plays a protective role against Aβ-induced neurotoxicity in human neuroblastoma cells (Hung et al., 2009). Further evidence came from the discovery of genetic risk factors and their molecular mechanisms. FAD-causing mutations in PSEN1 severely compromise autophagy-mediated recycling of proteins, affecting autophagy-dependent processes such as APP processing and Aβ accumulation (Nixon, 2006). Finally, several studies point to lysosomal acidification defects in different AD models causing a failure in lysosomal proteolysis (Avrahami et al., 2013; Nixon et al., 2011; Torres et al., 2012).

Support also comes from knowledge about lysosomal storage diseases (LSDs). LSDs are a family of disorders that result from recessively inherited gene mutations that perturb lysosomal homeostasis. Age of onset and clinical features vary, depending on the nature of accumulating substrate and the cell types affected. Common to LSDs is the initial accumulation of specific macromolecules or monomeric compounds inside organelles of the endosomal-autophagic-lysosomal system (Platt et al., 2012). Almost all LSDs present pathology of the CNS, and in some cases, neurodegeneration occurs in multiple brain

regions (thalamus, cortex, hippocampus, and cerebellum). For example, CTSD deficiency causes neuronal ceroid lipofuscinosis, a severe neurodegenerative disorder (Siintola et al., 2006). Niemann-Pick type C disease (NPC) is provoked by alterations of cholesterol trafficking and other lipids by the defective function or even absence of either two endosomal proteins, NPC1 or NPC2. This leads to an accumulation of autophagic vesicles and finally neuronal death. Interestingly, NPC patients show typical AD lesions like NFTs, intracellular Aβ42 accumulation and endosome deficits (Malnar et al., 2014). Indeed, LSD and AD display strong phenotypic overlap, including neuronal accumulation of autophagic or lysosomal vesicles, dystrophic axons, ectopic dendrites, cognitive deficits, and neurodegeneration. Many researchers claim that AD should be included in the group of LSDs due to these similarities (Nixon, 2005; Wolfe et al., 2013).

4. Induced pluripotent stem cells as Alzheimer's disease model

Induced pluripotent stem (iPS) cells have revolutionized the fields of *in vitro* models of human diseases. The iPS-derived differentiated cells allow researchers to study the impact of specific cell types in health and disease as well as performing therapeutic drug screens on a human genetic background. In particular, some of the potential reasons behind the clinical trials failure in AD are the species gap involved in proceeding from initial discoveries in rodent models to human studies, and the inadequate understanding of the biology of AD, starting therapies too late in the development due to the lack of phenotypic and genetic markers (Cummings et al., 2018). iPS cells overcome these obstacles and are allowing researchers to conduct in depth characterization of neural cells from both familial and sporadic AD patients. In contrast with the limited availability of viable neuronal cells from AD patients because of ethical and practical reasons, patient-derived skin or blood cells are an easily accessible source for reprogramming to human induced pluripotent stem (iPSCs) cells. These allows the subsequent differentiation to generate clinically relevant neuronal cells *in vitro* that can be used to investigate the pathogenesis of neuronal disorders, like AD (Yagi et al., 2011; Israel et al., 2010; Hossini et al., 2015). iPSC derived neurons are reliable models, not only for better understanding the etiopathological process of AD, but also for efficient anti-AD drugs screening. More importantly, human-sourced iPSCs may also provide a beneficial tool for cell-replacement therapy against AD (Yang et al., 2016).

Several groups have independently developed human iPSC neuronal differentiation protocols, often adapted from existing protocols for human embryonic stem cells (ESCs) or mouse iPSCs/ESCs (Zeng et al., 2010). These protocols are constantly being improved and revised, creating a plethora of techniques to differentiate hiPSCs to neuronal fates. The ability to differentiate, culture, and manipulate human neurons is of tremendous interest to labs seeking to study human neurodevelopment and neurological diseases (Srikanth et al., 2014). Many groups have taken advantage of somatic cell reprogramming technology to generate patient-specific iPSC lines in order to model neurodegenerative and neurodevelopmental disorders. Furthermore, there have been many advancements in protocols to create neurons of a particular identity like motor neurons, dopaminergic neurons or interneurons (Takazawa et al., 2012, Li et al., 2005). For the differentiation of iPSCs to forebrain neurons, two base protocols are often utilized: an embryoid aggregate-based technique and a monolayer dual SMAD inhibition method (Muratore et al., 2014).

Neuronal cultures derived of iPSC from AD patients produced more ROS and displayed higher levels of DNA damage. Furthermore, patient-derived cells showed increased levels of oxidative phosphorylation chain complexes, whereas mitochondrial fission and fusion proteins were not affected. Surprisingly, these effects neither correlated with Aβ nor phosphorylated and total tau levels. Synaptic protein levels were also unaffected in SAD derived neuronal cells. The increased ROS production may have an integral role in the development of SAD prior to the appearance of amyloid and tau pathology (Birnbaum et al., 2018).

Moreover, neurons from patients with FAD or SAD showed increased phosphorylation of tau protein at all investigated phosphorylation sites. Relative to the control neurons, neurons derived from patients with FAD and patients with SAD exhibited higher levels of extracellular amyloid-β 1-40 (Aβ1-40) and amyloid-β 1-42 (Aβ1-42). However, significantly increased Aβ1-42/Aβ1-40 ratios, which is one of the pathological markers of FAD, were observed only in samples of patients with FAD. Additionally, a significant upregulation of amyloid precursor protein (APP) synthesis and APP carboxy-terminal fragment cleavage was detected. Moreover, elevated sensitivity to oxidative stress, as induced by amyloid oligomers or peroxide, was detected in both FAD- and SAD-derived neurons (Ochalek et al., 2017).

In the field of treatment development, drug screenings have been performed in neurons from FAD and SAD patients (from a human iPSC-based platform), like the one leading to the selection of as a synergistic combination of bromocriptine, cromolyn, and topiramate as a cocktail showing a potent anti-Aβ effect (Kondo et al., 2017).

In light of these antecedents, we decided to generate iPSC-derived neurons from AD patients –who carried the AD associated TREM2 R47H variant– as a relevant model in which to validate the results obtained from the neuroblastoma cell line.

OBJECTIVES

The causes of sporadic Alzheimer's disease (SAD) are still unknown. However, it has been described that the oxidative stress (OS) associated with aging is an important risk factor for AD. Although the mechanisms that connect OS with neurodegeneration are not clear, there is evidence that the alteration of protein degradation systems can be part of these mechanisms. Lysosomal dysfunction is an early pathogenic event in the cascade that leads to neuronal death from different triggers, for example infectious agents capable of colonizing the brain such as Herpes Simplex virus 1 (HSV-1). The endo-lysosomal system is the preferential place where the amyloidogenic processing of APP takes place, raising the possibility that proteases related to this system could act as non-canonical APP secretases and constitute novel therapeutic targets for AD.

To analyze the role of lysosome related proteases on the metabolism and processing of the APP and on the functional changes of the lysosomal pathway induced by OS in the absence and presence of HSV-1, the following objectives were proposed:

1. Study of APP expression and processing in the presence or absence of the radical generating system X-XOD to select APP derivatives differentially expressed as a response to OS.

2. Selection of proteases modulated by OS whose cleavage specificities are compatible with the pattern of APP derivatives from objective 1. Study of their roles in the proteolytic processing of APP and in the lysosomal pathway alterations induced by OS.

3. Analysis of the effect of HSV-1 in the alterations on the processing of APP and the lysosomal pathway induced by OS. Involvement of the selected proteases.

4. Analysis of the processing of APP and of the lysosomal pathway in response to OS, in induced pluripotent stem cells (iPSCs) derived neurons from SAD patients.

MATERIALS & METHODS

1. Cell lines and cell culture

SK-N-MC human neuroblastoma cells (HTB-10) were obtained from the American Type Culture Collection (ATCC). Cells were cultured as monolayer in minimal Eagle's medium (MEM) supplemented with 10% heat-inactivated fetal calf serum (FCS), 1 mM sodium pyruvate, non-essential amino acids (NEAAs), 2 mM glutamine, and 50 µg/mL gentamycin, at 37°C in a humidified 5% CO_2 atmosphere. Exponentially growing cells, at 80–90% confluence, were splitted into multiwell culture plates one day before treatment. On the day of treatment, cells were placed in fresh medium 1 h before addition of the compounds. Culture medium components were purchased from Gibco Laboratories.

2. Generation of cell lines with stable gene-silencing of MMP-14 or CTSB

For the generation of cell lines with a stable knockdown of MMP-14 or CTSB, cells were transfected with a short hairpin RNA (shRNA) clone specific to MMP-14 or CTSB and with a scrambled control shRNA clone (Mission control shRNA library from Sigma, Figure 8) Sequences of shRNA are described in Table 1. Transfections were performed with jetPEI reagent according to the manufacturer's recommendations (Polyplus transfection). Briefly, SK-N-MC cells were cultured in 6 well plates until 70% confluency and then transfected by the mixture of 3 µg DNA and 6 µL jetPEI transfection reagent, both diluted in 150 mM NaCl. The mixture was incubated for 30 min at room temperature (RT) and was then added to the cells (200 µL per well). 48 h after transfection, cells were trypsinized and re-plated at low densities (dilutions 1:50, 1:500, 1:5.000) in P100 dishes with the selection antibiotic puromycin at a final concentration of 0.25 µg/mL. The effective concentration was previously determined in a dose-response experiment of SK-N-MC cells with puromycin concentrations between 0 and 10 µg/mL. Medium supplemented with puromycin was replaced every 2-3 days. Clones were picked manually and expanded until enough cells were available for generating a frozen stock and for isolating total RNA and protein extracts for analysis. Finally, clones with a low expression of MMP-14 or CTSB were selected for further analyses.

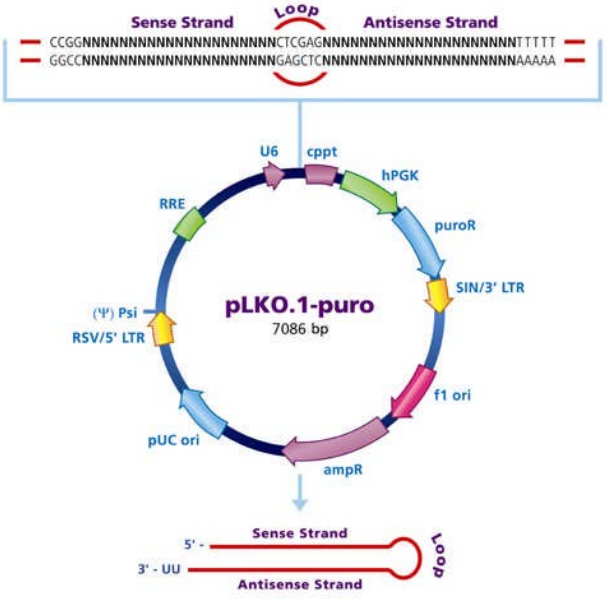

Figure 8. **MISSION shRNA clone.** Constructed within the lentivirus plasmid vector pLKO.1-puro from Sigma.

Table 1. Mission control shRNA DNA clone sequences

Item Number	Sequence	
TRCN0000003658	CCGGGCTGGTCAACTATGTCAACAACTCGAGTTGTTGA CATAGTTGACCAGCTTTTT	CTSB
TRCN0000050855	CCGGCGATGAAGTCTTCACTTACTTCTCGAGAAGTAAG TGAAGACTTCATCGTTTTTG	MMP-14
SHC005	CCGGTACAACAGCCACAACGTCTATCTCGAGATAGAC GTTGTGGCTGTTGTATTTTT	Control

3. Induction of oxidative stress

Induction of mild oxidative stress was performed as previously used by our group (Recuero et al., 2009) through the addition of xanthine (10 µM) - xanthine oxidase (50 mU/mL) (X-XOD) to fresh medium (mechanism in Figure 9). In case of combination with HSV-1, X-XOD was added after the virus adsorption and maintained until the end of infection. The effects of their addition were measured 24 h later. Xanthine (X) was purchased from Sigma and xanthine oxidase (XOD) from Roche.

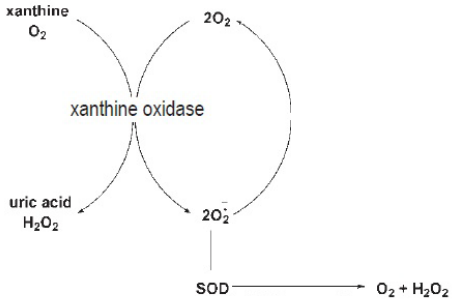

Figure 9. Generation of ROS. Mild oxidative stress generation system xanthine-xanthine oxidase

4. Infection conditions

The HSV-1 strain KOS 1.1 was obtained, propagated and titered on a monolayer of Vero cells following described methods (Carrascosa et al., 1982) and stored at -70°C. For infection experiments, cells were seeded in complete media at 70-80% confluency and exposed to HSV-1 at 37°C for 1 h. Control infections were performed using a virus-free suspension. In order to remove unbound virus, the medium was changed, and cells were incubated in complete medium at 37ºC. Multiplicity and time of infection (moi - expressed in plaque forming units per cell [pfu/cell]) were moi 1 analyzed at 24 hpi (hours post infection). The infectious titers of HSV-1 were determined by plaque assays with Vero cells as previously described (Santana et al., 2012).

5. Inhibitors

CA-074 Me (CTSB inhibitor) and GM6001 (MMPs inhibitor) were purchased from Enzo and NSC405020 (MMP-14 inhibitor) from APExBIO**.** For CA-074 Me treatments (usually used at a concentration of 5 µM, if changes it is indicated in each experiment), the inhibitor was added for 1 h and the cell cultures then placed in fresh medium for the rest of the experiment. For NSC405020 treatments (used at a concentration of 100 µM), the inhibitor was added for 24 h. For GM6001 treatments (used at a concentration of 10 µM), the inhibitor was added for 24 h. The concentration of DMSO (vehicle) in the cell culture was 0.1% or lower.

6. Analysis of cell viability

Cell injury was evaluated using the 3-(4,5-dimethyl-thiazol-2-yl)-2,5diphenyl tetrazolium bromide (MTT; Sigma) assay (Hansen et al., 1989) as previously used by our group (Recuero et al., 2009). Briefly, cells were seeded in 96 well plates, and 2 h before the end of treatment incubated with 0.5 mg/mL MTT at 37ºC. The MTT/formazan released from the cells during overnight (ON) incubation at 37ºC with 100 µL extraction buffer (20% sodium dodecyl sulphate [SDS], 50% formamide adjusted to pH 4.7 with 0.02% acetic acid and 0.025 N HCl) was determined. Optical densities were measured at 550 nm using a microplate reader (Bio-Rad, Model 680).

7. Western blot analysis

Treated cells were washed in PBS and lysed in the lysis buffer containing PBS, 1% Triton X-100 and the Complete Mini protease inhibitor cocktail (Roche) on ice for 30 min, vortexing every 10 min. Supernatants were collected after centrifugation at 13,000 *g* for 30 min at 4°C. CTSB was analyzed in the lysates used in the enzyme activity experiments (described in point 13). The protein concentration of the lysates was quantified by the bicinchoninic acid assay (BCA) according to the manufacturer's instructions (Pierce). Cell lysates were mixed with Laemmli loading buffer (25 mM Tris-HCl pH 6.3, 10% glycerol, 2% SDS, 5% betamercaptoethanol [β-ME], and 0.01% bromophenol blue) and incubated at 100°C for 3 min. Protein separation was performed using Laemmli discontinuous SDS-polyacrylamide gel electrophoresis with acrylamide concentrations of the resolving gel adjusted to the molecular weight of the protein of interest. To define the size of the proteins separated by electrophoresis the molecular weight markers Precision Plus Protein Standards Dual Color (Bio-Rad) were loaded. Proteins were then transferred by semi-dry transfer (30 min at RT, 20V) to a nitrocellulose membrane with a pore-size of 0.45 µm (Bio-Rad). Total protein stain with Ponceau S was performed to check for transfer efficiency. Membranes were subsequently blocked ON at 4ºC in 3% BSA and 0.2% Tween-20 in phosphate-buffered saline (PBS). The primary antibody diluted in PBS, 1% BSA and 0.1% Tween-20 was incubated for 2 h at RT. After washing in PBS, 0.05% Tween-20, the blots were incubated with the corresponding horseradish peroxidase (HRP)-coupled secondary antibodies (Vector; dilution 1:50.000) for 2 h at RT. Alternatively, blots were blocked ON at 4ºC in 5% milk and 0.1% Tween-20 in tris-buffered saline (TBS) and incubated with the

primary and secondary antibody diluted in TBS, 5% milk and 0.1% Tween-20. All primary used antibodies and their dilutions are listed in Table 2. Immunodetection was performed using ECL™ Western blotting Detection Reagents according to manufacturer's instructions (GE Healthcare Life Sciences). To quantify the intensity of protein band, densitometric analysis was performed using the Quantity One® Software (Bio-Rad).

The APP antibodies used in the present study were: anti-AβPP (22C11) directed against amino acids 66-81 of AβPP, 6E10 directed against amino acids 1-16 of human Aβ, anti-oligomer A11 and anti-C-terminal against amino acids 676-695 (Figure 10). The ability of each antibody to recognize different metabolites according to their epitope location in AβPP has been described (Recuero et al., 2010).

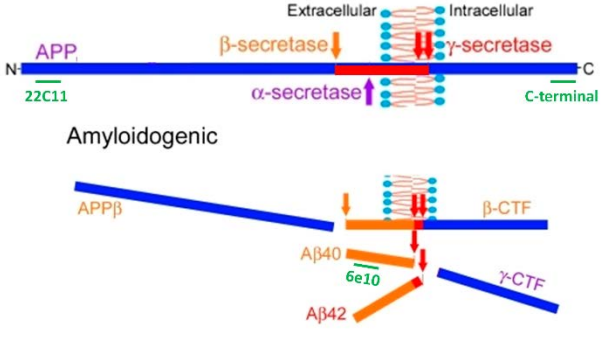

Antibodies	hAPP	sAPPα	sAPPβ	αCTF	βCTF	γCTF/AICD	Aβ	Aβ oligomers
22C11	X	X	X					
6E10	X	X			X		X	X
C-terminal	X			X	X	X		
A11								X

Figure 10. Scheme and table of APP antibodies against different regions.

8. Immunocytochemistry

Cells grown on coverslips were fixed with 4% formaldehyde for 20 min protected from light at RT and washed 3 times with PBS for 10 min. Fixed cells were then permeabilized and blocked ON at 4ºC with a blocking solution containing 0.2% Triton X-100 and 2% horse serum in PBS (pH 7.4), followed by incubation with the corresponding primary antibody (Table 2 and 3) for 2 h at RT diluted in blocking solution and protected from light. After 3 washing steps in blocking solution for 10 min at RT, cells were incubated with Alexa Fluor-coupled secondary antibodies (Invitrogen; dilution 1:1.000). for 90 min at RT and protected

from light. Cells were counterstained with Dapi (5 µg/mL) in PBS for 10 min at RT to visualize the nuclei, followed by 3 more washing steps in PBS. Afterwards, coverslips were washed in water and dehydrated in 100% EtOH. Finally, coverslips were mounted with Mowiol mounting medium (Sigma) on a microscope slide.

Cells were examined using a LSM 710 laser scanning confocal microscope (Zeiss) coupled to a vertical M2 AxioImager (Zeiss) equipped with a 63X/1.4 Plan-Apochromat oil objective lens, or using a Zeiss Axiovert 200 fluorescence microscope equipped with a 63 X oil-immersion objective. Pictures were taken with a Spot RT digital camera (Diagnostic) using Zeiss ZEN 2010 imaging system software. Images were processed using Adobe Photoshop CS3.

9. Primary antibodies

Table 2. Primary antibodies used for Western blot and immunocytochemistry

Antigen	Clonality	Host	Dilution		Reference
			WB	IF	
22C11	monoclonal	mouse	1:4000	1:50	Millipore (MAB348)
6E10	monoclonal	mouse	1:500	1:50	Covance (SIG-39300)
C-terminal	polyclonal	rabbit	1:1000	1:100	Sigma (A8717)
A11	polyclonal	rabbit	1:500	1:100	Origene (TA326459)
MMP-14	monoclonal	rabbit	1:2000	1:100	Abcam (ab51074)
CTSB	polyclonal	rabbit	1:200	---	SantaCruz (sc-6493)
CTSB	polyclonal	goat	---	1:200	SantaCruz (sc-6493)
CD222	monoclonal	mouse	---	1:50	BioLegend (315902
CD63	monoclonal	mouse	1:100	1:50	DSHB (H5C6)
EEA1	monoclonal	mouse	1:1000	1:50	BD Biosciences (610457)
LAMP2	monoclonal	mouse	1:1000	1:50	DSHB (H4B4)
Rab7	monoclonal	rabbit	1:1000	1:100	Cell Signaling Technology (9367)
Tubulin	monoclonal	mouse	1:10000	---	Sigma (T5168)

Table 3. Primary antibodies used for characterization of iPSCs-derived cells by immunocytochemistry

Antigen	Clonality	Host	Dilution	Reference
Nestin	polyclonal	rabbit	1:200	Sigma Aldrich (N5413)
MAP2	polyclonal	rabbit	1:200	SySy (188002)
GFAP	polyclonal	guinea pig	1:200	SySy (173004)
Doublecortin	polyclonal	guinea pig	1:200	Millipore (AB2253)
β-III-tubulin	monoclonal	mouse	1:200	Cell Signaling (4466S)

10. Cell fractionation for endo-lysosome and cytosol enrichment

The partial purification of lysosomes was performed as previously described by Avrahami with minor modifications (Avrahami et al., 2013). Briefly, cells were washed once in PBS, collected with washing buffer (125 mM KCl, 30 mM Tris pH 7.5, 5 mM MgOAc, 1 mM β-ME) and centrifuged at 800g for 5 min. Cells were resuspended in hypotonic buffer (10 mM KCl, 30 mM Tris pH 7.5, 5 mM MgOAc, 1 mM β-ME, Complete Mini protease inhibitor cocktail (Roche)) and broken with a 23G needle by 15 strokes (fraction F0: total cellular lysate). Homogenates were centrifuged at 1,000g for 5 min to precipitate nuclei. The supernatants (nuclei-free lysate: fraction F2) were again centrifuged at 100,000g for 1 h at 4ºC. The supernatant was stored (fraction Cyt) and the pellet (membrane fraction including lysosomes and endosomes: fraction L/LE) was lysed in RIPA buffer containing protease and phosphatase inhibitors. Western blot analysis was then performed with the different fractions.

11. Immunoprecipitation

Immunoprecipitation of cell lysates was performed in PBS containing 1% Triton X-100, employing the SureBeads™ Protein G Trial Kit (BioRad), following the manufacturer's instructions. Briefly, the magnetic beads were incubated with the antibody (2 µg) for 30 min, then washed three times with PBS- 0.1%Tween-20 and incubated with the lysates (100 µg) for 2 h, washed again three times with PBS- 0.1%Tween-20 and then what attached to the beads was eluted with 90 µL of Laemmli buffer for 10 min at 70 ºC. This elution was charged in an SDS-polyacrylamide gel and analyzed by Western blot.

12. Quantification of mRNA by reverse transcription followed by real-time PCR (RTqPCR)

Total RNA was purified with the High Pure RNA Isolation kit according to the manufacturer's instructions (Roche) as previously described (Recuero et al., 2009). To determine the RNA quantity, samples were analyzed with a NanoDrop® ND-1000 (NanoDrop Technologies). Complementary DNA (cDNA) was obtained from 0.5 µg of RNA by reverse transcription using the High Capacity RNA to cDNA Kit (Applied Biosystems). Real-time PCR was carried out with an ABI Prism 7900HT SD® (Applied Biosystems) using TaqMan assays or specific primers for the genes listed in Table 4. The

target-specific primer sequences were designed by using the ProbeFinder Assay Design Software (Roche). Samples were normalized with respect to the value obtained for the 18S or GAPDH gene due to its constant expression.

Table 4. Specific primers and TaqMan assays for real-time PCR

Gene	Primer	Sequence (5'-3')
Human CTSB	forward	TGGAGGGAGCTTTCTCTGTG
	reverse	TGACGTGTTGGTACACTCCTG
Human MMP-14	forward	CAGGAATGAGGATCTGAATGG
	reverse	CCGAGGGGTCACTGGAAT

Gene	TaqMan assay ID
18S	Hs99999901_s1
GAPDH	Hs02758991_g1
APP	HS00169098_m1

13. CTSB activity assay

The enzymatic activity of CTSB was assessed following the method described by Porter (Porter et al., 2013), with minor modifications. Cells were washed in PBS and lysed with 200 µL of lysis buffer (50 mM sodium acetate (pH 5.5), 0.1 M NaCl, 1 mM EDTA, and 0.2% Triton X-100) for 1 h at 4°C with shaking. Lysates were centrifuged at 13,000 *g* for 10 min and the supernatant (clarified lysate) used to determine proteolytic activity. For the activity assays, 50 µg of clarified lysate were incubated at 37°C for 90 min in lysis buffer (100 µL) in the presence of 20 µM z-RR-AMC fluorogenic substrate (P-137; Enzo Life Sciences). This synthetic substrate has a 7-amino-4-methylcoumarin (AMC) tag next to the cleavage site. While attached to the substrate, its fluorescence is quenched. Cleavage of the AMC peptide generates strongly fluorescent AMC that can be monitored fluorometrically. The fluorescence of AMC released as a result of proteolytic activity was quantified with an Infinite® 200 microplate reader (Tecan Trading AG), with excitation at 360 nm and emission at 430 nm, measuring each 30 min.

14. MMP-14/MMP-11 activity assay

The enzymatic activity of MMP-14/MMP-11 was assessed with the SensoLyte 520 kit (AnaSpec) following the manufacturer's instructions with minor modifications. Cells were washed in PBS and lysed with 200 µL of lysis buffer (component D) for 1 h at 4°C with

shaking. Lysates were centrifuged at 13,000 *g* for 10 min and the supernatant (clarified lysate) used to determine proteolytic activity. For the activity assays, 25 µL of clarified lysate were incubated at 37°C for 90 min with the fluorogenic substrate MCA-PLA-C(OMeBz)-WAR(Dpa)-NH_2 (Calbiochem) diluted in 25 µL of lysis buffer. This synthetic substrate has a 7-amino-4-methylcoumarin (AMC) tag next to the cleavage site. Cleavage of the AMC peptide generates strongly fluorescent AMC that can be monitored fluorometrically. The fluorescence of AMC released as a result of proteolytic activity was quantified with an Infinite® 200 microplate reader (Tecan Trading AG), with excitation at 320 nm and emission at 400 nm, measuring each 30 min.

15. LysoTracker fluorogenic assay

Lysosomal burden was evaluated using the acidotropic probe Lysotracker® Red DND-99 (LTR; Molecular Probes). 1 h before the end of treatments, cells were labelled with 1 µM LTR for 1 h at 37°C in culture medium and were then washed with PBS. Cells were lysed with RIPA buffer for 45 min at 4ºC and the lysates were centrifuged at 13,000g for 10 min. The protein concentration of the lysates was quantified by the BCA method and the fluorescence of 25 µg of total protein was recorded using a FLUOstar® OPTIMA microplate reader (BMG LABTECH) with excitation at 560 nm and emission at 590 nm. The LysoTracker® probe, which consist of a fluorophore linked to a weak base that is only partially protonated at neutral pH, is freely permeant to cell membranes and typically concentrate in acid spherical organelles.

16. Induced pluripotent stem cells (iPSCs) culture and differentiation to neurons

iPSCs were cultured in iPSC media (composed by mTeSR1, mTeSR1 supplement from StemCell Technologies and Penicillin/Streptomycin from Invitrogen). Cells were maintained at 37°C/5% CO2 and were split as necessary based on colony growth (~6 days). iPSCs were manually groomed by removing any colonies with irregular borders, spontaneous differentiation or transparent centres, prior to splitting.

To obtain iPSCs-derived neurons from SAD patients we tried two protocols: an embryoid aggregate protocol based on methods developed for human embryonic stem cells (hESCs), and another protocol based on a dual SMAD inhibition cultured in monolayer.

16.1. Embryoid aggregate differentiation protocol

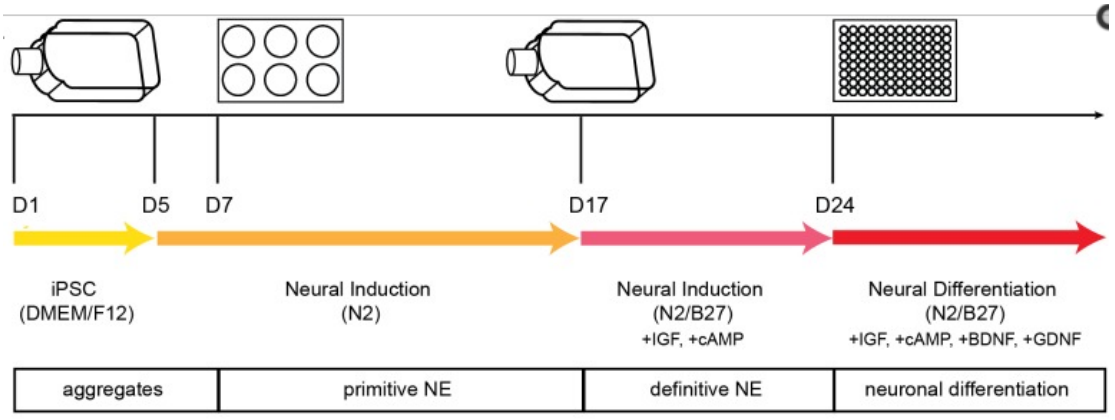

Figure 11. Time course of differentiation for embryoid aggregates. iPSC colonies were dissociated from mouse embryonic fibroblasts at day 1 (D1) and cultured as aggregates in suspension. Aggregates were plated onto culture dishes at day 7 (D7), forming primitive neuroepithelial (NE) structures. By day 17 (D17), definitive NE structures were present; NE structures were manually isolated and further cultured in suspension. Cells were plated for final differentiation at day 24 (D24). Arrows indicate media changes across differentiation. Boxes indicate differentiation state (image from Muratore et al., 2014).

Figure 11 shows the schematic timeline for the aggregate protocol. For the induction of forebrain neurons, iPSCs were differentiated using an embryoid body-based protocol (Zeng et al., 2010). Colonies with irregular borders, spontaneous differentiation or transparent centres were removed prior to splitting. Aggregates were formed by dissociating iPSCs as large clusters at day 1, followed by suspension in culture for five days in serum-free iPS media (without FGF2), with media changes every day. At day 5, aggregates were washed with N2 neural induction media and then fed with N2 neural induction media. On day 7, aggregates were plated on Matrigel® at about 20–30 aggregates/well for the formation of primitive neuroepithelial cells in N2 neural induction media. At day 17, neural rosette structures were selected, with STEMDiff neural rosette selection reagent from plates (used per the manufacturer's instructions, StemCell Technologies), added 1 h at 37°C, and suspended in non-adherent culture flasks for another week in N2/B27 neural induction media with cAMP and IGF-1, changing media every 2 days. This step aims to select for definitive neuroepithelial cells since many non-neuroepithelia cell types adhere to the flask. At day 24, aggregates were plated on Matrigel® (10 aggregates/well of 6 well plate) and allowed to mature for an additional 15–30 days in neural differentiation media with ROCK inhibitor (Stem RD, 10 µM). A full media change was performed every 2–3 days.

16.2. Dual SMAD inhibition differentiation protocol

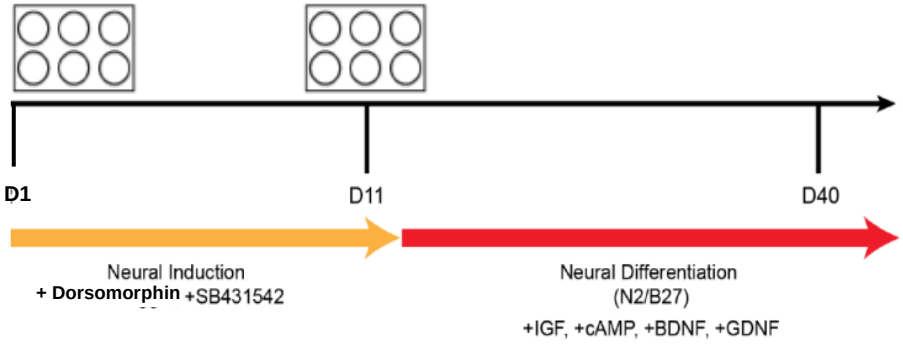

Figure 12. Time course of differentiation using dual-SMAD inhibition. iPSC colonies were dissociated at day 1 (D1) and plated as a monolayer. Small molecules and growth factors were added as indicated. At day 11 cells were split and replated in neural differentiation media (image modified from Muratore et al., 2014).

Figure 12 shows the schematic timeline for the dual SMAD inhibition monolayer protocol, an alternate method for the induction of forebrain neurons. iPSCs were differentiated using a monolayer protocol (Chambers et al., 2009). iPSCs were manually groomed by removing any colonies with irregular borders, spontaneous differentiation or transparent centers. To initiate differentiation, cells were dissociated with TrypLE (Invitrogen) for 5 min at 37°C. The cells were then disaggregated to form a single cell suspension, centrifuged 100g for 5 min and plated as a monolayer (day 0) with a concentration of 20,000 cells/cm2 in iPSCs media (mTeSR1). After cells reached 90% confluency (D1), media was changed to N2/B27 neural induction media supplemented with Dorsomorphin (200 ng/mL) and SB431542 (10 mM). Cells were split at day 11 using TrypLE and re-plated in neural differentiation media onto 6-well plates coated with Matrigel®.

16.3. iPSCs differentiation media

Culture medium components were purchased from Gibco Laboratories.

N2 neural induction medium. DMEM/F12, N2 supplement, MEM-NEAA (Lonza), Penicillin/Streptomycin (Invitrogen) and Heparin (Sigma-Aldrich).

N2/B27 neural induction medium. DMEM/F12, N2 supplement, B27 supplement, MEM-NEAA (Lonza), Penicillin/Streptomycin (Invitrogen) and Heparin (Sigma-Aldrich), with the addition of fresh cAMP (Sigma, 1 µM) and IGF1 (Immuno Tools, 10 ng/mL) to the medium.

Neural differentiation medium. Neurobasal medium, N2 supplement, B27 supplement, MEM-NEAA (Lonza) and Penicillin/Streptomycin (Invitrogen), with the addition of fresh cAMP (Sigma, 1 µM), BDNF, GDNF, and IGF-1 (all ImmunoTools, 20 ng/mL) to the medium.

17. Statistical analysis

Graph values are expressed as mean ± standard error of the mean (SEM) or standard deviation (SD). Unless otherwise indicated in specific experiments, differences between groups were analyzed using the 2-tailed Student t test. Significance was recorded as *$p<0.05$; **$p<0.01$; ***$p<0.001$.

RESULTS

1. Analysis of APP processing in the presence of oxidative stress

Besides the canonical pathway, recent studies describe additional routes of proteolytic processing of APP (non-canonical) that seem to be, at least partly, executed by enzymes of the lysosomal pathway (cysteine proteases, metalloproteinases), and generate proteolytic fragments capable of inhibiting neuronal activity in the hippocampus (Willem et al.2015). Based on data from our experimental model demonstrating that OS alters the lysosomal degradation system and the processing/metabolism of APP (Recuero et al., 2013), these new proteolytic processing routes of APP could, as with canonical pathways, be altered in aging and thus be part of the pathogenic mechanisms of neurodegeneration. Proteins involved in these alterations, and in particular the proteases of the lysosomal pathway capable of acting as APP secretases, would be potential targets to regulate neurodegeneration.

With the aim of analyzing the effects of OS on APP processing, SK-N-MC human neuroblastoma cells were treated with the free radical generating system xanthine/xanthine oxidase (X-XOD), that produces a mild OS in these cells (Recuero et al., 2009).

As a previous step the cell damage induced by this system was monitored by phase contrast microscopy, and the apoptotic cellular death was controlled analyzing by fluorescence microscopy the nuclear morphology of the cells stained with 4', 6-diamidino-2-phenylindole (DAPI). As previously reported by our group in this cell model, at 24 hours no adverse effects were observed, but at 48 hours a high proportion of cells showed condensed nuclear chromatin, revealing the apoptosis induced by X-XOD that was still undetectable at 24h (Recuero et al., 2010). These results confirmed that the behavior of the cells allows the performance of all the studies under conditions of minimal cell damage, previous to the outcome of the apoptotic death.

1.1 APP proteolytic fragment pattern induced by OS

Probably the most studied modification of APP is its proteolytic processing, which is intimately linked with its intracellular trafficking and generates, apart from Aβ peptides, multiple fragments with either neuroprotective or neurotoxic capabilities (Nhan et al., 2015).

In our cell model the levels of Aβ are low due to the lack of APP transfection, therefore we decided to study the levels of amyloid oligomers, that are more neurotoxic, with the A11 antibody, a structural antibody that recognizes oligomers.

To study the proteolytic processing of APP we performed Western Blot analysis of SK-N-MC cell lysates with anti-APP antibodies: anti N-terminal (22C11), anti C-terminal and anti β amyloid (6E10). Given that amyloid oligomers are more neurotoxic we also used an anti-oligomer antibody (A11). The results revealed specific bands corresponding to APP (full length APP - blue arrow), higher molecular weight bands probably corresponding to post-translational modifications (e.g. glycosilation), and lower molecular weight bands probably representing proteolytic fragments. In Figure 13 the specific bands that significantly change in X-XOD treated cells are noted with red arrows: the most prominent one has an approximate molecular weight of 85 kDa and would correspond to a N-terminal part of APP since it is recognized only by 22C11; furthermore, the sequencing of this band revealed us that it contains APP N-terminal sequences, but not the Aβ or CTF parts. In addition, there was an increase of CTFs (band of around 15 kDa recognized by anti C-terminal antibody) that we have studied previously (Recuero et al., 2013), and a band of around 56 kDa recognized by A11 (anti oligomer).

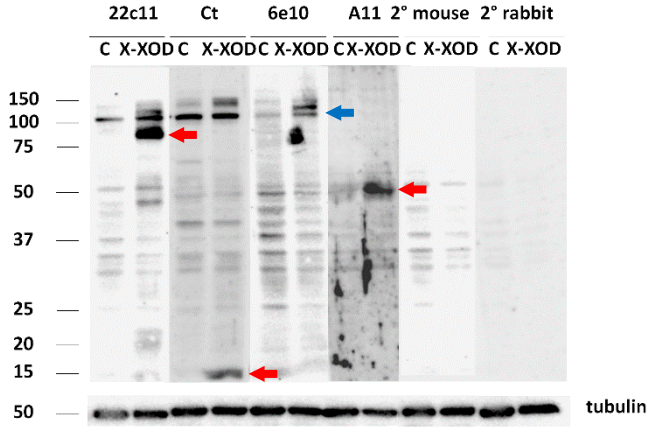

Figure 13. APP processing changes induced by OS. X-XOD induces three derivatives of APP of about 85 kDa, 56 kDa and 15 kDa CTF (previously studied). SK-N-MC cells were treated with X-XOD. After incubation for 24 h, cells were lysed and western blotting was performed using anti-N terminal APP (22C11), anti-C terminal APP (Ct), anti-Aβ (6E10) and anti-oligomer (A11) antibodies. α-tubulin blot is shown as loading control.

In summary, OS induced two prominent bands recognized by APP specific antibodies that will be the focus of our subsequent studies in this thesis: one of 85 kDa recognized by the N-terminal specific antibody 22C11 (herein referred to as APP85) and another one of about 56 kDa recognized by the oligomer specific A11 antibody.

1.2. Subcellular location of APP derived products

Because APP is majoritarily located in membranes of the lysosomal system, and its processing takes place mainly in the endo-lysosomes (Soldano et al., 2012), we decided to explore the subcellular location of the APP derivatives that accumulate under OS conditions. For this purpose, cells were fractionated, following the method of Avrahami (Avrahami et al., 2013), to separate out a fraction enriched in lysosomes and late-endosomes (L/LE). APP was preferentially located in the L/LE fraction, as well as the oligomeric form (56 kDa) recognized by A11, whereas the APP85 band recognized by 22C11 was evenly distributed in both fractions (Cyt and L/LE). In the X-XOD treated cells, all the bands, including APP and their derivatives and the endo-lysosomal markers LAMP1, Rab7 an EEA1 were clearly increased. We also analyzed the location of the two candidate proteases that will be studied in this thesis (CTSB and MMP-14, see next chapter for the selection process), which were also located in the L/E fraction. MMP-14 levels increased in X-XOD treated cells, whereas CTSB was clearly reduced.

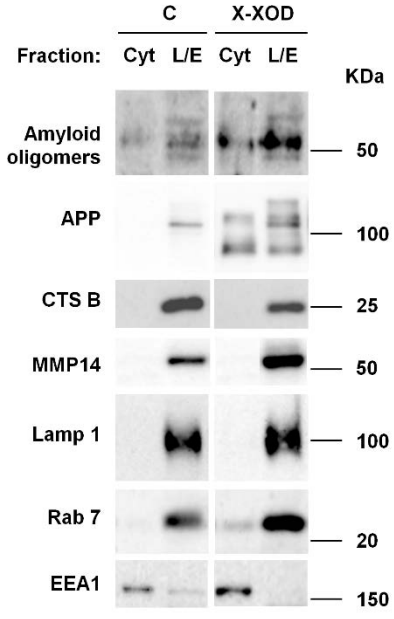

Figure 14. APP, amyloid oligomers and selected proteases were located in L/LE fraction. SK-N-MC cells were treated with X-XOD for 24 h and then fractionated by differential centrifugation. Western blotting was performed using anti-oligomer (A11), anti-APP (22C11), anti-CTSB, anti-MMP-14, anti-LAMP1, anti-Rab7 and anti-EEA1 antibodies. The protein quantity determined by a BCA assay was used as the loading control. A representative blot of three independent experiments is shown. Cyt: cytosol fraction; L/LE: lysosome-late endosome fraction.

1.3. Identification of the 56 kDa band induced by OS as oligomeric Aβ

Since products of APP containing the whole Aβ peptide are the result of the amyloidogenic pathway, classically considered as the pathogenic one, we considered of high interest to follow these amyloid-containing products. The direct detection of the peptide is not possible in our cells due to its very low levels (Santana et al., 2013), and that was the initial reason why we decided to take advantage of the A11 antibody. This antibody specifically detects soluble amyloid assemblies distinct from fibrillar Aβ; it is claimed to recognize a peptide backbone epitope that is common to amyloid oligomers, but is not found in native proteins, amyloid monomer or mature amyloid fibrils (datasheet from Origene, TA326459). Because A11 is able to cross-react with amyloid structures of proteins different from Aβ and APP fragments, immunoprecipitation assays were carried out to assure that the 56 kDa band recognized by this antibody correspond to Aβ oligomers.

Immunoprecipitation of the A11 band with the monoclonal antibody 6E10 (which recognizes Aβ, βCTF and APP), but not with the C-terminal APP antibody, indicated it to be an Aβ oligomeric form derived from APP proteolysis (Figure 15). Based on its electrophoretic migration, this amyloid oligomer probably corresponds either to the 56 kDa soluble Aβ assembly known as Aβ*56 (detected in brain of AD transgenic rat model by Lesne et al., 2006) or to the more recently described oligomeric Aβ assemblies found in both aging and AD brains (Baker-Nigh et al., 2015).

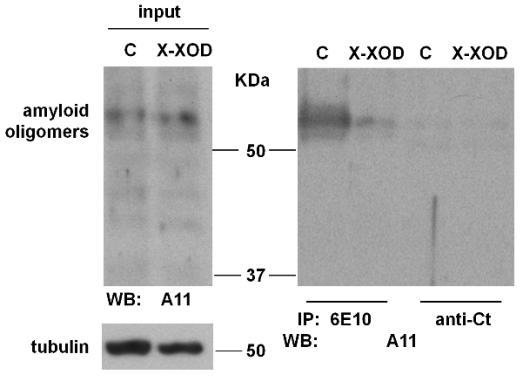

Figure 15. Immunoprecipitation of the A11-recognized band with 6E10 and C-terminal antibodies. SK-N-MC cells were treated with X-XOD. After incubation for 24 h, immunoprecipitation was performed using the 6E10 antibody and the anti-APP C-terminal fragment antibody, followed by Western blotting with antibody A11. A representative blot of three independent experiments is shown.

2. Involvement of candidate proteases in APP processing and in lysosomal function

Increasing evidence indicate that the lysosomal system is altered in AD. Lysosomal hydrolase-containing compartments are massively accumulated in atrophic and degenerating neurons or their processes, and they are released into the extracellular space where they then contribute to senile plaque formation (Cataldo et al., 1991). Increased expression of lysosomal enzymes is observed during the early stages of AD (Cataldo et al., 1996). It has been reported that, in neuronal cells, APP is enriched in the lysosomes, and that it is rapidly and directly trafficked toward this compartment (Haas et al., 2012). Thus, the endosomal/lysosomal system may play a central role in the pathophysiology of AD, and the type of proteolysis that APP undergoes may be related to the mechanism by which the protein is mobilized to the lysosomes (Lorenzen et al., 2010).

In order to study the role of non-canonical secretases capable of mediating the changes in the processing of APP and in the lysosomal pathway induced by OS in our cellular model, we chose candidate proteases based on the following criteria: i) their recognition sites in APP should be compatible with the proteolytic fragments observed in Figure 13, ii) their expression should be modulated by OS and iii) they should be located or related with the endo-lysosomal system. These criteria were applied to the APP secretases previously described in the literature (see a scheme in Figure 16), that were expressed in the SK-N-MC cells and modulated in our model of OS (Table 5). Moreover, we analyzed their intracellular location, being of relevance their presence in lysosomes, in accordance with studies of our group that revealed the profound impairment of the lysosome system induced by OS in SK-N-MC cells infected with HSV-1 (Kristen et al., 2018).

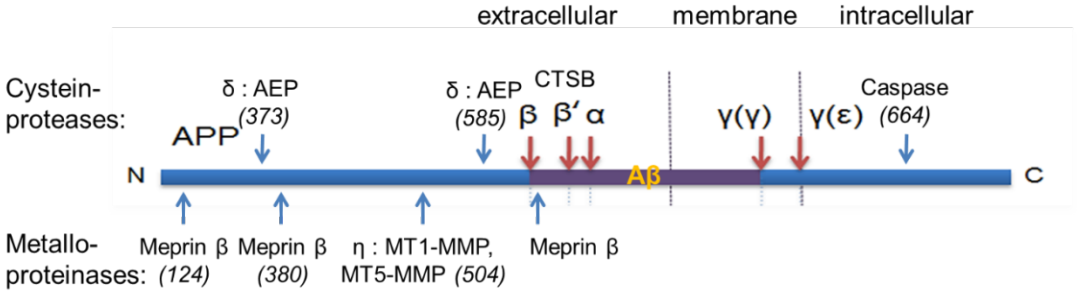

Figure 16. Scheme of APP (APP695 isoform) cleavage by canonical (red arrows) and non-canonical secretases (blue arrows). Cysteine proteases are represented at the upper part of the figure and metalloproteinases at the bottom part of the figure. The residue by which APP is cleaved is indicated in brackets.

Table 5. Modulation of metalloproteinases and cysteine proteases expression by OS.

Gene	fold 24h	fold 36h
MEP1A	0,96	0,94
MMP1	1,02	4,85
MMP11	1,07	1,04
MMP14	**1,37**	**2,01**
MMP15	0,88	1,20
MMP17	0,90	0,95
MMP19	0,87	1,10
MMP19	0,91	1,13
MMP21	1,00	0,97
MMP23B	0,80	0,92
MMP25	0,90	0,86
MMP25	1,08	0,94
MMP28	0,70	0,84
MMP9	1,11	1,11
LGMN	0,89	1,17

Gene	fold 24h	fold 36h
CTSA	1,39	1,50
CTSA	1,07	1,54
CTSB	**0,74**	**0,60**
CTSC	0,89	1,30
CTSC	0,84	0,68
CTSC	0,78	0,92
CTSD	0,79	1,19
CTSE	0,90	0,98
CTSF	1,51	1,18
CTSG	0,85	0,89
CTSH	0,95	0,73
CTSK	1,15	0,94

SK-N-MC cells were treated with X-XOD for 24 h or 36 h. mRNA levels were analyzed in whole human genome expression microarrays**.** Candidate genes with basal expression levels above a given threshold (4.0 arbitrary units) were selected. Expression is shown as the fold change of X-XOD treated compared to control cells at 24 and 36 hours.

With these criteria, cathepsin B and Matrix metalloproteinase 14 were selected as the strongest candidates. Their enzymatic activity and protein levels were modulated by pharmacological inhibition or by gene silencing and their involvement on the APP processing and on the lysosomal pathway changes induced by OS were studied.

2.1 Cathepsin B

Cathepsins reside in the endo-lysosome system where β-secretase activity mainly occurs (Soldano et al., 2014). Cathepsin B (CTSB) is a cysteine protease with the ability to cleave APP at the same site than β–secretase (Hook et al., 2005) and degrades the Aβ42 peptide, starting at its C-terminal (Mueller-Steiner et al., 2006). Moreover, mature and proenzyme forms of CTSB have been identified at early endosomes in most cases of AD patients, but only a small proportion at endosomes of normal brains (Cataldo et al., 1995). In this way, it likely plays an important role in the formation of the amyloid oligomers that we have detected in our model of mild OS.

2.1.1. Pharmacological inhibition of CTSB

CA-074 Me is an epoxysuccinyl peptide that acts as a potent and specific irreversible cell permeable cathepsin B inhibitor. Methyl ester (Me) is hydrolyzed by intracellular esterases releasing the active inhibitor. CA-074 Me action mechanism is not fully characterized, but some authors have described that its specificity for CTSB would be explained if it binds to CTSB in a substrate-like mode (Buttle et al., 1992).

2.1.1.1 Effect of OS or CA-074 Me on CTSB

Cathepsin B (CTSB) activity was assessed in SK-N-MC cells treated with the X-XOD free radical generating system for 24 h. To compare the effect of mild OS with the pharmacological inhibition of CTSB, cells were treated with CA-074 Me. CTSB activity was quantified using a fluorimetric assay. X-XOD treated cells showed CTSB activity to be reduced by up to 58% (Figure 17A) ($p<0.001$ compared to control culture). CA-074 Me reduced CTSB activity in a dose-dependent manner (Figure 17B) - by 97% ($p<0.001$) at its highest concentration (5 μM), 71% ($p=0.0012$) at an intermediate concentration (1 μM), and 48% ($p=0.011$) at the lowest concentration (0.2 μM).

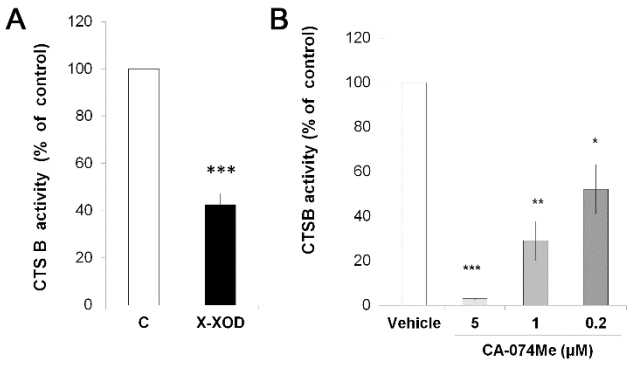

Figure 17. X-XOD and CA-074 Me reduce CTSB activity. SK-N-MC cells were treated with X-XOD or with the indicated concentrations of CA-074 Me. After incubation for 24 h, CTSB activity induced by OS (A) and CTSB inhibitor (B) were measured. Proteolysis of the fluorogenic substrate z-RR-AMC was used to monitor CTSB activity. The graphs show the mean (±SEM) fluorescence values expressed as a percentage of the control or vehicle value. ∗p<0.05, ∗∗p<0.01 and ∗∗∗p<0.01 (t-test, n=3).

To deepen in the effect of these treatments on CTSB, the active enzyme levels were examined by Western blotting in the same cell lysates, using a CTSB-specific antibody that recognizes the enzyme (25 kDa) and its precursor (pro-enzyme, 37-42 kDa). CTSB is synthesized as a pre-proenzyme, following removal of the signal peptide the inactive pro-enzyme undergoes further modifications including removal of the pro region to result in the active enzyme. X-XOD (Figure 18A) induced a significant reduction in CTSB mature/active-form levels (0.61±0.08-fold vs. control; p=0.098). The CTSB inhibitor CA-074 Me (Figure 18B) also induced significant reductions (0.45±0.04-, 0.61±0.16- and 0.59±0.01-fold vs. control at 5 (p<0.001), 1 (p=0.049) and 0.2 (p=0.006) µM respectively).

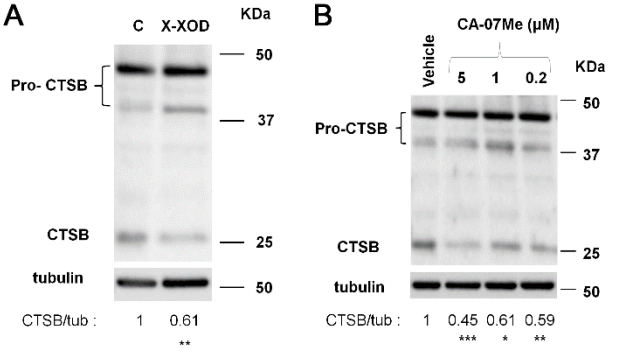

Figure 18. X-XOD and CA-074 Me reduce CTSB levels. SK-N-MC cells were treated with X-XOD or with the indicated concentrations of CA-074 Me. After incubation for 24 h, CTSB protein levels induced by OS (A) and CTSB inhibitor (B) were measured. Western blotting was performed using the anti-CTSB antibody. α-tubulin blot is shown as loading control. The

bands correspond to the pro-enzyme (top) and active enzyme (down) forms of CTSB. The data show the mean (±SEM) densitometry values (normalized by α-tubulin). Control or vehicle values were set at 1. ∗p<0.05, ∗∗p<0.01 and ∗∗∗p<0.01 (t-test, n=4).

To confirm that the reduced activity was not due to any treatment-caused lessening of cell viability, MTT reduction assays were performed. Figure 19 (A and B) shows that none of the treatments reduced cell viability at 24 h of culture.

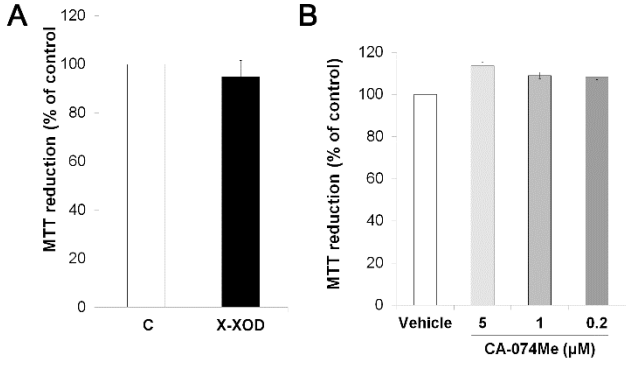

Figure 19. Cell viability is not affected by X-XOD or CA-074 Me. The cells were treated with X-XOD or with the indicated concentrations of CA-074 Me. After incubation for 24 h, cell injury was analyzed via the MTT reduction assay. Values are expressed relative to the optical density of the control at 550 nm. Each value represents the mean of three replicates ± S.E.M.

2.1.1.2. Effect of OS or CA-074 Me on APP processing

The effect of mild OS on soluble amyloid oligomer levels was examined in cell lysates by Western blotting (Figure 20) using the polyclonal antibody A11. This antibody specifically detects soluble amyloid assemblies distinct from fibrillar Aβ. Since the amyloid oligomer derives from APP proteolytic processing, APP protein was analyzed in the same cell lysates by Western blotting using the 22C11 antibody which recognizes full-length APP and APP fragments containing the N-terminal region (sAPP). Figure 20A shows that treatment with X-XOD for 24 h led to a 3.85±1.07-fold increase in cellular APP levels (p=0.037) and a significant increase in a single band at 56 kDa (1.36±0.06-fold; p<0.001). The above results indicate that, during that period just before the transmission of cell death signals (24 h), the X-XOD system increases APP levels and intracellular soluble amyloid oligomer.

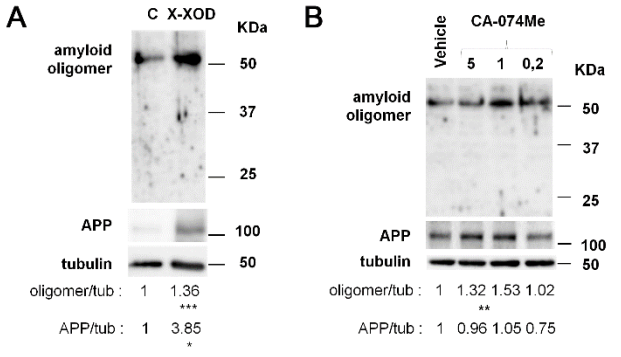

Figure 20. X-XOD and CA-074 Me increase amyloid oligomers levels. SK-N-MC cells were treated (A) with X-XOD or (B) with the indicated concentrations of CA-074 Me. After incubation for 24 h, Western blotting was performed using anti-N terminal APP antibody (22C11) and anti-oligomer antibody (A11). Representative blots for X-XOD (A) and CA-074 Me (B) treatments are shown. α-tubulin blot is shown as loading control. In the upper panel the band corresponds to high molecular weight amyloid oligomer, in the intermediate panel to APP, and in the lower to α-tubulin. The data show the mean (± SEM) densitometry values (normalized by α-tubulin). Control or vehicle values were set at 1. ∗p<0.05, ∗∗p<0.01 and ∗∗∗p<0.01 (t-test, n=4).

The effect of the CTSB inhibitor CA-074 Me was also examined. Figure 20B shows that in the presence of CA-074 Me, the levels of amyloid oligomer were also increased, by 1.32±0.07- and 1.53±0.40-fold at the ($p=0.005$) and 1 μM ($p>0.05$) concentrations of the inhibitor respectively, resulting to be significant only for the higher concentration. In contrast, the levels of APP protein were not significantly affected by CA-074 Me treatment. Together, these results show that the inhibition of CTSB activity via mild OS or the pharmacological inhibitor leads to increased levels of amyloid oligomers, suggesting that the CTSB pathway is a participant in the formation of amyloid oligomers.

2.1.1.3. Effect of CA-074 Me on the CTSB enzymatic activity produced by OS

The mechanisms by which OS and the inhibitor works are different as deduced above. To deepen into it, we decided to analyze their effect together studying X-XOD treated cells in presence of CA-074 Me. Firstly, the quantification of CTSB activity with both treatments together (Figure 21) revealed a complete inhibition (up to 98%; $p<0.001$ vs. control culture), whereas the results with X-XOD or CA-074 Me alone were similar to those described above (Figure 17).

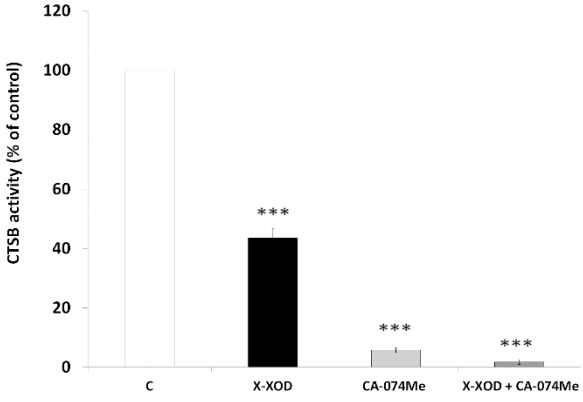

Figure 21. X-XOD combined with CA-074 Me reduces CTSB activity almost completely. SK-N-MC cells were treated with X-XOD in the presence or absence of CA-074 Me. After incubation for 24 h, CTSB activity was analyzed. Proteolysis of the fluorogenic substrate z-RR-AMC was used to monitor CTSB activity. The graph shows the mean (±SEM) fluorescence values expressed as a percentage of the control value. ∗p<0.05, ∗∗p<0.01 and ∗∗∗p<0.01 (t-test, n=4)

The MTT reduction assay was performed to confirm that there was not a treatment-induced lessening of cell viability by the combination of the treatments (Figure 22).

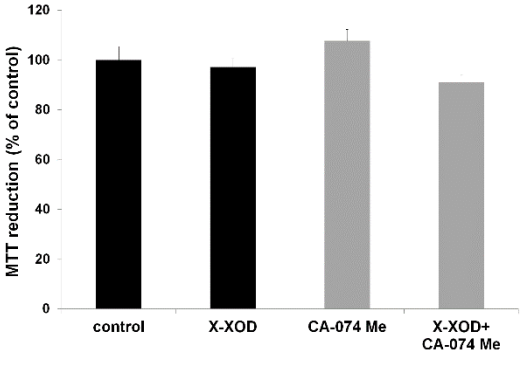

Figure 22. Cell viability is not affected by the combination of X-XOD with CA-074 Me. The cells were treated with X-XOD) in the presence or absence of CA-074 Me. After incubation for 24 h, cell injury was analyzed via the MTT reduction assay. Values are expressed relative to the optical density of the control at 550 nm. Each value represents the mean of three replicates ± S.E.M.

2.1.1.4. Effect of CA-074 Me on the APP processing induced by OS

Although the two treatments (X-XOD system and the CTSB inhibitor) induced an increase of amyloid oligomer species, their effect on APP levels was different; whereas X-XOD increases APP levels, CTSB inhibitor does not (Figure 20). This suggested that X-XOD induced OS and the CTSB inhibitor modulate APP metabolism by different mechanisms. To

deepen in that complexity of APP metabolism modulation, the effect on the levels of amyloid oligomers and APP of mild OS in the presence of the CTSB inhibitor was then examined by Western blotting, using the A11 and 22C11 antibodies respectively. Figure 23A shows that the increase in the 56 kDa amyloid oligomer induced by X-XOD was attenuated, in the presence of CA-074 Me (0.65±0.15-fold over X-XOD alone, p=0.05). The increase in APP protein induced by X-XOD was, however, significantly enhanced in the presence of CA-074 Me (3.03±0.57-fold over X-XOD alone; p=0.0083). The effect of both treatments together on soluble APP (sAPP) secretion was also examined by Western blotting using the 6E10 antibody, which recognizes secreted APP derived from non-amyloidogenic α-cleavage (sAPPα). Figure 23B shows a 1.25±0.03-fold increase in sAPPα at the culture medium of cells treated for 24 h with X-XOD compared to control cells (p=0.011). This increase was further enhanced in the presence of CA-074 Me (1.37±0.05-fold over X-XOD alone; p=0.027). These results indicate that the APP processing induced by mild OS is modulated by inhibiting CTSB, leading to an increase in intracellular APP and secreted sAPPα.

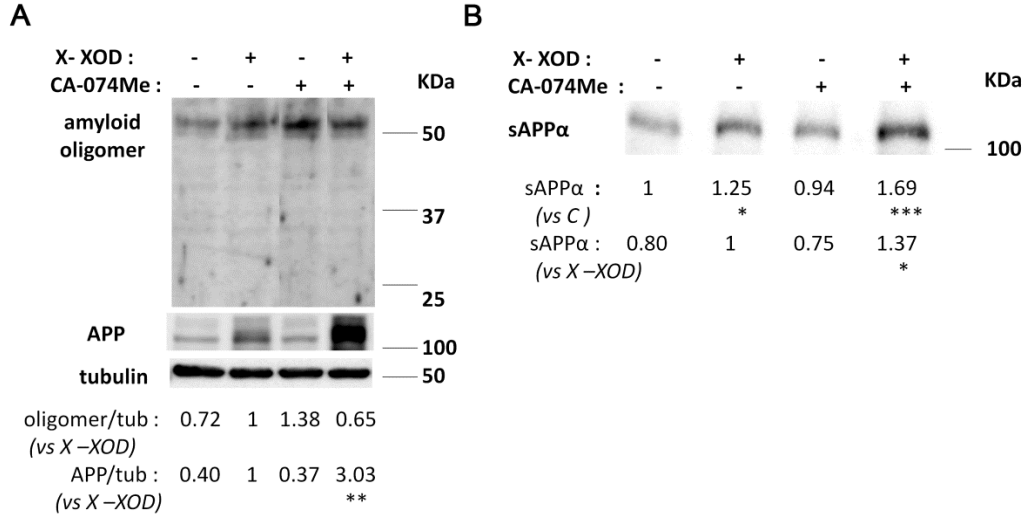

Figure 23. **CA-074 Me varies the APP metabolism/processing response to X-XOD.** SK-N-MC cells were treated with X-XOD in the presence or absence of CA-074 Me. After incubation for 24 h, cell cultures were examined A) intracellularly and B) extracellularly. (A) Intracellular: Western blotting analysis was performed using anti-N-terminal APP antibody (22C11) and the anti-oligomer antibody A11. A representative experiment is shown. α-tubulin blot is shown as loading control. In the upper panel, the band corresponds to high-molecular weight amyloid oligomer, in the intermediate to APP, and in the lower panel to α-tubulin. The data show the mean (± SEM) densitometry values (normalized by α-tubulin). Values for X-XOD were set at 1. ***p<0.001 (t-test, n=5). (B) Extracellular: secreted APP in the culture medium, derived from nonamyloidogenic α-cleavage

(sAPP α), was analyzed by Western blotting with the 6E10 antibody. The data show the mean (± SEM) densitometry values. Values for control or X-XOD were set at 1. ∗p<0.05, ∗∗∗p<0.01 (t-test, n=4).

An immunofluorescence assay was performed to observe the intracellular pattern of APP with these treatments. As it was described previously by this group, APP was mainly localized in endolysosomal compartments (Recuero et al., 2013). APP immunoreactivity increase in the presence of OS and we can observe some condensed pattern (Figure 24). Moreover, the levels in cells treated with OS and CA-074 Me are even higher, which correlates with the results obtained by Western blot.

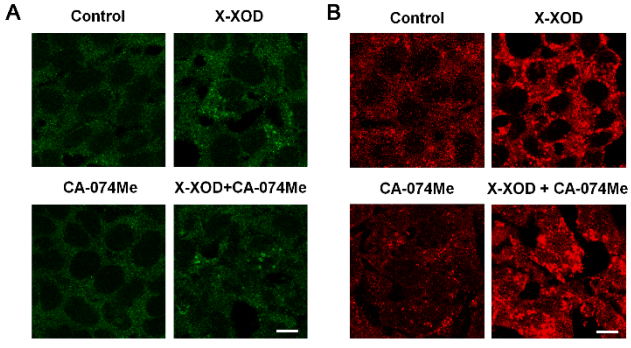

Figure 24. CA-074 Me promotes the APP accumulation induced by X-XOD. SK-N-MC cells treated with X-XOD, in the presence or absence of CA-074 Me, for 24 h were examined by confocal microscopy. The representative panel shows immunofluorescence images for (A) the 22C11 (green) and (B) anti-C-terminal (red) antibodies. Original magnification: 63×. Scale bar: 10 μm. No staining was observed when the primary antibodies were omitted.

These data indicate that the inhibition of CTSB increase the APP levels induced by OS and that CTSB modulates the APP processing at various levels, including the formation of amyloid oligomers.

2.1.1.5. Effect of CA-074 Me on the lysosomal pathway changes induced by OS

The autophagy–lysosomal pathway (ALP) is involved in the degradation of long-lived proteins. Deficits in the ALP result in protein aggregation, the generation of toxic protein species, and accumulation of dysfunctional organelles, which are hallmarks of AD. In AD defects in endocytosis and lysosomal function appear at the earliest stages of disease development, preceding the classical neuropathological hallmarks, and progress to widespread failure of intraneuronal waste clearance, neuritic dystrophy and neuronal cell death. Several genetic factors that cause or increase AD risk are also direct causes of

endosomal-lysosomal dysfunction, underscoring the essential partnership between this dysfunction and APP metabolites in AD pathogenesis.

To analyze the lysosomal pathway, representative markers were measured by Western blot using antibodies specific for LAMP2 (lysosome membrane-associated protein) and CD63 (lysosomal membrane integral protein). As shown in Figure 25, the levels of lysosomal proteins increased in X-XOD treated cells, being the increase even higher in combination with the CA-074 Me inhibitor. The effect of the inhibitor by its own was also an increase of lysosomal markers.

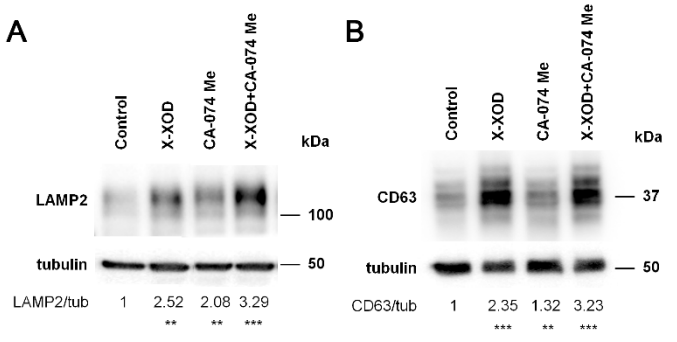

Figure 25. CA-074 Me potentiates the increase in lysosomal markers induced by X-XOD. SK-N-MC cells were treated with X-XOD, in the presence or absence of CA-074 Me. After incubation for 24 h, Western blotting was performed using (A) anti-LAMP2 and (B) anti-CD63 antibodies. Representative experiment is shown. α-tubulin blot is shown as loading control. The data show the mean (± SEM) densitometry values (normalized by α-tubulin). Control value was set at 1. $*p<0.05$, $**p<0.01$ and $***p<0.01$ (t-test, n=3)

The lysosomal burden was measured using LysoTracker® that is a fluorescent acidotropic probe for labeling and tracking acidic organelles. As shown in Figure 26, in the fluorimetric assay of cells in the absence (black) or in the presence of the inhibitor CA-074 Me (grey) the lysosomal burden increase significantly in X-XOD treated cells by up to 183,6 % without inhibitor ($p=0.001$) and even more, by up to 239%, in the presence of CTSB inhibitor ($p<0.001$).

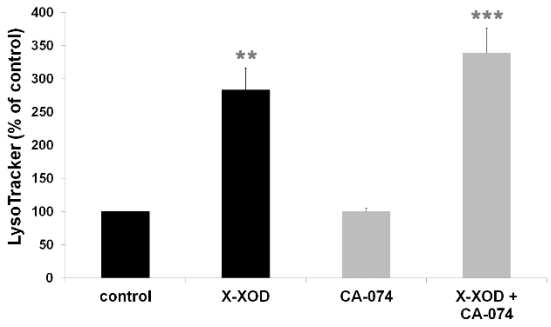

Figure 26. CA-074 Me favors the increase of lysosomal burden induced by X-XOD. SK-N-MC cells were treated with X-XOD in the presence or absence of CA-074 Me. After incubation for 24 h, lysosomal quantity was analyzed by fluorimetric measurement of LysoTracker. The graph shows the mean (±SEM) fluorescence values expressed as a percentage of the control value. ∗p<0.05, ∗∗p<0.01 and ∗∗∗p<0.01 (t-test, n=4)

To analyze the intracellular location pattern of endolysosomal vesicles, immunofluorescence assays with the LysoTracker probe and LAMP2, CD63 and Rab7 specific antibodies were performed. As it is observed in Figure 27, all the markers increase in the presence of OS, being that increase even higher in cells treated with X-XOD together with CA-074 Me, as was especially evident for CD63 (Figure 27C). These results correlate with the Western blot data (Figure 25), confirming the increase in lysosomal burden induced by OS and CTSB inhibition.

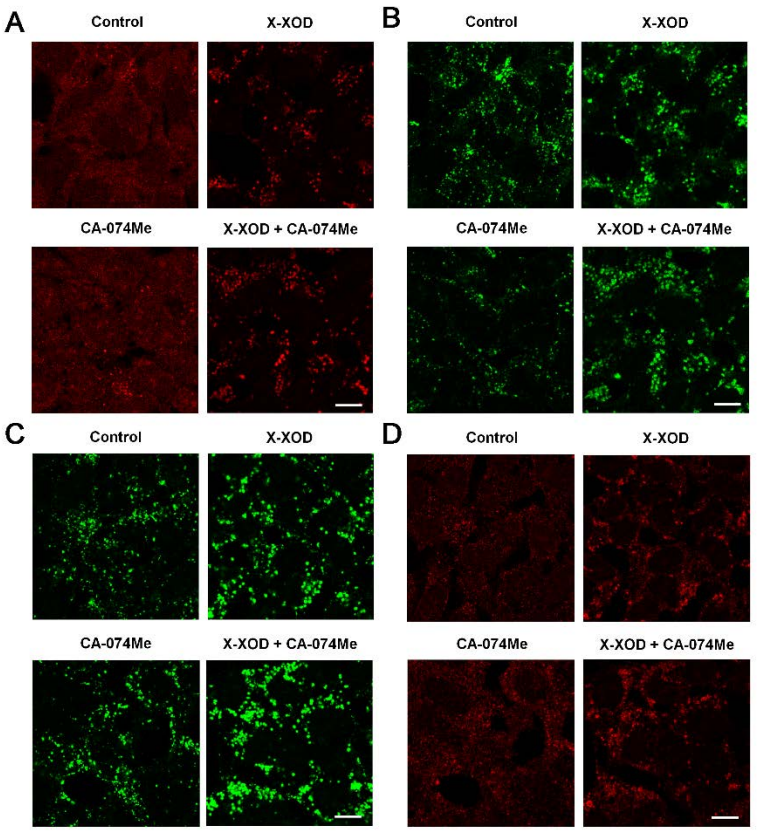

Figure 27. CA-074 Me favors the accumulation of lysosomes induced by X-XOD. SK-N-MC cells treated with X-XOD, in the presence or absence of CA-074 Me, for 24 h were examined by confocal microscopy. The representative panel shows immunofluorescence images for (A) LysoTracker probe, (B) anti-LAMP2, (C) anti-CD63 and (D) anti-Rab7 antibodies. Original magnification: 63×. Scale bar: 10 μm. No staining was observed when the primary antibodies were omitted.

Taken together, the results support the involvement of CTSB in the regulation of APP metabolism induced by mild OS and its role on the lysosomal pathway, and support the potential relevance of CTSB in AD.

2.1.2. Gene silencing of CTSB

To study the role of CTSB in the APP processing and in the lysosomal dysfunction induced by OS in a more stable cell model, we decide to generate SK-N-MC cells stably transfected with a shRNA specific for CTSB, as described in Methods. Cells were transfected and several CTSB deficient clones were selected, expanded and analyzed.

2.1.2.1. Characterization of CTSB deficient cell line

To characterize the transfected cell lines CTSB activity and levels analysis were performed, and the clones with lower activity and expression were selected for the subsequent studies.

Figure 28A shows that in some clones CTSB activity decreased significantly, which was corroborated by Western blot analyses (Figure 28B). The clone 14 had consistent results in both assays, therefore it was selected to work with. In comparison with SK-N-MC cells, the CTSB-deficient cell line 14 showed a clear reduction in activity and protein levels (approximately 75% reduction in both assays). The cell line transfected with a scrambled shRNA (clone 8) showed no decrease in CTSB. Determination of the CTSB mRNA levels by RT-qPCR confirmed the results obtained by Western blot as shown in Figure 28C. Moreover, mRNA levels of APP were also measured to take into account the possible changes in APP basal levels in the studies of APP processing (Figure 28D). A moderate decrease in the mRNA levels of APP (around 20%) was observed in the selected clone 14.

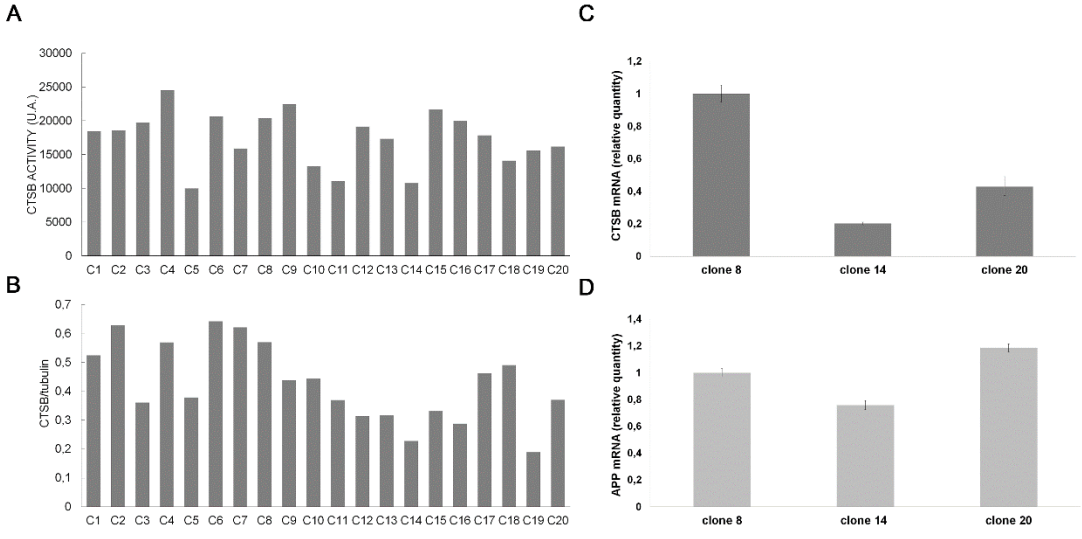

Figure 28 Selection of CTSB deficient clones. (A) Analysis of the clones by CTSB activity. (B) Analysis of the clones by Western blot with an anti-CTSB antibody. (C) Analysis of the clones by RT-qPCR of CTSB and (D) APP.

Once selected the clone to work with, CTSB deficient cells and non-deficient cells were treated with X-XOD. CTSB activity of deficient cells decreased by up to 80% ($p<0.001$) in comparison to non-deficient cells (black). A reduction of activity by up to 78 % ($p=0.0035$) in comparison to untreated deficient cells was observed (Figure 29), similar to the results

obtained in the non-deficient (71% of reduction, p<0.001) and in the SK-N-MC parental cells (previous chapter).

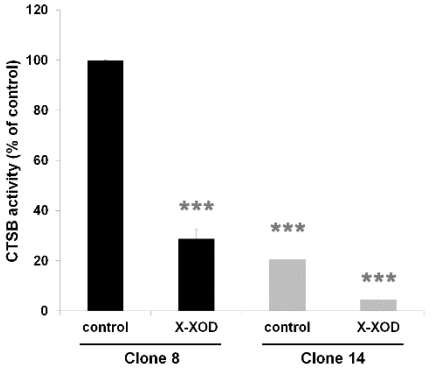

Figure 29. X-XOD reduces the residual CTSB activity in deficient cells. CTSB deficient cells (grey) were treated with X-XOD. After incubation for 24 h, CTSB activity was analyzed. Proteolysis of the fluorogenic substrate z-RR-AMC was used to monitor CTSB activity. The graph shows the mean (±SEM) fluorescence values expressed as a percentage of the untreated non-deficient cells (black) value. ∗p<0.05, ∗∗p<0.01 and ∗∗∗p<0.01 (t-test, n=4).

2.1.2.2. Effect of OS on APP processing in CTSB deficient cells

To study the effect of CTSB deficiency on APP processing induced by mild OS, deficient cells were treated with X-XOD and APP fragments were examined in cell lysates by Western blotting using the antibody 22C11 (Figure 30). We observed a significant increase of APP in the presence of X-XOD. The increase in APP induced by OS was higher in the CTSB deficient (2.5 fold) than in the clone 8 (1.7) although the difference didn't reach statistical significance.

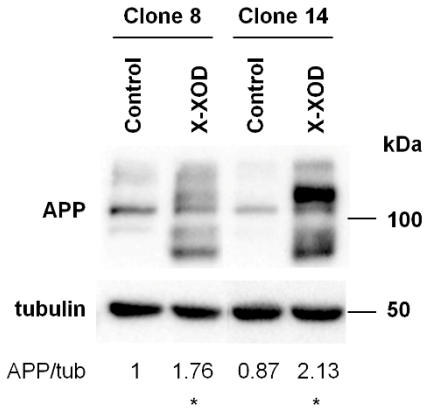

Figure 30. X-XOD induces higher increase of APP levels in CTSB deficient cells. CTSB deficient cells were treated with X-XOD. After incubation for 24 h, Western blotting was performed using anti-N terminal APP antibody (22C11). A representative experiment for X-XOD treatment is shown. α–tubulin blot is shown as loading control. The data show the mean (± SEM) densitometry values (normalized by α-tubulin). Control value was set at 1. ∗p<0.05, ∗∗p<0.01 and ∗∗∗p<0.01 (t-test, n=3).

The immunofluorescence assay of these cells with antibodies specific for APP, N-terminal (22C11) and for the C-terminal (anti-Ct) (Figure 31), revealed an increase of the levels of immunofluorescence and a more punctate pattern in the presence of X-XOD in the CTSB deficient cells. A similar effect was observed in X-XOD treated non-deficient cells. Comparing deficient cells with non-deficient cells, there was an increase of APP markers fluorescence associated to the CTSB deficiency.

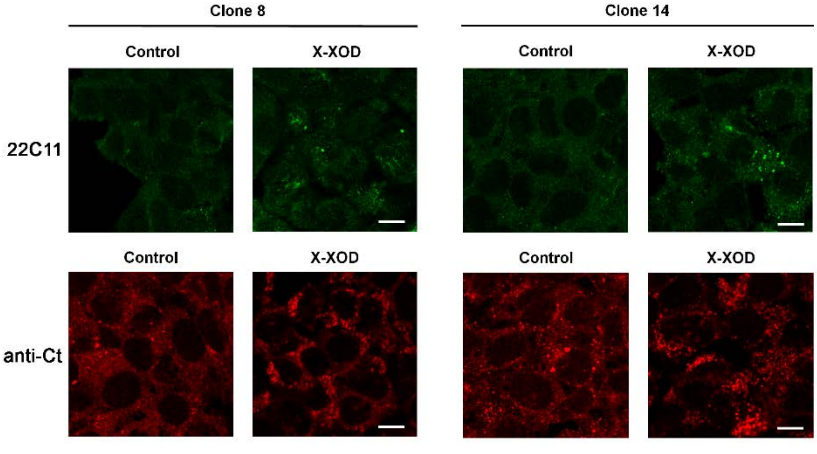

Figure 31. CTSB deficiency helps to the APP accumulation induced by X-XOD. CTSB deficient cells treated with X-XOD for 24 h were examined by confocal microscopy. The representative panel shows immunofluorescence images for the 22C11 (green) and anti-C-terminal (red) antibodies. Original magnification: 63×. Scale bar: 10 μm. No staining was observed when the primary antibodies were omitted.

2.1.2.3. Study of lysosomal pathway changes in CTSB deficient cells

As described in chapter 2.1.1.5, lysosomal markers were measured by Western blot using the antibodies specific for LAMP2 and CD63. X-XOD treated CTSB deficient cells showed higher levels of lysosomal proteins, especially CD63, than X-XOD treated non-deficient cells, indicating that CTSB deficiency promotes the increase of lysosomal markers induced by OS.

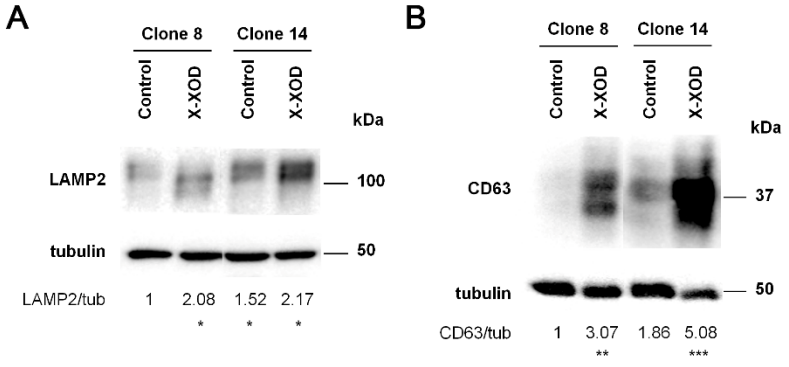

Figure 32. CTSB deficiency cooperates to the lysosomal markers levels increase induced by X-XOD. CTSB deficient cells were treated with X-XOD. After incubation for 24 h, Western blotting was performed using anti-LAMP2 (A) and anti-CD63 (B) antibodies. Representative experiment for X-XOD treatment is shown. α-tubulin blot is shown as loading control. In the upper panel the bands correspond to LAMP2 or CD63 and in the lower to α-tubulin. The data show the mean (± SEM) densitometry values (normalized by α-tubulin). Control value was set at 1. $*p<0.05$, $**p<0.01$ and $***p<0.01$ (t-test, n=3)

The lysosomal burden was measured with LysoTracker probe. As shown in Figure 33, LysoTracker basal levels decreases slightly but significantly (20% decrease, p=0.029) in deficient cells compared to non-deficient cells. As for the effect of OS, X-XOD treatment increased the lysosomal burden in both lines to similar levels with respect to their respective untreated cells (220% in clone 8 and 200% in clone 14, Figure 33).

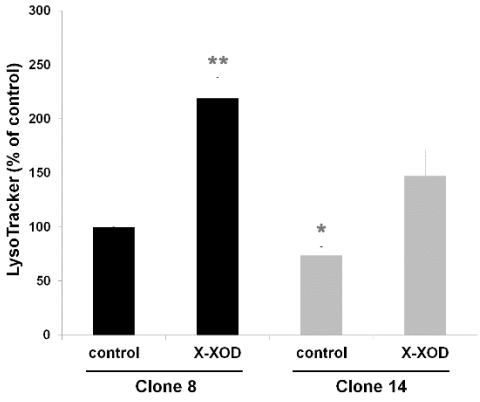

Figure 33. CTSB deficiency decrease lysosomal burden. CTSB deficient cells were treated with X-XOD. After incubation for 24 h, lysosomal quantity was analyzed by fluorimetric measurement of LysoTracker. The graph shows the mean (±SEM) fluorescence values expressed as a percentage of the control value. ∗p<0.05, ∗∗p<0.01 and ∗∗∗p<0.01 (t-test, n=3)

The immunofluorescence assay of the CTSB deficient cells with the markers specific of the lysosomal pathway, LysoTracker probe and CD63, revealed an increase of their immunoreactivity in the presence of X-XOD in CTSB deficient cells in comparison to non-deficient ones (Figure 34). The levels of lysosomal markers in immunofluorescence correlated with those obtained with Western blot analysis.

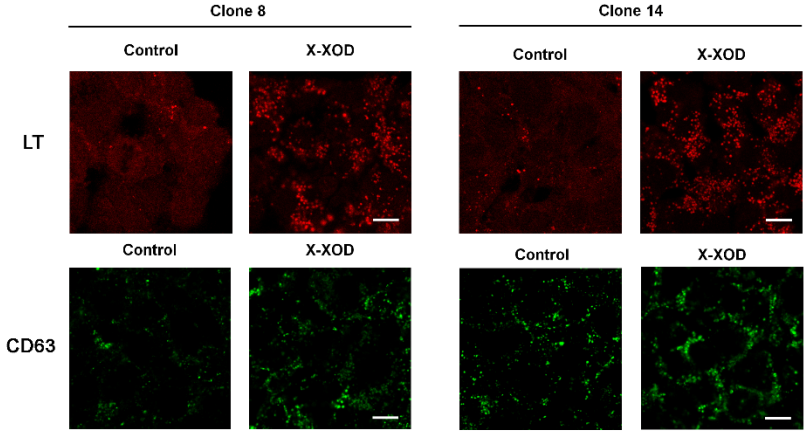

Figure 34. CTSB deficiency improves the lysosomal accumulation induced by X-XOD. CTSB deficient cells were treated with X-XOD for 24 h and were examined by confocal microscopy. The representative panel shows immunofluorescence images for LysoTracker probe and anti-CD63 antibody. Original magnification: 63×. Scale bar: 10 μm. No staining was observed when the primary antibodies were omitted.

In summary, the analysis of the lysosomal pathway indicated that, in the CTSB deficient cells, all the markers increased in the presence of OS to levels higher than those of the non-

deficient cells, with the exception of Lysotracker probe analyzed by fluorimetry. These results are, therefore, in agreement with those obtained with the CTSB inhibitor CA-074 Me.

2.2. Matrix metalloproteinase 14

Matrix metalloproteinase 14 (MMP-14 or MT1-MMP) was the first MMP to be identified as an integral membrane protein with a single transmembrane domain and a short cytoplasmic C-terminal tail. MMP-14 is expressed in a variety of tissues including brain and is inhibited by the endogenous tissue inhibitor of MMPs 2 (TIMP2). MMP-14 might be responsible, considering its potential cleaveage sites, of the APP85 that appears in our model of mild OS.

2.2.1. Pharmacological inhibition of MMP-14

There is a high structural homology between MMP catalytic domains which difficult the design of specific inhibitors of MMP-14. The modifications of other regulatory sites (e.g. linker or hemopexin domain) of the enzyme that affect the optimal conformation are becoming better tools (Sela-Passwell et al., 2010).

NSC405020 is a cell-permeable pentanylbenzamide compound that acts as an allosteric, reversible, and selective inhibitor of the collagenolytic activity of MMP-14. It specifically targets the hemopexin (PEX) domain but not the catalytic domain of MMP-14, therefore it does not inhibit directly the catalytic activity of MMP-14, but influences the enzyme activity. NSC405020 directly interacts with and binds to PEX in a vicinity of Met-328, Arg-330, Asp-376, Met-22 and Ser-470 of the druggable pocket in the full-length MMP-14 structure, which affects the conformation and flexibility of blades I to IV of the β-propeller resulting in the decrease of the PEX-dependent homodimerization of cellular MMP-14 (datasheet from APExBIO, A4051).

2.2.1.1. Effect of NSC405020 on MMP-14 enzymatic activity induced by OS

Metalloproteinase 14 (MMP-14) activity was assessed in SK-N-MC cells treated with the X-XOD free radical generating system for 24 h. To compare the effect of mild OS with the pharmacological inhibition of MMP-14, cells were treated with NSC405020 (a specific inhibitor of this protease) or with GM6001 (a broad-spectrum hydroxamate inhibitor of MMPs). MMP-14 activity was quantified using a fluorimetric assay with a substrate for

MMP-14 and MMP-11, given that we did not find a more specific tool to analyze the activity of this metalloproteinase (although herein referred to as MMP-14 activity). X-XOD treated cells showed MMP-14 activity similar to control, whereas the generic matrix metalloproteinases inhibitor GM6001, alone or in combination with OS, reduced MMP-14 activity by 15% ($p=0.0136$). In contrast, the NSC405020 inhibitor increased the MMP-14 activity by 30% ($p<0.001$), possibly due to its lack of direct action on the catalytic pocket of the enzyme and/or a compensatory activation of MMP-11 (Figure 35).

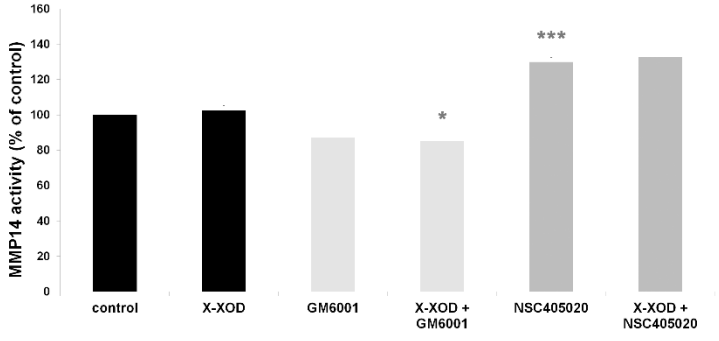

Figure 35. NSC405020 increases MMP-14 activity. SK-N-MC cells were treated with X-XOD in the presence or absence of NSC405020 or of GM6001. After incubation for 24 h, MMP-14 activity was analyzed. Proteolysis of the fluorogenic substrate MCA-PLA-C(OMeBz)-WAR(Dpa)-NH_2 was used to monitor MMP-14 activity. The graph shows the mean (±SEM) fluorescence values expressed as a percentage of the control value. ∗p<0.05, ∗∗p<0.01 and ∗∗∗p<0.01 (t-test, n=4)

To confirm that there was not any treatment-caused lessening of cell viability, MTT reduction assays were performed. Figure 36 shows a reduction of cell viability induced by NSC405020 at 24 h of culture.

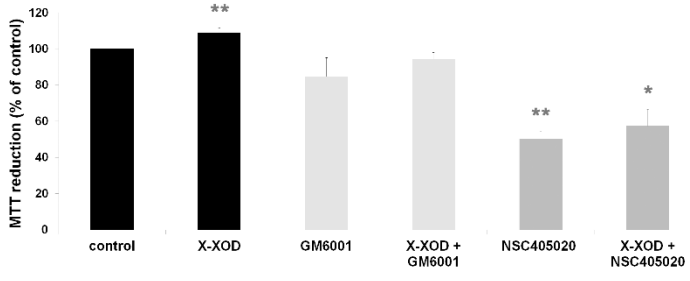

Figure 36. **Cell growth is inhibited by NSC405020.** The cells were treated with X-XOD in the presence or absence of NSC405020 or of GM6001. After incubation for 24 h, cell injury was analyzed via the MTT reduction assay. Values are expressed relative to the optical density of the control at 550 nm. Each value represents the mean of three replicates ± S.E.M. ∗p<0.05, ∗∗p<0.01 and ∗∗∗p<0.01 (t-test, n=4).

Although there was a decrease of cell viability, when cells treated with this compound were observed at the microscope there was not cell death. This phenomenon may be due to a standby of cell growth. The cells stopped growing when this compound was added to the culture media, probably due to the role of NSC405020 as an anti-tumoral drug, able to repress the growth of tumor cells through its binding to the PEX domain of MMP-14 (Remacle et al., 2012).

MMP-14 protein levels were then examined by Western blotting, using an MMP-14-specific antibody that recognizes the monomeric form (active enzyme), the dimeric form and some degraded forms of MMP-14 (Figure 37). The levels of the monomeric form, which is the active enzyme, increased significantly in cells treated with X-XOD as well as in cells treated with X-XOD and GM6001. In cells treated with X-XOD and NSC405020 the increase was impaired. The inhibitors had not significant effects on protein levels by themselves.

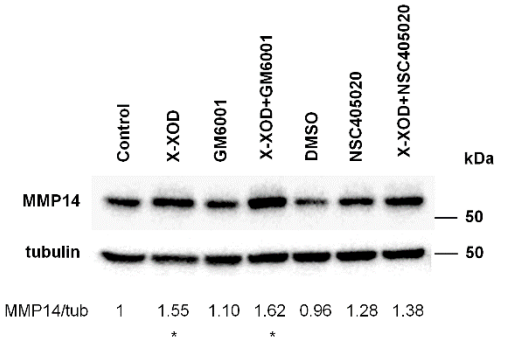

Figure 37. X-XOD increases MMP-14 levels, but when combined with NSC405020 impairs the increase. SK-N-MC cells were treated with X-XOD in the presence or absence of NSC405020 or of GM6001. After incubation for 24 h, Western blotting was performed using anti-MMP-14 antibody. α-tubulin blot is shown as loading control (lower panel). Representative experiment is shown. ∗p<0.05, ∗∗p<0.01 and ∗∗∗p<0.01 (t-test, n=4).

The immunofluorescence assay of these treated cells with an antibody specific for MMP-14 revealed a different location pattern in the presence of X-XOD, more punctated. A more condensed pattern was observed in the presence of the NSC405020 inhibitor, probably due to its role on conformation and dimerization of the MMP-14 protein. Similar effect to NSC405020 was observed in GM6001 treated cells in the presence of X-XOD, suggesting that the effect of the inhibitors on MMP-14 levels and in the intracellular location pattern is increased by the induction of OS.

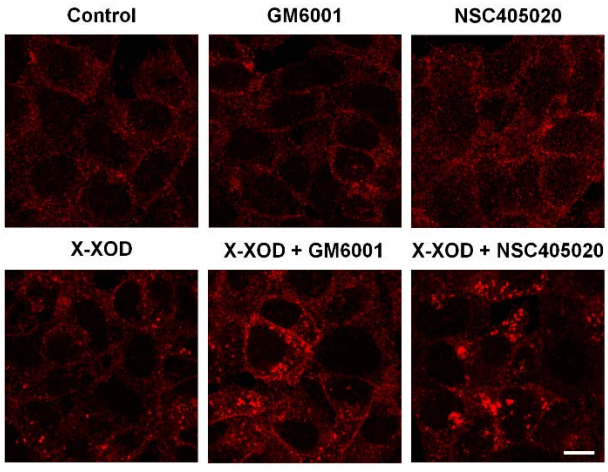

Figure 38. MMP-14 accumulates in the presence of X-XOD combined with NSC405020. SK-N-MC cells treated with X-XOD, in the presence or absence of NSC405020 or of GM6001, for 24 h were examined by confocal microscopy. The representative panel shows immunofluorescence images for anti-MMP-14 antibody. Original magnification: 63×. Scale bar: 10 µm. No staining was observed when the primary antibodies was omitted.

2.2.1.2. Effect of NSC405020 on APP processing induced by OS

Regarding the APP processing, the effect of mild OS and the inhibitor NSC405020 on APP fragments was examined in cell lysates by Western blotting using the antibody 22C11 (Figure 39). The most striking effect of the inhibitor was a marked decrease of the APP85 induced by X-XOD (as observed in Figure 13) in the SK-N-MC cells. This decrease (80%) is higher than that of APP levels in X-XOD combined with NSC405020 treated cells compared to X-XOD alone (less than 40%) indicating that it is due to an alteration in APP proteolysis more than a mere result of APP level changes. No effect on the levels of APP or APP85 was observed in cells treated with the broad-spectrum inhibitor GM6001, indicating that the inhibition of APP85 induced by OS was MMP-14 specific.

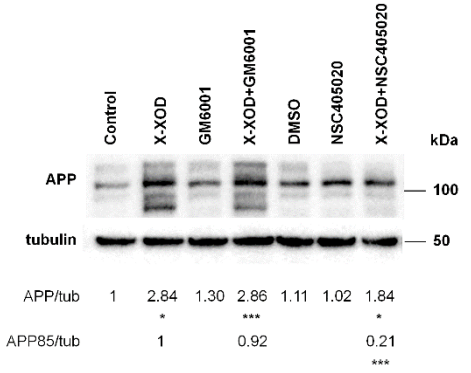

Figure 39. **NSC405020 prevents the formation of the 85kDa APP fragment induced by OS.** SK-N-MC cells were treated with X-XOD in the presence or absence of NSC405020 or of GM6001. After incubation for 24 h, cell cultures were examined by Western blot using the anti-N-terminal APP antibody (22C11). A representative experiment is shown. In the upper panel, the bands correspond to APP and APP fragments, and in the lower panel to α-tubulin. The data show the mean (± SEM) densitometry values (normalized by α-tubulin). Values for control were set at 1 in APP. Values for X-XOD were set at 1 in APP85. ∗p<0.05, ∗∗p<0.01 and ∗∗∗p<0.01 (t-test, n=4).

The immunofluorescence assay of these treated cells with antibodies specific for APP (22C11 for the N-terminal (A) and Ct for the C-terminal (B)) revealed an increase of the levels of immunofluorescence and a different pattern in the presence of X-XOD, more punctated (Figure 40). In the presence of X-XOD and the NSC405020 inhibitor a decrease of immunofluorescence with respect to X-XOD alone was observed. These correlated with the Western blot where APP band decreased and the APP85 even disappeared. No additional effect of GM6001 in signal intensity was observed in X-XOD treated cells, but a reorganization of APP seemed to appear.

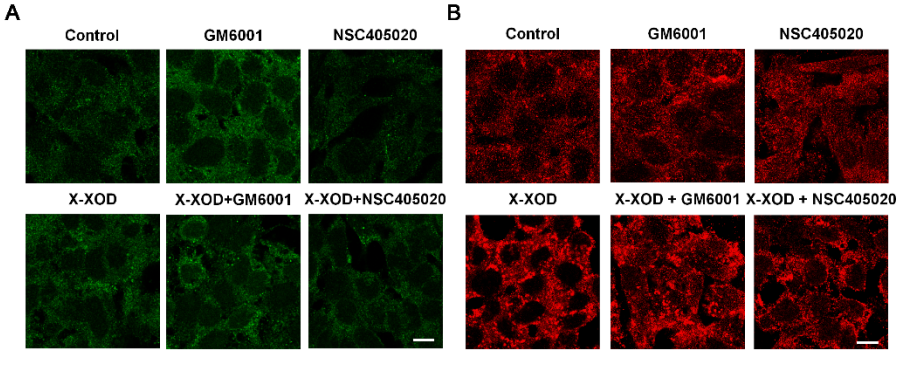

Figure 40. NSC405020 reduces the accumulation of APP induced by OS. SK-N-MC cells treated with X-XOD, in the presence or absence of NSC405020 or of GM6001, for 24 h were examined by confocal microscopy. The representative panel shows immunofluorescence images for (A) the 22C11 (green) and (B) anti-C-terminal (red) antibodies. Original magnification: 63×. Scale bar: 10 μm. No staining was observed when the primary antibodies were omitted.

Taken these results together, they support the involvement of MMP-14 in the regulation of APP metabolism by mild OS. The inhibition of MMP-14 decreases the levels of APP85, what suggest to be the η secretase in our cell model, and supports the role of MMP-14 in AD pathogenesis.

2.2.1.3. Effect of NSC405020 on lysosomal pathway changes induced by OS

The lysosomal markers were measured by Western blot using the antibodies specific for LAMP2 and CD63 (Figure 41). The lysosomal markers increased in cells treated with X-XOD, and also in X-XOD and GM6001 treated cells. In contrast, cells treated with X-XOD and NSC405020 decreased its levels of lysosomal proteins compared to X-XOD alone. These results suggest that MMP-14 has a role in the lysosomal pathway. The inhibition of MMP-14 decreased the lysosomal markers induced by OS, parallely to the results observed with these treatments on the APP85.

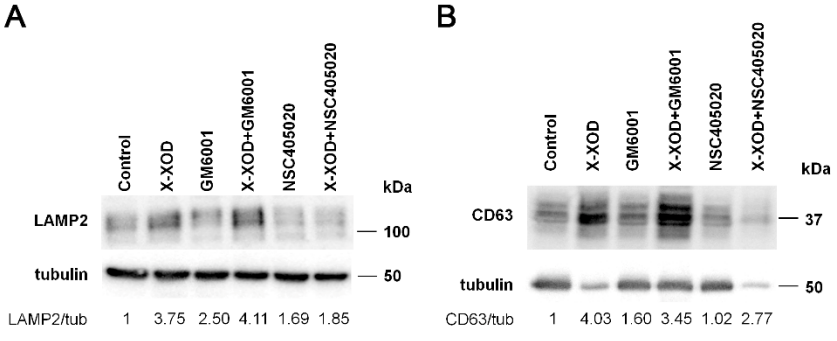

Figure 41. **NSC405020 diminishes the lysosomal markers levels increase induced by OS.** SK-N-MC cells were treated with X-XOD in the presence or absence of NSC405020 or of GM6001. After incubation for 24 h, cell cultures were examined by Western blot using the anti-LAMP2 and anti-CD63. α-tubulin blot is shown as loading control. A representative experiment is shown. The data show the mean (± SEM) densitometry values (normalized by α-tubulin). (n=4).

The lysosomal burden was measured using the acidotropic probe LysoTracker®. As shown in Figure 42, X-XOD treated cells increased significantly the LysoTracker fluorescence (increased by 183%, p=0.0014). Although the increase in cells treated with X-XOD and NSC405020 in comparison to control cells was still significant (increased by 57%, p<0.0001), its level decreased significantly in comparison to X-XOD alone (p=0.0087), impairing the increase of the lysosomal burden. GM6001 and NSC405020 had no significant effect on the lysosomal burden.

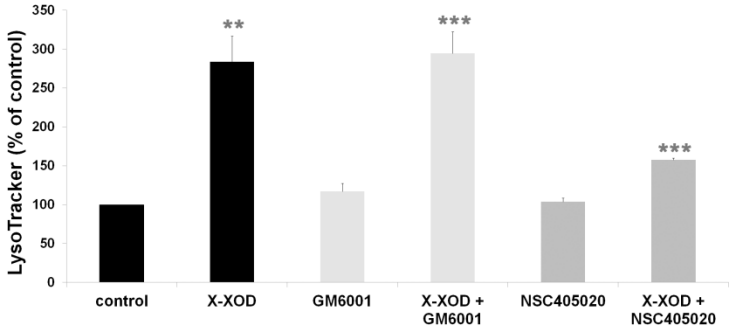

Figure 42. NSC405020 impairs the increase of lysosomal burden induced by X-XOD. SK-N-MC cells were treated with X-XOD in the presence or absence of NSC405020 or of GM6001. After incubation for 24 h, lysosomal quantity was analyzed by fluorimetric measurement of LysoTracker. The graph shows the mean (±SEM) fluorescence values expressed as a percentage of the control value. ∗p<0.05, ∗∗p<0.01 and ∗∗∗p<0.01 (t-test, n=4).

To analyze the intracellular location pattern of the endolysosomal markers, immunofluorescence assays were performed. As it is observed in Figure 43, all the markers increased in the presence of OS, but this increase was impaired in cells treated with X-XOD in combination with NSC405020. No effect was observed in the presence of the GM6001 inhibitor. These results correlate with the ones obtained by Western blot (Figure 41) and with the fluorimetric quantification of LysoTracker, indicating that MMP-14 inhibition avoid the increment of lysosomal burden induced by OS.

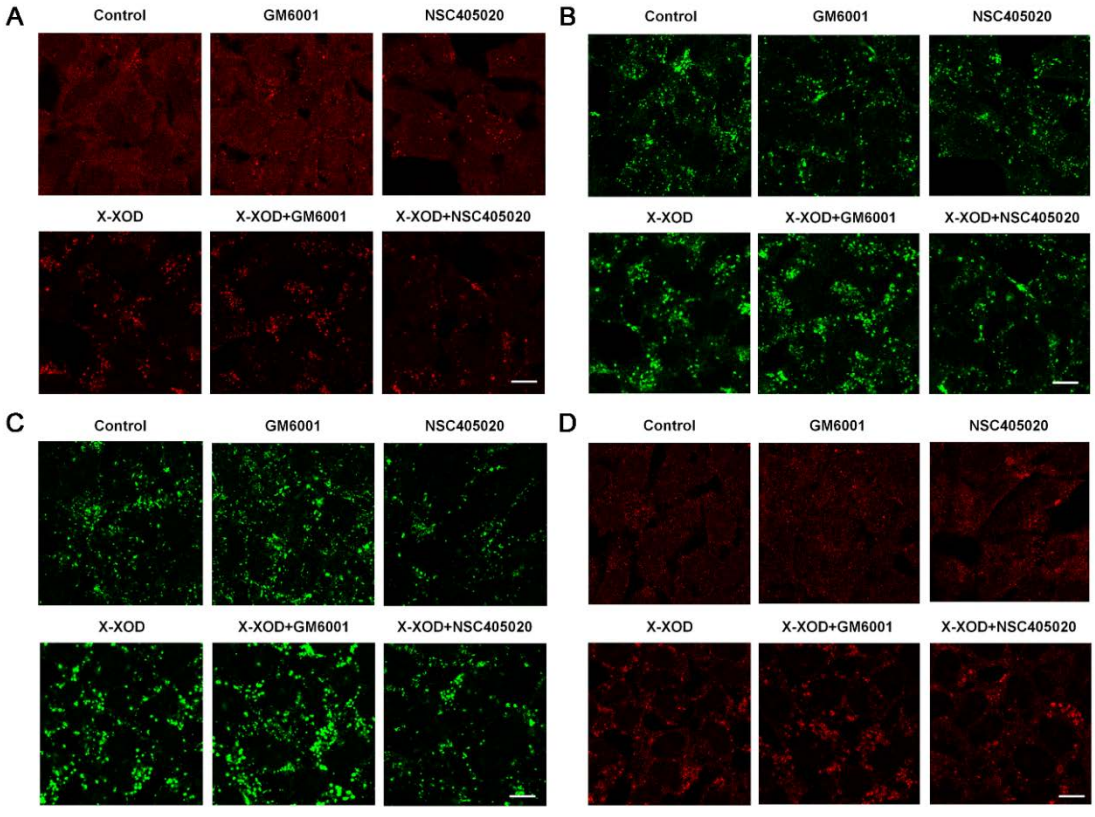

Figure 43. NSC405020 impairs the accumulation of lysosomes induced by X-XOD. SK-N-MC cells treated with X-XOD, in the presence or absence of NSC405020 or of GM6001, for 24 h were examined by confocal microscopy. The representative panel shows immunofluorescence images for (A) LysoTracker, (B) anti-LAMP2, (C) anti-CD63 and (D) anti-Rab7 antibodies. Original magnification: 63×. Scale bar: 10 μm. No staining was observed when the primary antibodies were omitted.

Taken all the above results together, MMP-14 seems to be part of the mechanism mediating the connection between lysosomal alterations and APP proteolysis, specially the disappearance of the APP85, that mild oxidative stress induces in our SK-M-NC neuroblastoma cell model.

2.2.2. Gene silencing of MMP-14

To study the role of MMP-14 on APP processing and on the lysosomal dysfunction induced by OS our next step was to generate a suitable cell model. To achieve this, SK-N-MC cells were stably transfected with a shRNA specific for MMP-14. Several MMP-14 deficient clones were selected, expanded and analyzed by Western blot. The clone with lower expression (clone 3) was selected for the following studies. Moreover, cells were transfected with a scrambled shRNA (clone 8).

2.2.2.1. Characterization of MMP-14 deficient cell line – MMP-14 enzymatic activity

MMP-14 activity was quantified as described before (chapter 2.2.1.1) The deficient clone 3 showed a significant reduction in comparison to non-deficient clone 8 cells (by up to 28%, p=0.00157) (Figure 44A). The activity did not decrease as much as expected probably due to the substrate, that is processed by MMP-11 and MMP-14, as previously mentioned. However, the Western blot showed a significant decrease of MMP-14 levels (Figure 44B), approximately a 75% reduction, confirming the silencing of MMP-14. X-XOD treatment did not produce significant changes, although a trend for an increase in the protein levels was observed in both cell lines, in accordance with the effects observed in the SK-N-MC parental cell line. Determination of the relative MMP-14 mRNA levels by RT-qPCR confirmed the results obtained by Western blot as shown in Figure 44C. Moreover, mRNA levels of APP were also measured to take into account the possible changes in APP basal levels in the studies of APP processing (Figure 44D). There was no changes on mRNA levels of APP in MMP-14 deficient cells compared to control clone 8.

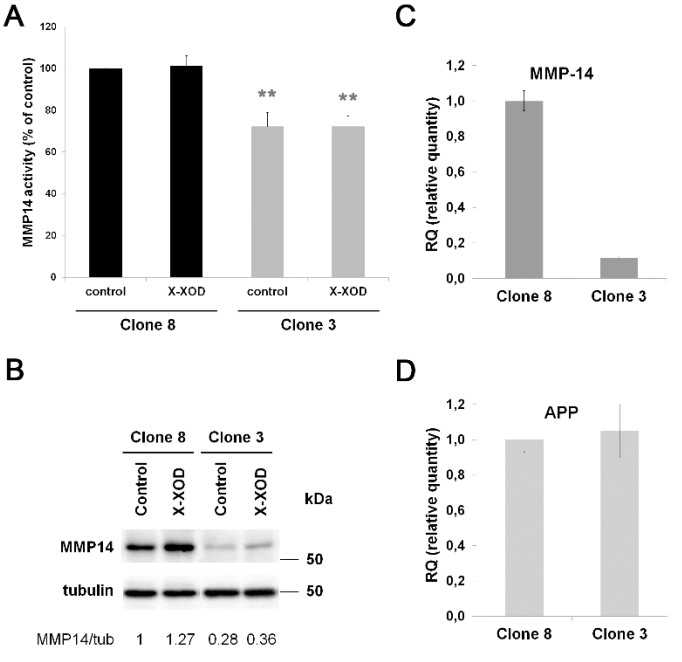

Figure 44. Characterization of MMP-14 deficient cells. (A) Analysis of the clones by MMP-14 activity, (B) Analysis of the clones by Western blot with an anti-MMP-14 antibody, (C) Analysis of the clones by RT-qPCR of MMP-14 and (D) APP. SK-N-MC deficient cells were treated with X-XOD. After incubation for 24 h, MMP-14 activity or expression was analyzed. A.

Proteolysis of the fluorogenic substrate MCA-PLA-C(OMeBz)-WAR(Dpa)-NH_2 was used to monitor MMP-14 activity. The graph shows the mean (±SEM) fluorescence values expressed as a percentage of the control value. ∗p<0.05, ∗∗p<0.01 and ∗∗∗p<0.01 (t-test, n=4). B. Western blot analysis with anti-MMP-14 antibody. α-tubulin blot is shown as loading control. The data show the mean (± SEM) densitometry values (normalized by α-tubulin). Values for control were set at 1.

2.2.2.2. Characterization of APP proteolytic fragments induced by OS in MMP-14 deficient cells

Regarding the APP processing, the effect of mild OS in deficient cells was examined in cell lysates by Western blotting using the antibody 22C11 (Figure 45). We observed a significant decrease of the APP85 that appears in the presence of X-XOD in non-deficient cells.

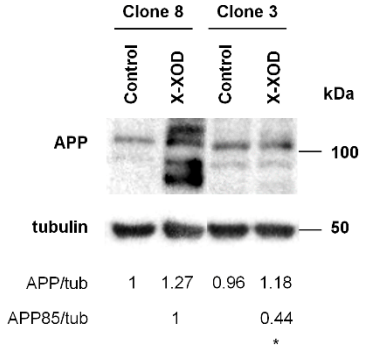

Figure 45. **MMP-14 deficiency precludes the formation of an X-XOD induced APP85.** MMP-14 deficient cells were treated with X-XOD. After incubation for 24 h, cell cultures were examined by Western blot using the anti-N-terminal APP antibody (22C11). α-tubulin blot is shown as loading control. A representative experiment is shown. In the upper panel, the bands correspond to APP and APP fragments, and in the lower panel to α-tubulin. The data show the mean (± SEM) densitometry values (normalized by α-tubulin). Values for control were set at 1 in APP. Values for X-XOD were set at 1 in APP85. ∗p<0.05, ∗∗p<0.01 and ∗∗∗p<0.01 (t-test, n=4).

As shown in Figure 46, the immunofluorescence assay of these treated cells with an antibody specific for the N-terminal region of APP (22C11) revealed an increase of the levels of APP and a different pattern in the presence of X-XOD, and apparently no differences between deficient and non-deficient cells.

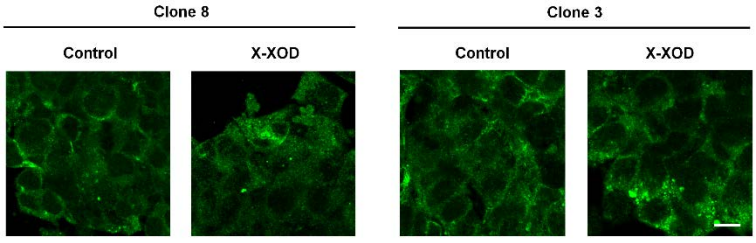

Figure 46. MMP-14 deficiency does not modify APP accumulation induced by X-XOD. MMP-14 deficient cells were treated with X-XOD for 24 h were examined by confocal microscopy. The representative panel shows immunofluorescence images for 22C11 (anti-N-terminal of APP) antibody. Original magnification: 63×. Scale bar: 10 µm. No staining was observed when the primary antibodies was omitted.

2.2.2.3. Study of the lysosomal pathway changes in MMP-14 deficient cells

Representative lysosomal markers were measured by Western blot using the specific antibodies for LAMP2 and CD63. X-XOD increased the levels of both markers, but to a lesser extent in the MMP-14 deficient cells.

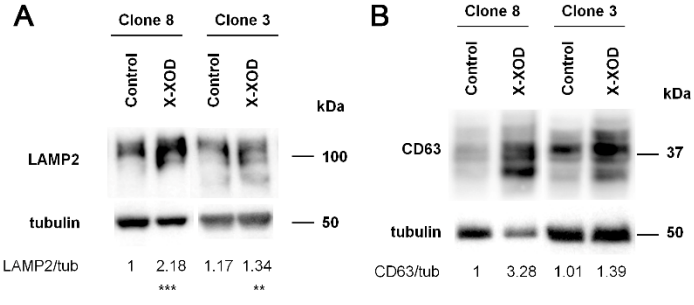

Figure 47. **MMP-14 deficiency impairs the increase of lysosomal markers induced by OS.** MMP-14 deficient cells were treated with X-XOD in the presence or absence of NSC405020. After incubation for 24 h, cell cultures were examined by Western blot using the anti-LAMP2 (A) and anti-CD63 (B) antibodies. α-tubulin blot is shown as loading control. A representative experiment is shown. The data show the mean (± SEM) densitometry values (normalized by α-tubulin). (n=4).

The lysosomal burden was measured as described before. Figure 48 shows that LysoTracker fluorescence of untreated deficient cells decreased significantly in comparison to untreated non-deficient cells (by up to 45%, $p=0.011$). There is also a significant decrease in X-XOD deficient treated cells in comparison to X-XOD non-deficient treated cells (by up to 57%, $p<0.001$), although the relative LysoTracker fluorescence in X-XOD treated compared to untreated cells was similar in both deficient and non-deficient cells (between 2 - 2.2 fold) . MMP-14 deficiency impairs the increase of lysosomal markers induced by OS.

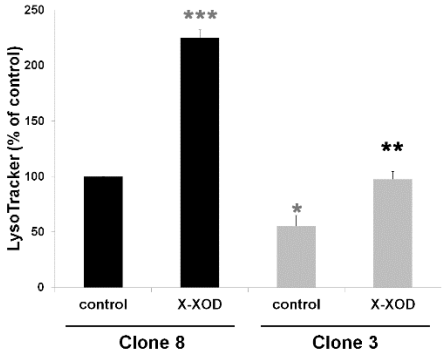

Figure 48. MMP-14 deficiency shows a diminution of the lysosomal burden. MMP-14 deficient cells were treated with X-XOD. After incubation for 24 h, lysosomal quantity was analyzed by fluorimetric measurement of LysoTracker. The graph shows the mean (±SEM) fluorescence values expressed as a percentage of the control value. ∗p<0.05, ∗∗p<0.01 and ∗∗∗p<0.01 (t-test, n=4).

In summary, the analysis of stable silenced cells reinforces the results obtained with NSC405020 inhibitor, indicating that MMP-14 is part of the lysosomal system and is involved in the proteolysis of APP, specifically in the generation of APP85 induced by OS.

3. Effect of Herpes Simplex virus 1 in the APP processing and in the lysosomal pathway changes induced by OS

Growing evidence support that chronic or latent infection of the CNS might be implicated in the etiology of AD (Miklossy, 2011). The idea of the so-called pathogen/infectious hypothesis came up in the 1960s and has gained support since then. First evidence came from the fact that several microbes can access the CNS, remain there in latent form by evading the host immune response, and that they are highly prevalent in the AD brain (Harris et al., 2015). The hypothesis states that in combination with genetic risk factors, these pathogens participate in the generation of the Aβ peptide, tau hyperphosphorylation and inflammation. Of all studied pathogens in relation with AD, HSV-1 has emerged as a major factor in the etiology of the disease (Itzhaki, 2014 and 2016). Moreover, HSV-1 is a ubiquitous neurotropic virus, with a worldwide seroprevalence of more than 80% in adults. It usually enters orofacial mucosal epithelia cells where productive infection takes place. From there, the virus can spread to neurons of the trigeminal ganglia innervating the epithelium where it can establish lifelong latency (Kennedy et al., 2015; Nicoll et al., 2012). After primary infection, the virus can replicate or stay latent in the neuron cell body until reactivation by diverse stimuli, like stress and immunosuppression associated with aging.

Our group has reported that OS modulates the lysosomal pathway in infected cells and that HSV-1 is able to induce the accumulation of Aβ. When OS is induced in infected neurons, the alterations in the lysosomal pathway and in amyloidogenesis are mutually potentiated (Kristen 2018).

To study the role of HSV-1 in relation with the candidate genes studied in the previous chapters, all the experiments were repeated in infected cells. Previously, we assess the multiplicity of infection (moi) at 24 h needed for infecting the majority of the cells without a massive cell lose. Immunofluorescence assay was performed with an HSV-1 specific antibody in cells infected at a moi ranging from 0.1 to 1 pfu/cell (Figure 49). Immunofluorescence analysis confirmed that almost all cells were infected at the maximum viral dose for that time of infection, and that X-XOD decreased the infection, as had been previously described by our group (Santana et al., 2013). So, a moi of 1 pfu/cell will be used for all the experiments.

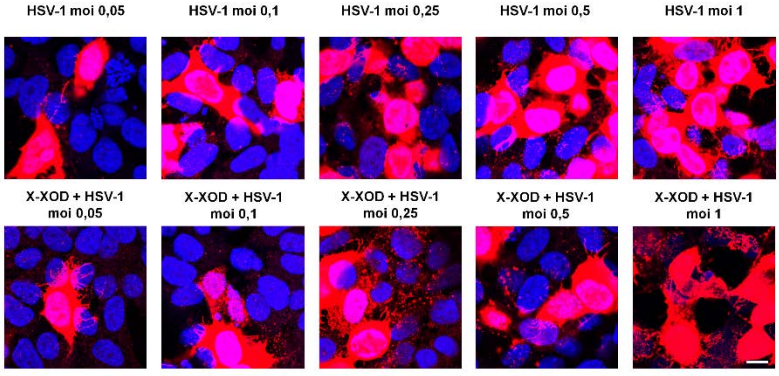

Figure 49. Dose curve of HSV-1 infection. SK-N-MC cells were infected with HSV-1 at different moi, from 0,05 to 1 pfu/cell, and treated with X-XOD. After incubation for 24 h were examined by confocal microscopy. The panel shows immunofluorescence images for the anti-HSV-1 antibody. Original magnification: 63×. Scale bar: 10 μm. No staining was observed when the primary antibodies were omitted.

3.1. Involvement of Cathepsin B

To study the interplay between OS and the virus to modulate APP processing and the lysosomal pathway markers, as well as the potential role of CTSB in these events, cells were studied as described in previous chapters (2.1.1 and 2.1.2) but adding HSV-1 to the treatments. To investigate the possible participation of CTSB in the results obtained, SK-N-MC cells treated with the specific inhibitor and the stable cell line silenced for CTSB (Clone 14), along with the control cell line (Clone 8) were examined. Because the studied effects were almost identical in the cells treated with the inhibitor CA-074 Me or genetically silenced for CTSB, we present the experiments performed with the inhibitor here and the results of silenced cells are attached as Annex I to the thesis.

3.1.1. Effect of HSV-1 on CTSB enzymatic activity

The effect of HSV-1 alone or in combination with X-XOD was analyzed in SK-N-MC cells in the absence or presence of the CTSB inhibitor CA-074 Me. CTSB activity was quantified using the same fluorometric assay, used in previous chapters. SK-N-MC cells infected with HSV-1 displayed a reduction of CTSB activity in infected cells that was similar in the absence (23%; p=0.016) or presence of OS (23%; p=0.018) compared to their uninfected partners (control and X-XOD treated cells respectively) (Figure 50). The CTSB inhibitor, as

previously described, decreased the activity by up to 96% ($p<0.001$) consequently the effect of the infection was undetected in the cells treated with the inhibitor.

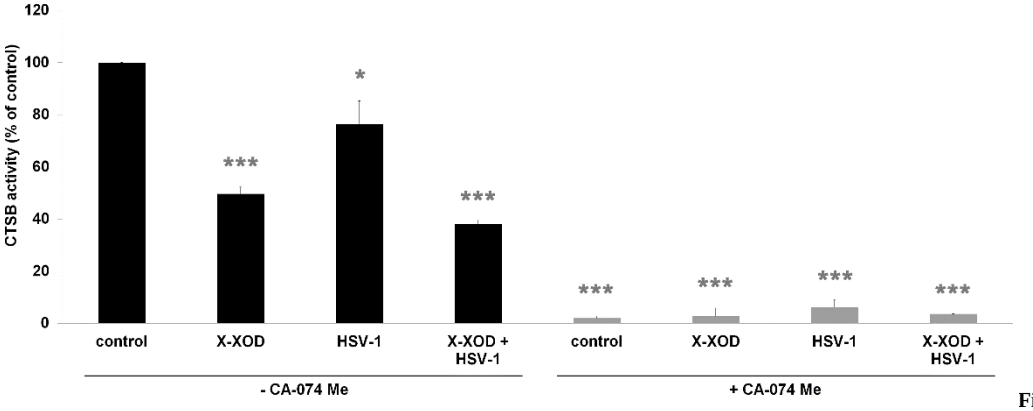

Figure 50. HSV-1 reduces CTSB activity. SK-N-MC cells were infected with HSV-1 and treated with X-XOD in the presence (grey) or absence (black) of CA-074 Me. After incubation for 24 h, CTSB activity was analyzed. Proteolysis of the fluorogenic substrate z-RR-AMC was used to monitor CTSB activity. The graph shows the mean (±SEM) fluorescence values expressed as a percentage of the control value. ∗p<0.05, ∗∗p<0.01 and ∗∗∗p<0.01 (t-test, n=4).

In summary, the effect of HSV-1 infection was a reduction of CTSB activity. Since HSV-1 is known to inhibit the transcription of numerous cellular genes, CTSB mRNA levels were measured by RT-qPCR to determine if the changes in activity were attributable to transcriptional changes. As it is observed in Figure 51, the levels of CTSB mRNA do not change in the presence or absence of HSV-1, therefore there were no transcriptional effects responsible for the results obtained by Western blot.

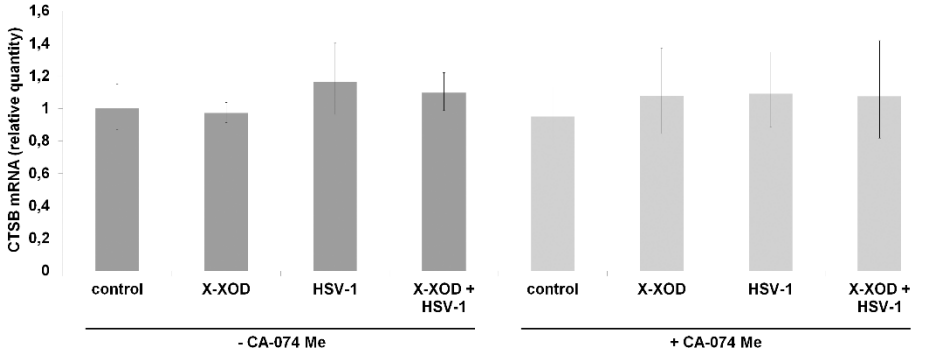

Figure 51. HSV-1 does not change CTSB mRNA levels. SK-N-MC cells were infected with HSV-1 in the presence or absence of X-XOD and the inhibitor CA-074 Me for 24 hours. The mRNA transcribed from CTSB was quantified by RT-qPCR (as described in Methods) and normalized in terms of the GAPDH RNA levels. The relative quantity with respect to control cultures was determined by the ΔΔCt method using the RQ manager 1.2.1. software (Applied Biosystems). Error bars represent the 95% confidence interval.

3.1.2. Effect of HSV-1 on APP processing

The effect of HSV-1 infection on the levels of APP and amyloid oligomers induced by mild OS were studied in the absence or presence of the CTSB inhibitor by Western blotting, using the 22C11 and the A11 antibodies. Figure 52 shows that the levels of APP protein slightly decreased by HSV-1 infection in comparison to not infected cells. This inhibition was more evident in cells treated with X-XOD or CA-074 Me. Interestingly, in the presence of the inhibitor CA-074 Me the amyloid oligomers increased significantly in HSV-1 infected cells whereas APP was decreased, suggesting that CTSB modulates APP metabolism at several levels and the possible interaction od CTSB and HSV-1.

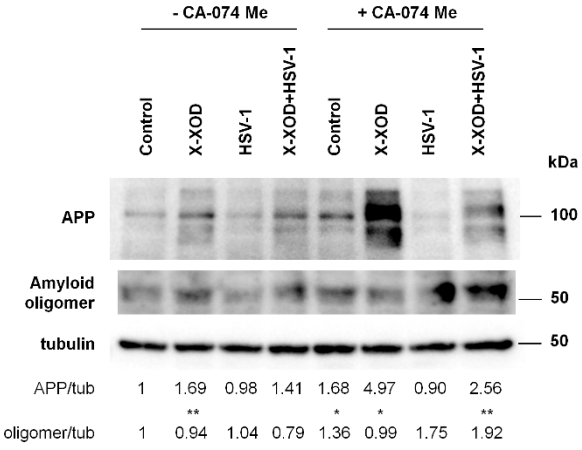

Figure 52. **HSV-1 promotes the accumulation of amyloid oligomers induced by CTSB inhibition.** SK-N-MC cells were infected with HSV-1 and treated with X-XOD. After incubation for 24 h, cell cultures were examined by Western blot using the anti-N-terminal APP antibody (22C11). Tubulin blot is shown as loading control. A representative experiment is shown. In the upper panel, the bands correspond to APP and APP fragments, and in the lower panel to α-tubulin. The data show the mean (± SEM) densitometry values (normalized by α-tubulin). Values for control were set at 1. ∗p<0.05, ∗∗p<0.01 and ∗∗∗p<0.01 (t-test, n=4).

APP mRNA levels were measured by RT-qPCR to assess if the results obtained by Western blot were due to transcriptional changes. As it is observed in Figure 53, the levels of APP mRNA do not change in the presence or absence of HSV-1, therefore there were no transcriptional effects responsible for the results obtained by Western blot.

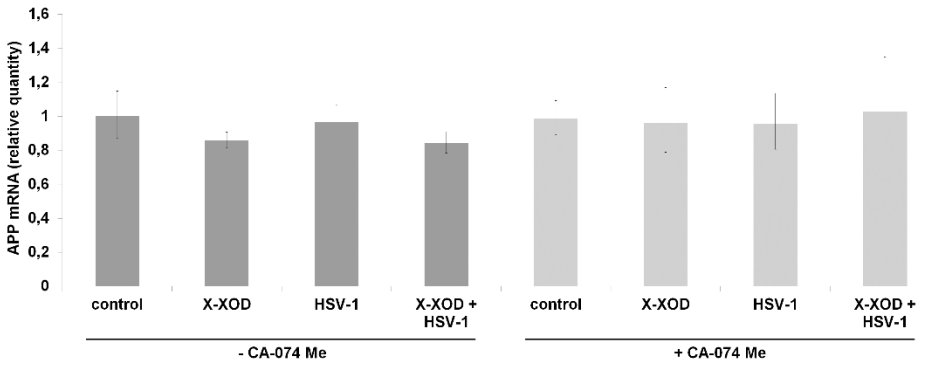

Figure 53. HSV-1 does not change the levels of APP mRNA. SK-N-MC cells were infected with HSV-1 in the presence or absence of X-XOD and the inhibitor CA-074 Me for 24 hours. The mRNA transcribed from APP was quantified by RT-qPCR (as described in Methods) and normalized in terms of the GAPDH RNA levels. The relative quantity with respect to control cultures was determined by the ΔΔCt method using the RQ manager 1.2.1. software (Applied Biosystems). Error bars represent the 95% confidence interval.

An immunofluorescence assay was performed to analyze the effect of these treatments in HSV-1 infected cells on the subcellular distribution of APP (Figure 54). HSV-1 reorganizes the location of APP in the cell, condensing the fluorescence at some brilliant points. This condensation could be the reason why the levels of immunofluorescence not always seemed to decrease in the presence of HSV-1 (lower panel) as in the results obtained by Western blot (Figure 53). This reorganization is similar in all the treatments, suggesting no interactions with HSV-1.

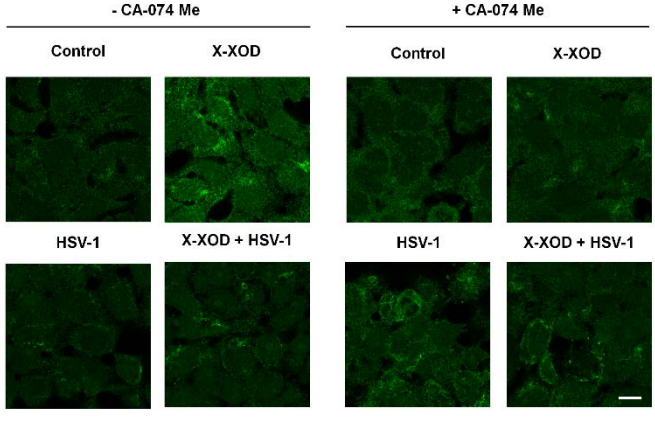

Figure 54. HSV-1 reorganizes the intracellular location of APP. SK-N-MC cells were infected with HSV-1 and treated with X-XOD in the presence or absence of CA-074 Me. After incubation for 24 h were examined by confocal microscopy. The representative panel shows immunofluorescence images for the 22C11 (anti N-terminal) antibody. Original magnification: 63×. Scale bar: 10 μm. No staining was observed when the primary antibodies were omitted.

3.1.3. Effect of HSV-1 on the lysosomal pathway changes

To analyze the lysosomal pathway some representative markers were measured by Western blot using the antibodies specific for LAMP2 and CD63 (Figure 55). A decrease of lysosomal proteins in the infected cells was observed in comparison to non-infected. In the presence of X-XOD the reduction is even higher suggesting that the HSV-1 infection reduces the number of vesicles of the lysosomal pathway.

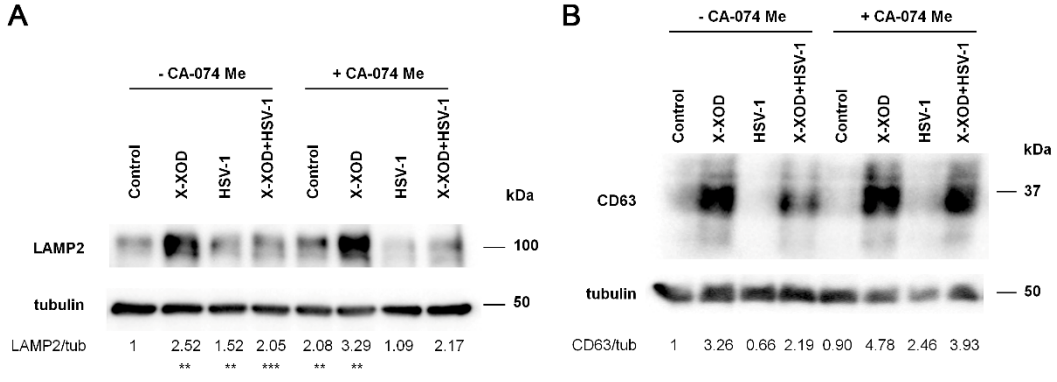

Figure 55. **HSV-1 impairs the increase of the lysosomal markers induced by OS.** SK-N-MC were infected with HSV-1 cells and treated with X-XOD in the presence or absence of CA-074 Me. After incubation for 24 h, cell cultures were examined by Western blot using the anti-LAMP2 and anti-CD63 antibodies. Tubulin blot is shown as loading control. A representative experiment is shown. The data show the mean (± SEM) densitometry values normalized by α-tubulin (n=4).

The lysosomal burden was measured using the acidotropic probe LysoTracker®. In the fluorometric assay the cells without the inhibitor (black) and the cells treated with the inhibitor CA-074 Me (grey) did not change the burden of acidic vesicles by the effect of HSV-1 infection (Figure 56). The effect of CA-074 inhibitor without infection is higher than its control, as it had been described above (Figure 25). According to this assay, this result is in disagreement with the Western Blot data of LAMP2 and CD63, probably due to their different targets; LAMP2 and CD63 are antibodies against lysosomal membrane and Lysotracker is a probe with affinity for acid pH.

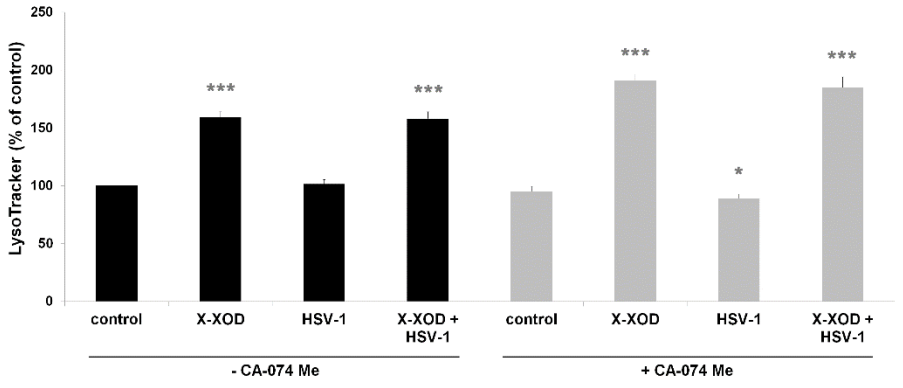

Figure 56. HSV-1 does not change the lysosomal burden. SK-N-MC infected with HSV-1 cells were treated with X-XOD in the presence (grey) or absence (black) of CA-074 Me. After incubation for 24 h, lysosomal quantity was analyzed by fluorometric measurement of LysoTracker. The graph shows the mean (±SEM) fluorescence values expressed as a percentage of the control value. ∗p<0.05, ∗∗p<0.01 and ∗∗∗p<0.01 (t-test, n=4)

To analyze the intracellular location pattern of the endolysosomal markers, immunofluorescence assays were performed. As it is observed in Figure 57 (A-LTR, B-LAMP2 and C-CD63) there is a fluorescence decrease of the lysosomal markers in cells infected (lower panel) in comparison to not infected (higher panel), especially in LAMP2 and CD63 immunofluorescence. These results correlate with the ones obtained by Western blot.

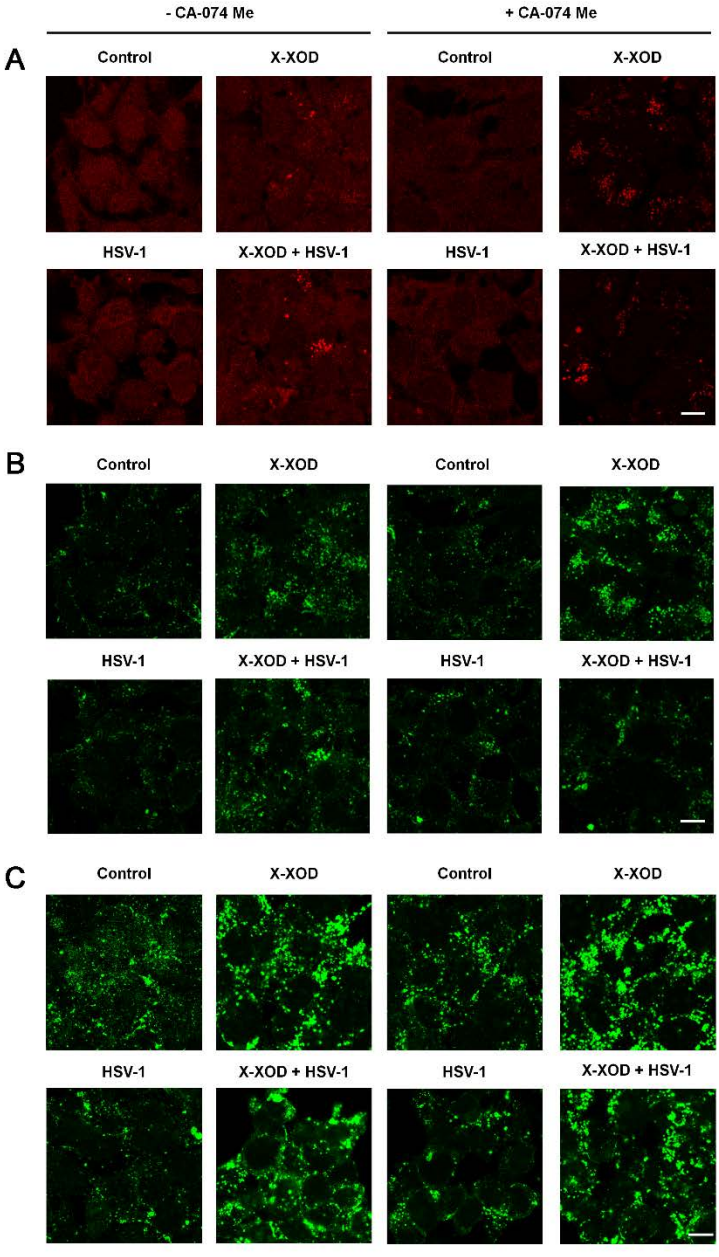

Figure 57. HSV-1 impairs the accumulation of lysosomes induced by OS. SK-N-MC cells infected with HSV-1 were treated with X-XOD, in the presence or absence of CA-074 Me, for 24 h and were examined by confocal microscopy. The representative panel shows immunofluorescence images for (A) LysoTracker probe, (B) anti-LAMP2 and (C) anti-CD63 antibodies. Original magnification: 63×. Scale bar: 10 μm. No staining was observed when the primary antibodies were omitted.

Taken the results together, we conclude that the HSV-1 infection in the modulation of CTSB has effect on APP processing at different stages, although the APP levels are reduced,

surprisingly, there is an increase of the Aβ aggregation. Regarding the lysosomal pathway, HSV-1 infection reduces CTSB activity and lysosomal markers but does not produce changes in the lysosomal burden.

3.2. Involvement of Matrix metalloproteinase 14

To study the potential role of MMP-14 in the interplay between OS and the virus to modulate APP processing and the lysosomal pathway markers, cells were studied as described in previous chapters (2.2.1 and 2.2.2) but adding HSV-1 to the treatments. To investigate the possible participation of MMP-14 in the results obtained, SK-N-MC cells treated with the specific inhibitor and the stable cell line silenced for MMP-14 (Clone 3), together with the control cell line (Clone 8) were examined. Because the studied effects were almost identical in the cells treated with the inhibitor or genetically silenced, we present the experiments performed with the inhibitor here and the results of MMP-14 silenced cells are added as an Annex I.

3.2.1. Effect of HSV-1 on MMP-14 enzyme levels

MMP-14 levels were analyzed by Western blotting, using the MMP-14-specific antibody (Figure 58). The levels of the monomeric form (active) showed a trend to be decreased in infected cells, although differences were small and not significant.

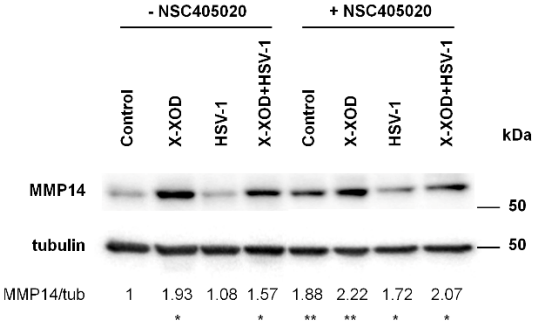

Figure 58. **HSV-1 impairs the increase of MMP-14 levels induced by OS.** SK-N-MC cells were infected with HSV-1 and treated with X-XOD in the presence or absence of NSC405020. After incubation for 24 h, cell cultures were examined by Western blot using the anti-N-terminal APP antibody (22C11). Tubulin blot is shown as loading control. A representative experiment is shown. In the upper panel, the bands correspond to APP and APP fragments, and in the lower panel to α-tubulin. The data show the mean (± SEM) densitometry values (normalized by α-tubulin). Values for control were set at 1. ∗p<0.05, ∗∗p<0.01 and ∗∗∗p<0.01 (t-test, n=4).

MMP-14 mRNA levels were analyzed by RT-qPCR to observe if the results obtained by Western blot were attributable to transcriptional changes (Figure 59). The inhibitor NSC405020 produced transcriptional changes that increased in the presence of X-XOD, therefore the results obtained by Western blot with the inhibitor NSC405020 may be due to these transcriptional changes. In contrast, in the absence of the inhibitor there was no transcriptional changes, neither HSV-1 had effect on mRNA levels.

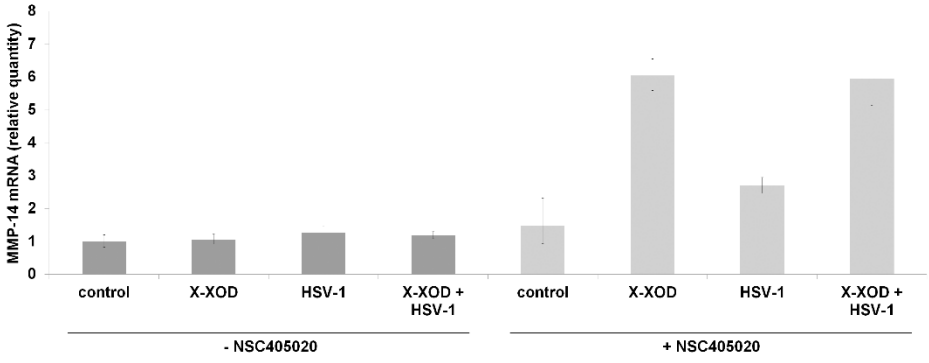

Figure 59. HSV-1 does not affect the levels of MMP-14 mRNA. SK-N-MC cells were infected with HSV-1 in the presence or absence of X-XOD and the inhibitor NSC405020 for 24 hours. The mRNA transcribed from MMP-14 was quantified by RT-qPCR, as described in Methods, and normalized in terms of the GAPDH RNA levels. The relative quantity with respect to control cultures was determined by the ΔΔCt method using the RQ manager 1.2.1. software (Applied Biosystems). Error bars represent the 95% confidence interval.

In contrast with the previous data, immunofluorescence assay with an antibody specific for MMP-14 revealed an apparent increase of immunofluorescence levels, even higher in cells infected in the presence of X-XOD, with a more condensed pattern (Figure 60). In the presence of the inhibitor NSC405020 this increase is lower, especially in infected cells treated with X-XOD, in contrast to the results obtained in MMP-14 Western blot. The clear change in MMP-14 pattern induced by the virus, and the inhibition of this change in the presence of NSC4050250 make us suspect the existence of direct interactions between MMP-14 and HSV-1.

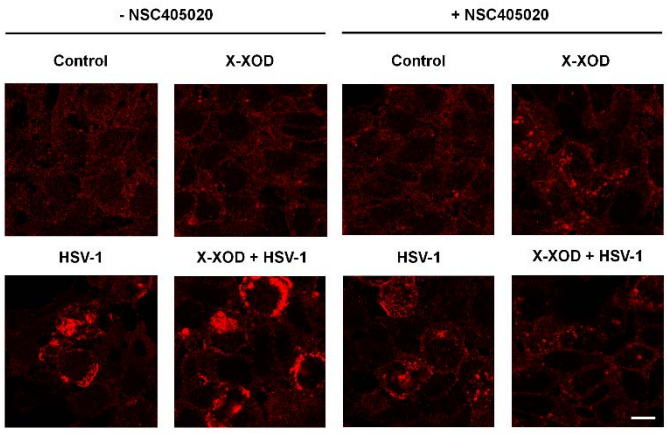

Figure 60. HSV-1 induces the intracellular accumulation of MMP-14 that decreases with NSC405020. SK-N-MC infected cells were treated with X-XOD, in the presence or absence of NSC405020, for 24 h and were examined by confocal microscopy. The representative panel shows immunofluorescence images for anti-MMP-14 antibody. Original magnification: 63×. Scale bar: 10 μm. No staining was observed when the primary antibodies was omitted.

3.2.2. Effect of HSV-1 on APP processing

Regarding the APP processing, the effect of the HSV-1 infection on APP proteolysis was examined in cell lysates by Western blotting using the antibody 22C11 (Figure 61). We observed in infected cells a decrease of APP together with a significant decrease of the APP85 that appears in the presence of X-XOD. This decrease was higher in the presence of the inhibitor NSC405020, suggesting again a possible interaction between MMP-14 and HSV-1.

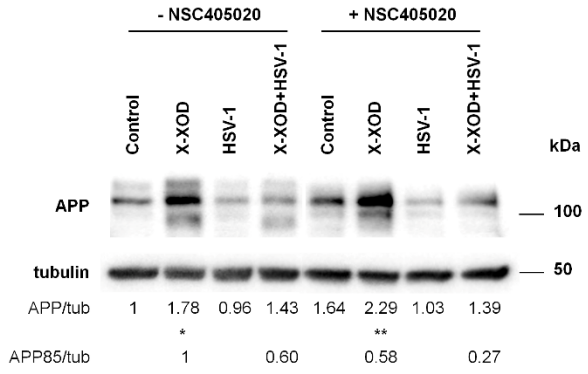

Figure 61. **HSV-1 decreases the levels of APP and APP85 induced by OS.** SK-N-MC cells were infected with HSV-1 and treated with X-XOD in the presence or absence of NSC405020. After incubation for 24 h, cell cultures were examined by Western blot using the anti-N-terminal APP antibody (22C11). A representative experiment is shown. In the upper panel, the bands correspond to APP and APP fragments, and in the lower panel to α-tubulin. The data show the mean (± SEM) densitometry values (normalized by α-tubulin). Values for control were set at 1. ∗p<0.05, ∗∗p<0.01 and ∗∗∗p<0.01 (t-test, n=4).

APP mRNA levels by RT-qPCR were analyzed to observe if the results obtained by Western blot were due or not to transcriptional changes (Figure 62). The inhibitor NSC405020 increased the mRNA levels of APP in the presence of X-XOD but no changes were observed in infected cells. The effect observed in APP processing by MMP-14 was not due to transcriptional changes.

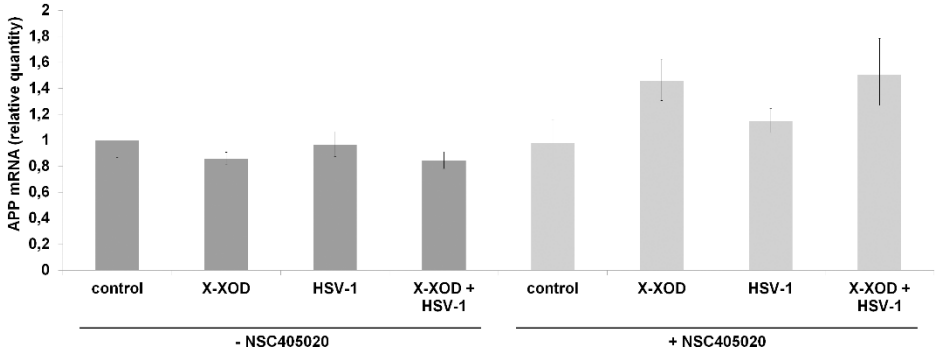

Figure 62. HSV-1 does not change the APP mRNA levels. SK-N-MC cells were infected with HSV-1 in the presence or absence of X-XOD and the inhibitor NSC405020 for 24 hours. The mRNA transcribed from each gene APP was quantified by RT-qPCR, as described in Methods, and normalized in terms of the GAPDH RNA levels. The relative quantity with respect to control cultures was determined by the ΔΔCt method using the RQ manager 1.2.1. software (Applied Biosystems). Error bars represent the 95% confidence interval.

An immunofluorescence assay was performed with 22C11, the antibody specific for the N-terminal region of APP, to observe the intracellular pattern of APP in these HSV-1 infected cells (Figure 63 - lower panel). HSV-1 reorganizes the location of APP in the cell, condensing at some points. This might be the reason why the levels of immunofluorescence in NSC405020 treated cells did not seem to decrease in the presence of HSV-1 (lower panel) as in the results obtained by Western blot.

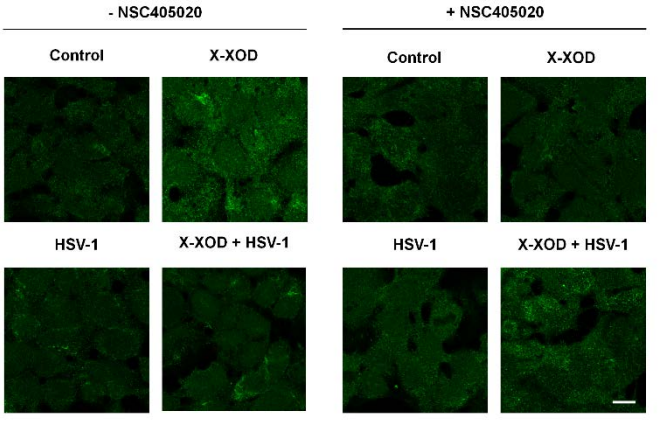

Figure 63. HSV-1 accumulates intracellular APP. SK-N-MC infected cells were treated with X-XOD, in the presence or absence of NSC405020, for 24 h and were examined by confocal microscopy. The representative panel shows immunofluorescence images for 22C11 (anti-N-terminal) antibody. Original magnification: 63×. Scale bar: 10 μm. No staining was observed when the primary antibodies was omitted.

3.2.3. Effect of HSV-1 on the lysosomal pathway changes

The lysosomal markers were measured by Western blot using the specific antibodies for LAMP2 and CD63 (Figure 64). The lysosomal markers decreased in HSV-1 infected cells in the presence of X-XOD. Apparently, the presence of the inhibitor in infected cells decrease the levels of LAMP2 but not the levels of CD63. However, the results observed previously without infection are better reproduced with anti-CD63 antibody.

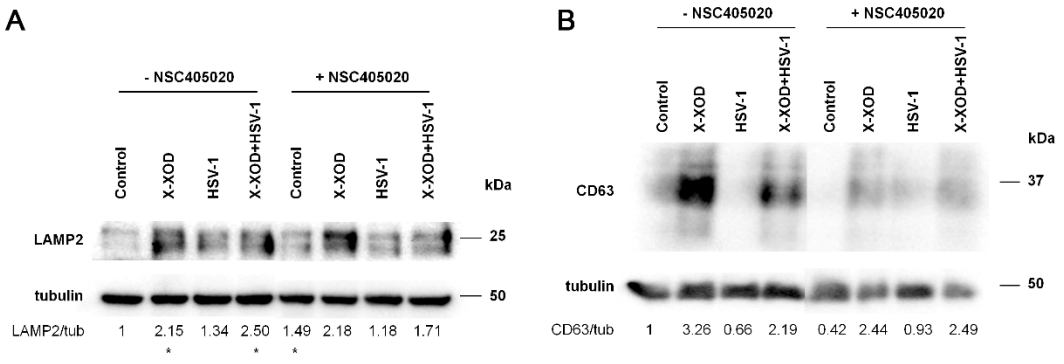

Figure 64. **HSV-1 alters the lysosomal levels induced by OS.** SK-N-MC infected with HSV-1 cells were treated with X-XOD in the presence or absence of NSC405020. After incubation for 24 h, cell cultures were examined by Western blot using the anti-LAMP2 and anti-CD63. Tubulin blot is shown as loading control. A representative experiment is shown. The data show the mean (± SEM) densitometry values (normalized by α-tubulin) (n=4).

The lysosomal burden was measured as described above using the acidotropic probe LysoTracker®. Fluorometric assay was performed and the infected cells did not change the burden of acidic vesicles in comparison to X-XOD treated cells (Figure 65). In the absence of X-XOD, the levels of infected cells in the presence of the inhibitor NSC405020 (grey) were higher than in control cells without the inhibitor (black).

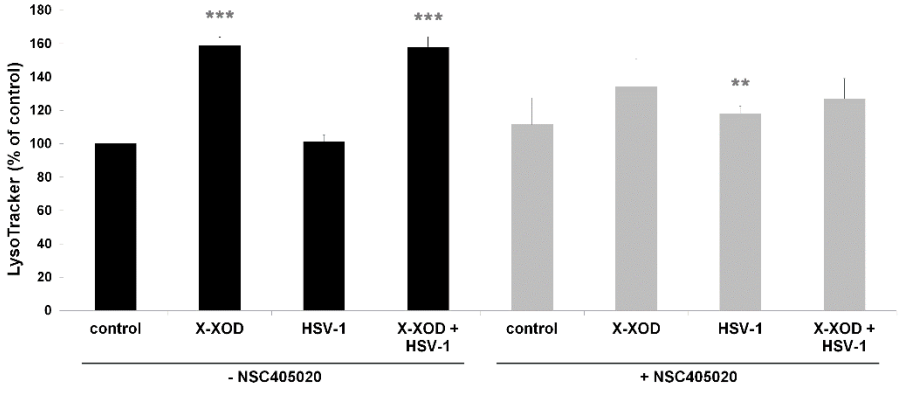

Figure 65. HSV-1 does not affect the lysosomal burden. SK-N-MC infected cells were treated with X-XOD in the presence (grey) or absence (black) of NSC405020. After incubation for 24 h, lysosomal quantity was analyzed by fluorometric measurement of LysoTracker. The graph shows the mean (±SEM) fluorescence values expressed as a percentage of the control value. ∗p<0.05, ∗∗p<0.01 and ∗∗∗p<0.01 (t-test, n=4)

To analyze the intracellular location pattern of endolysosomal markers, immunofluorescence assays were performed. As it is observed in Figure 66 (A-LTR, B-LAMP2 and C-CD63) all the markers decrease in infected cells, especially LAMP2 and CD63. These results correlate with the ones obtained by Western blot (Figure 75).

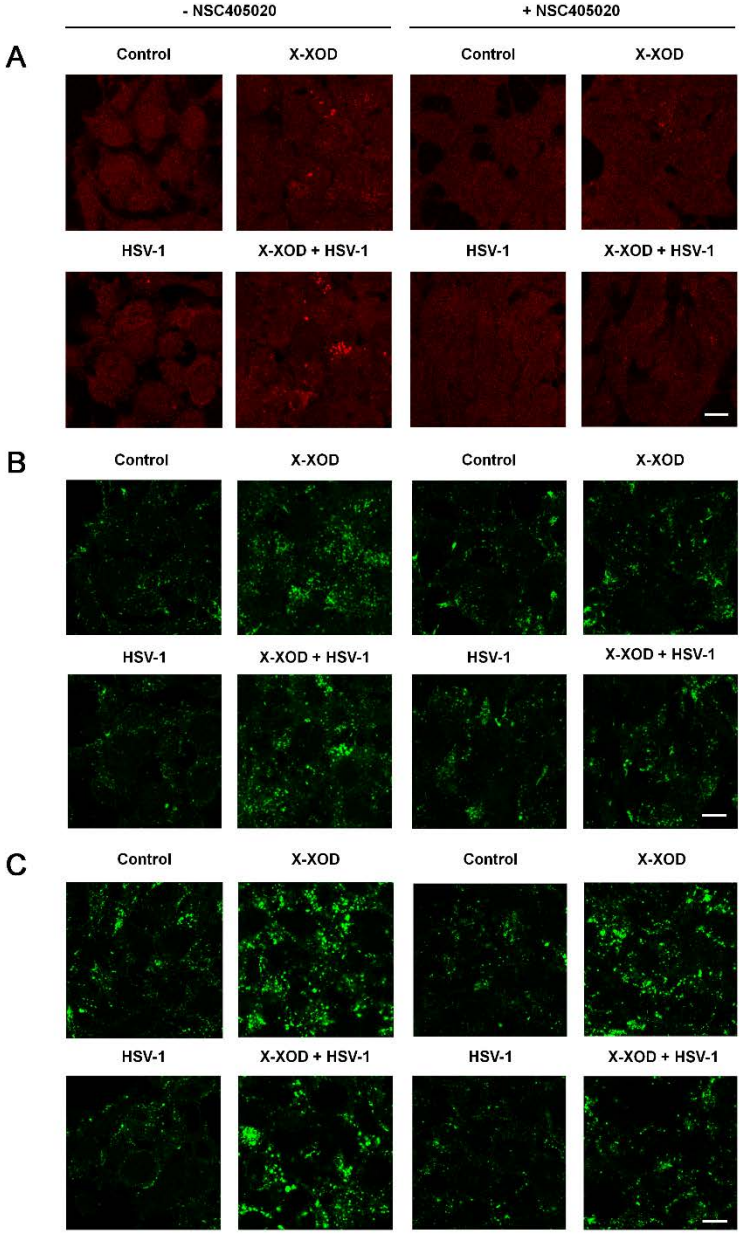

Figure 66. HSV-1 decreases the levels of lysosomes induced by OS. SK-N-MC infected with HSV-1 cells were treated with X-XOD, in the presence or absence of NSC405020, for 24 h and were examined by confocal microscopy. The representative

panel shows immunofluorescence images for (A) LysoTracker probe, (B) anti-LAMP2 and (C) anti-CD63 antibodies. Original magnification: 63×. Scale bar: 10 μm. No staining was observed when the primary antibodies were omitted.

3.2.4. Effect of MMP-14 on HSV-1 infection

Since data of the previous chapter suggested an interaction between MMP-14 and HSV-1, the efficency of HSV-1 infection was assesed in cells treated with NSC405020 or deficient for MMP-14. Interestingly, the levels of glycoprotein B (gB, envelope glycoprotein of HSV-1) were undetectable in cells treated with the inhibitor NSC405020 (Figure 67A). The same effect was seen in the MMP-14 deficient clone 3 (Figure 67B), although the effect was less pronounced than with the inhibitor

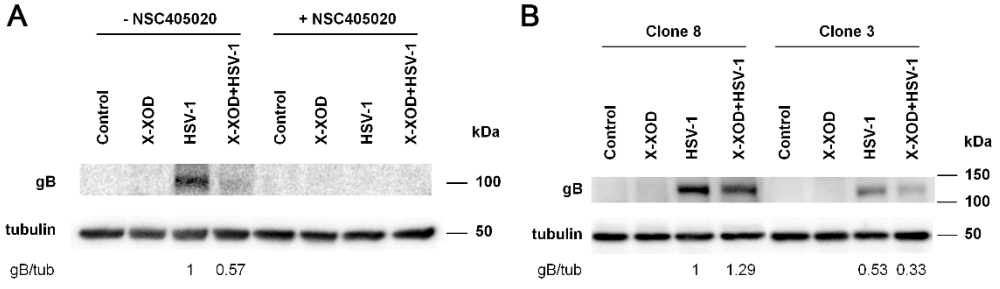

Figure 67. **MMP-14 inhibition decreases HSV-1 gB protein levels.** SK-N-MC infected with HSV-1 cells were treated with X-XOD in the presence or absence of NSC405020. After incubation for 24 h, cell cultures were examined by Western blot using the anti-gB antibody (envelope glycoprotein of HSV-1). Tubulin blot is shown as loading control. A representative experiment is shown. The data show the mean (± SEM) densitometry values (normalized by α-tubulin) (n=4).

To confirm these results, immunofluorescence assay was performed using an anti-HSV-1 antibody. As it is observed in Figure 68, NSC405020 strongly decreased the number of HSV-1 infected cells. These data indicate that MMP-14 plays a role in the HSV-1 capacity of infection in our neuroblastoma cell model.

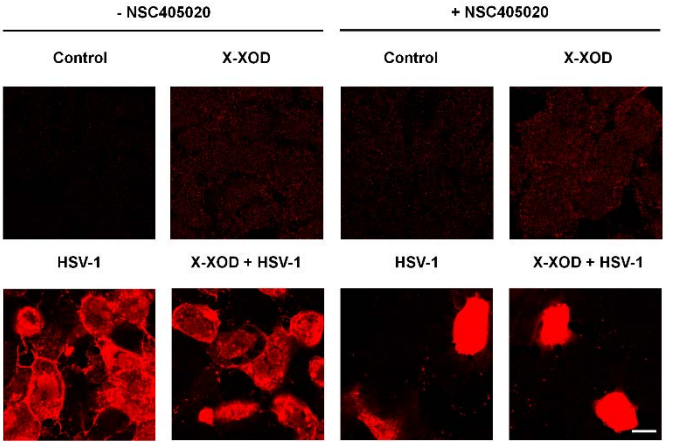

Figure 68. NSC405020 decreases the efficiency of HSV-1 infection. SK-N-MC infected with HSV-1 cells were treated with X-XOD, in the presence or absence of NSC405020, for 24 h were examined by confocal microscopy. The representative panel shows immunofluorescence images for anti-HSV-1 antibody. Original magnification: 63×. Scale bar: 10 μm. No staining was observed when the primary antibodies were omitted.

4. iPSCs derived neurons obtained from SAD patients

We wanted to analyze the effect of OS on APP processing and on the lysosomal pathway in a more physiological model, for that we used iPSC-derived cells, a more suitable model given that has a background of AD patients. The discovery of iPS cells generation from somatic adult cells using a cocktail of four transcription factors (Takahashi and Yamanaka, 2006) paved the way to model diseases by using patient-derived cells which can then be differentiated into disease relevant cell types. Furthermore, considering the unavailability of *in vitro* human disease models, human iPS cells could help to provide large numbers of patient-specific neuronal cells for research and clinical objectives. To complement the findings obtained in the SK-N-MC neuroblastoma model, we decided to take advantage of this technology to get a cell model closer to the physiological state in which to validate the previous results. As the starting material, we used iPSCs generated from T lymphocytes, thanks to a collaboration with Dr. Adjaye's laboratory (Martins et al., 2018).

4.1. iPSCs differentiation to neurons

For this purpose, we started with six iPS cell lines: two controls and four AD patients bearing the AD risk variant R47H in TREM2. These lines were previously derived from lymphoblasts and characterized by Dr. James Adjaye's group. Their basic characteristics are summarized in Table 6.

Table 6. iPSCs lines characteristics.

iPSC internal code	Disease status	TREM2 genotype	APOE genotype	Age	Age at onset	Gender
106	Control	wt	34	69	-	M
116	Control	wt	33	75	-	F
125	AD	TREM2 p.R47H	34	67	65	M
105	AD	TREM2 p.R47H	44	65	60	M
126	AD	TREM2 p.R47H	44	74	74	M
120	AD	TREM2 p.R47H	24	67	64	F

Disease status, TREM2 and APOE genotypes, as well as the age at examination and at disease onset, and gender of the lymphocyte donors is shown.

With the aim to obtain differentiated neurons from iPSCs of controls and SAD patients, we used two stablished differentiation protocol, described in detail in Methods. As observed in the table, two of the AD donors were APOE4 homozygous, and all of them were carriers of the risk variant p.R47H of TREM2. This variant, whose functional study constitutes one of

the main interests of Dr Adyaje's group, is claimed to increase SAD susceptibility to levels similar to that associated to the APOE ε4 allele, probably by mechanisms involving inflammation-induced bystander damage of neurons or the regulation of phagocytic pathways responsible for the removal of neuronal debris (Jiang et al., 2013). The aim of using these cell lines in the thesis was to check the similarities between the neuroblastoma cell model and iPS derived neurons in terms of their response to OS.

The first differentiation protocol we tried was an aggregate protocol based on methods developed for hESCs (Zeng et al., 2010). Briefly, aggregates were formed by dissociating iPSCs into large clusters, followed by suspension in serum-free iPS media (hES). Aggregates were then plated on Matrigel for the formation of primitive neuroepithelial cells in N2 neural induction media. Neural rosette structures were selected with STEMDiff reagent from plates and suspended in flasks in N2/B27 neural induction media. Aggregates were plated on Matrigel and allowed to mature in neural differentiation media. Although we obtain neurons (positive for MAP2 and Doublecortin, markers for neurons) as shown in Figure 69, the number of cells was not enough for performing any experiment.

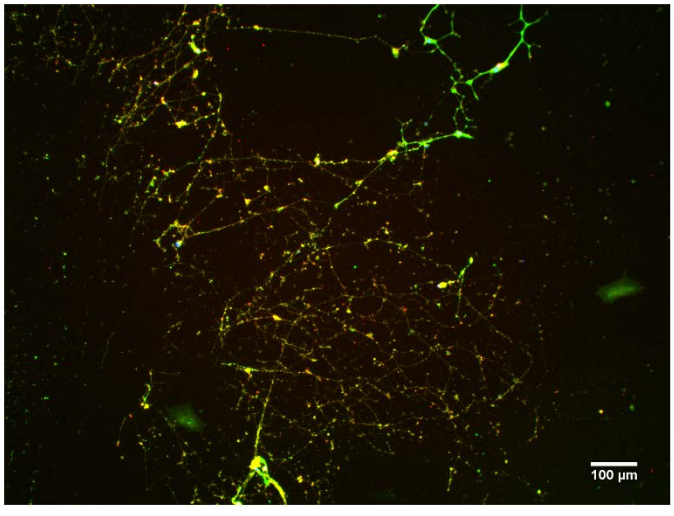

Figure 69. Neurons obtained with the embryoid aggregate protocol. Immunofluorescence of neurons obtained with the aggregate differentiation protocol, showing positive staining for MAP2 (green) and Doublecortin (red). Original magnification: 10x. Scale bar: (n=1).

We then moved to another protocol, based on a dual SMAD inhibition culture in monolayer (Chambers et al., 2009); for that, iPSCs cells were dissociated and plated to grow as a

monolayer in mTeSR1 media. After cells reached 90% confluency, media was changed to neural induction media supplemented with Dorsomorphin and SB431542. Cells were re-plated in neural differentiation media onto plates coated with a special Matrigel that promotes the adhesion and generation of NPCs. As a result of this protocol we were able to obtain neurons from the iPS cell line 105 and neural progenitor cells (NPCs, an intermediate differentiation step to neurons) from the iPS cell line 126 (Figure 70), both derived from AD patients, which were used on the following experiments.

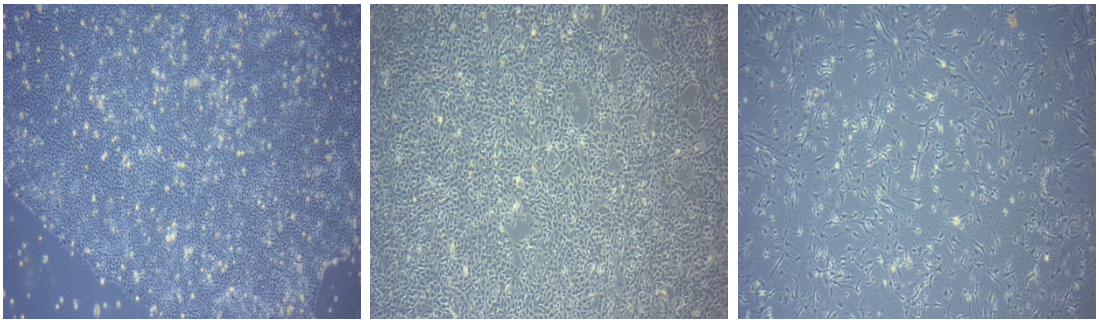

Figure 70. iPSCs differentiation during the dual SMAD inhibition protocol. iPSCs, NPCs (iPS cell line 126) and neurons (iPS cell line 105) images taken in phase contrast microscope are shown from left to right. Original magnification: 10x.

4.1.1. Characterization of the iPSCs derived cells

The neural progenitor cells (NPCs) obtained from iPSC 126 had the typical morphology of this cell type at the microscope. Its characterization was confirmed using antibodies specific for nestin, a marker for ectoderm differentiated cells and doublecortin. Nestin is an intermediate filament protein originally described as a neural stem cells marker that appears during development of the central nervous system (CNS) and is required for survival, renewal and mitogen-stimulated proliferation of neural progenitor cells. Doublecortin is a microtubule-associated protein that is required for normal migration of neurons into the cerebral cortex. As shown in Figure 71 the cells derived from iPSC 126 were positive for nestin and doublecortin, therefore they were considered as NPCs.

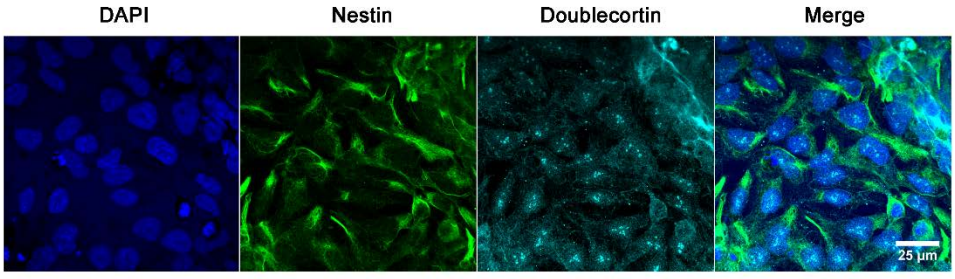

Figure 71. Neural progenitor cells (NPCs) obtained by the SMAD inhibition protocol. Immunofluorescence positive for nestin and doublecortin. Nuclei stained with DAPI. Original magnification: 63×. Scale bar: 25 µm.

We were also able to obtain cells differentiated to a more advanced stage, from the iPSC line 105. In this case, a mix of cell morphologies corresponding to different cell types similar to what APPens in the brain, the so-called brain microenvironment, was observed in the cultures (Figure 72A and B). As shown in Figure 72C, in the immunofluorescence assay with antibodies specific for MAP2 (neurons), GFAP (astrocytes) and beta III tubulin (nerve cells, including neurons and astrocytes), these different cell types could be identifyed.

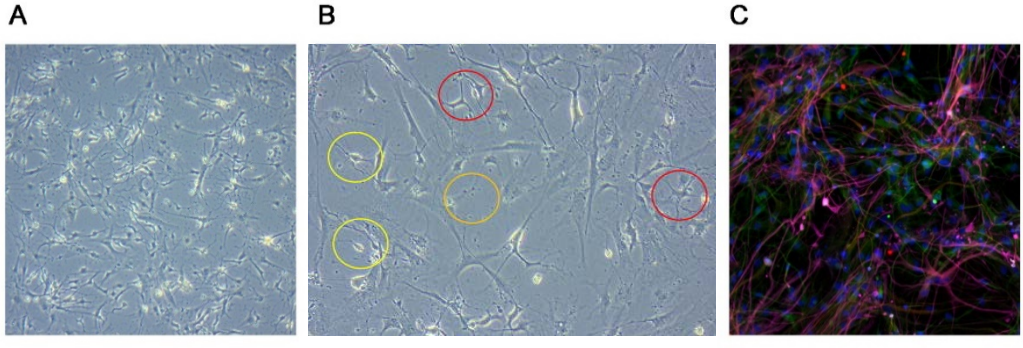

Figure 72. Advance stages of differentiation to brain microenvironment, obtained by the SMAD inhibition protocol. (A) Neurons images taken in microscope obtained from dual SMAD inhibition protocol. Original magnification: 10x. (B) Magnification of image A (20x). There are different cell types in the differentiated cells; neurons (yellow circles), astrocytes (red circles) and microglia (orange circle). (C) Immunofluorescence positive for MAP2, β-III tubulin and GFAP, markers for neurons and astrocytes respectively.

4.2. Analysis of the role of CTSB and MMP-14 on APP processing and on lysosomal pathway in neural iPSC derived cells

4.2.1. Modulation of CTSB and MMP-14 in the presence of OS

Differentiated cells derived from iPSCs were subjected to OS as it was performed previously in SK-N-MC cells, in the absence or presence of the inhibitor of CTSB, CA-074 Me, or the inhibitor of MMP-14, NSC405020. Besides the study of the effect of OS on the candidates, we also analyzed potential cross regulation between both proteins, previously described in the bibliography, by analyzing the activity of CTSB in cells treated with the MMP-14 inhibitor, and viceversa.

4.2.1.1. Effect of the inhibitors on CTSB activity in iPSCs derived cells

CTSB activity was assessed in NPCs and neurons treated with the free radical generating system X-XOD (black) and the inhibitors of CTSB and MMP-14, CA-074 Me (light grey) and NSC405020 (dark grey) respectively, for 24 hours. In NPCs (Figure 73A), X-XOD reduced CTSB activity by up to a 70% and CA-074 Me decreases the activity almost completely, very similar to what had been observed in SK-N-MC. In neurons (Figure 73B), the reduction of CTSB activity in X-XOD treated cells reached a 90%, an effect even higher than in the SK-N-MC cell model. Interestingly, NSC405020 inhibitor increased the CTSB activity almost an 80% suggesting the interaction between CTSB and MMP-14, at least in the most differentiated cells.

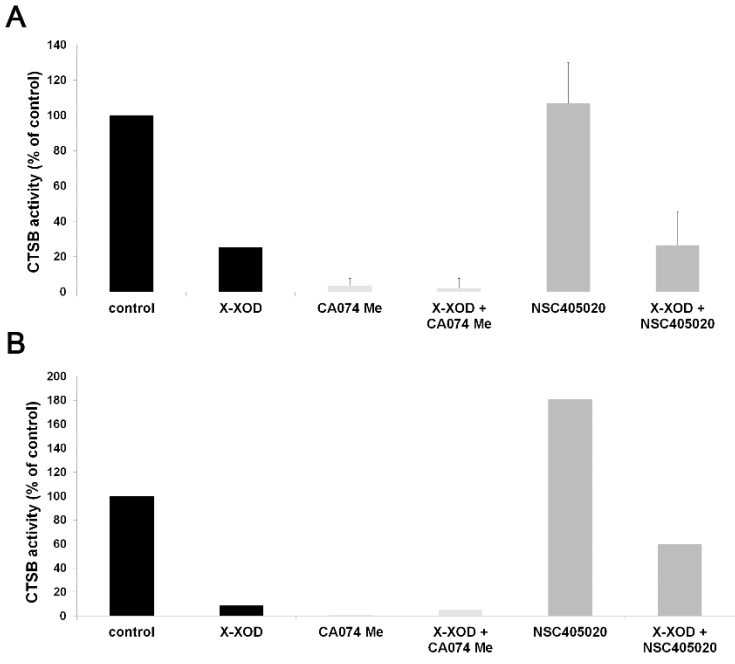

Figure 73. X-XOD and CA-074 Me reduces CTSB activity. NPCs (A) and neurons (B) were treated with X-XOD in the presence or absence of CA-074 Me or of NSC405020. After incubation for 24 h, CTSB activity was analyzed. Proteolysis of the fluorogenic substrate z-RR-AMC was used to monitor CTSB activity. The graph shows the mean (±SEM) fluorescence values expressed as a percentage of the control value (NPCs n=2, neurons n=1).

4.2.1.2. Effect of the inhibitors on MMP-14 levels in iPSCs derived cells

MMP-14 activity was assessed in NPCs in the presence or absence of X-XOD (black) and the inhibitors CA-074 Me (light grey) and NSC405020 (dark grey) for 24 h (Figure 74). X-XOD treated cells showed similar MMP-14 activity to control, and NSC405020 increased as it had been described previously in our cell model SK-N-MC (Figure 35). Interestingly, CA-074 Me inhibitor decrease the MMP-14 activity by up to 20% suggesting again the interaction between CTSB and MMP-14.

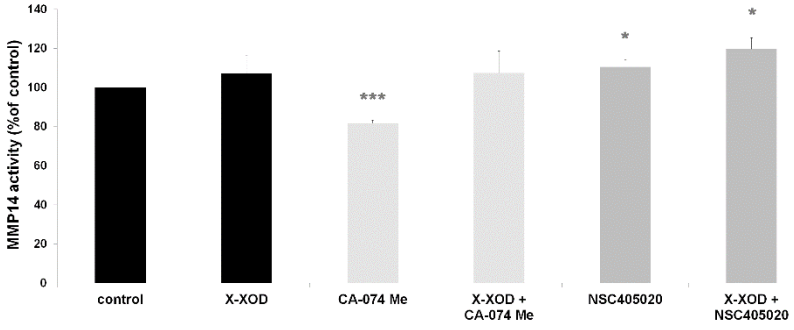

Figure 74. NSC405020 increases MMP-14 activity. NPCs were treated with X-XOD in the presence or absence of CA-074 Me or of NSC405020. After incubation for 24 h, MMP-14 activity was analyzed. Proteolysis of the fluorogenic substrate MCA-PLA-C(OMeBz)-WAR(Dpa)-NH_2 was used to monitor MMP-14 activity. The graph shows the mean (±SEM) fluorescence values expressed as a percentage of the control value. ∗p<0.05, ∗∗p<0.01 and ∗∗∗p<0.01 (t-test, n=4).

The levels of MMP-14 protein (monomeric active form) were measured by Western blot. Cells treated with X-XOD presented a marked increase in protein levels (Figure 75), similarly to the effect observed in SK-N-MC (Figure 37). This increase was lower in NSC405020 treated neurons, where the X-XOD effect seemed to be bigger, whereas the CTSB inhibitor CA-074 Me had no effect on MMP-14 protein levels.

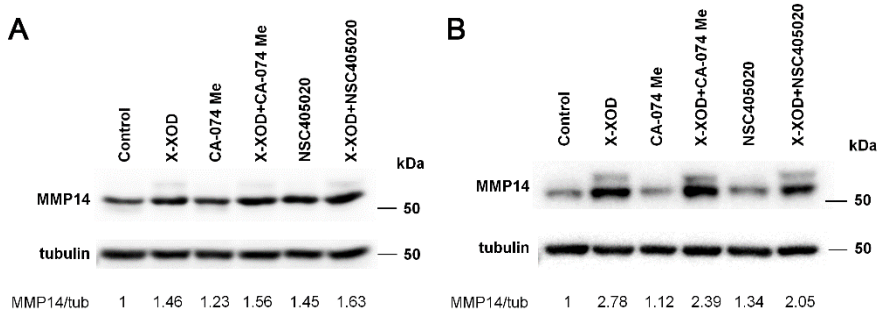

Figure 75. CA-074 Me and NSC405020 increase MMP-14 levels induced by OS. NPCs (A) and neurons (B) were treated with X-XOD in the presence or absence of CA-074 Me or of NSC405020. After incubation for 24 h, Western blotting was performed using anti-MMP-14 antibody. Tubulin blot is shown as loading control. In the upper panel the band corresponds to MMP-14 and in the lower to α-tubulin (NPCs n=3, neurons n=1)

MMP-14 was also analyzed by immunofluorescence assays and revealed the same effect in X-XOD treated cells than the ones obtained in Western blot (Figure 76). As it had been observed in SK-N-MC (Figure 38), MMP-14 accumulated in the presence of X-XOD combined with the inhibitor NSC405020. Further, CA-074 Me treatment seemed to increase

the immunofluorescence levels in comparison to its controls, in the presence or absence of X-XOD.

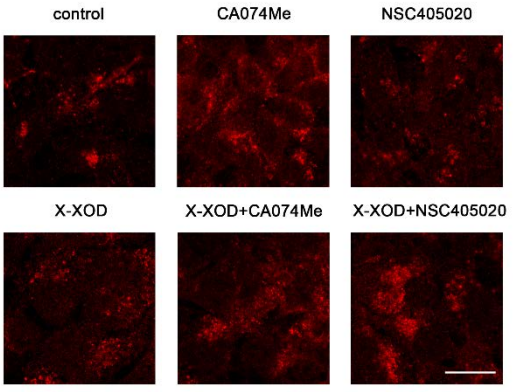

Figure 76. CA-074 Me and NSC405020 accumulates MMP-14 iduced by OS. NPCs treated with X-XOD, in the presence or absence of CA-074 Me or of NSC405020, for 24 h were examined by confocal microscopy. The representative panel shows immunofluorescence images for anti-MMP-14 antibody. Original magnification: 63×. Scale bar: 10 μm. No staining was observed when the primary antibodies was omitted.

In summary, the activity, the protein levels and the immunofluorescence of CTSB and MMP-14 showed the same response to the modulation of CTSB and MMP-14 in the iPSC derived NPCs and neurons than in our SK-N-MC cells. Furthermore, these results suggest an interaction between CTSB and MMP-14. The changes obtained with the inhibitors in both enzymatic activities respectively was not expected due to their specifity, but interestingly we observed a cross reaction of these proteases.

4.2.2. Effect of the inhibitors on APP proteolytic processing in iPSC derived cells

Regarding the APP processing, the effect of mild OS and the inhibitors CA-074 Me or NSC405020 were examined in cell lysates by Western blotting using the antibody 22C11 (Figure 77). No effect of the inhibitors was observed, in accordance with the SK-N-MC model (Figures 23 and 39). We observed an increase of APP in the presence of OS, more pronounced in its combination with CA-074 Me, specially in NPCs. In contrast, a decrease of APP in X-XOD treated cells combined with NSC405020, both in NPCs and in neurons, as well as a decrease of APP85, that appears in the presence of X-XOD, was observed. Although this decrease in neurons (Figure 77B) was lower than the previously observed in our SK-N-MC model, this result is not conclusive, given that was performed only in one AD

patient derived cell line, and our cell model support firmly the involvement of MMP-14 in the APP85 formation.

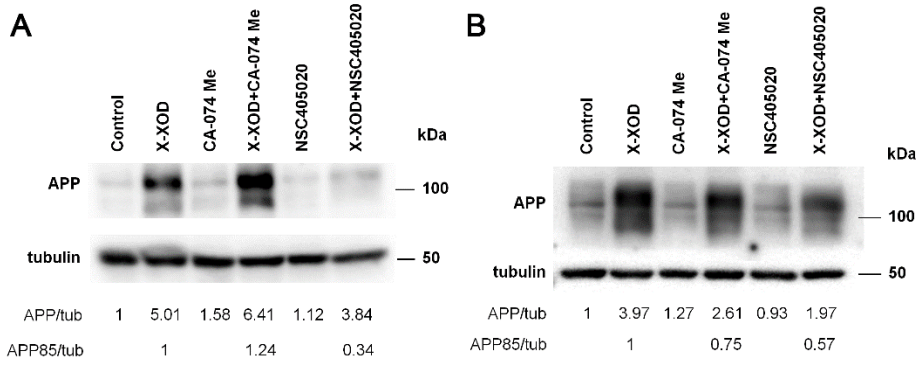

Figure 77. X-XOD induces the increase of APP and the appearance of APP85. CA-074 Me favors whereas NSC405020 prevents these effects. NPCs (A) and neurons (B) were treated with X-XOD in the presence or absence of CA-074 Me or of NSC405020. After incubation for 24 h, Western blotting was performed using 22C11 (anti-N-terminal) antibody. Tubulin blot is shown as loading control. In the upper panel the band corresponds to APP and its fragments and in the lower to α-tubulin (n=1).

To analyze the intracellular location and pattern of APP, immunofluorescence assays were performed in NPCs (Figure 78) with antibodies corresponding to different regions of the APP (A- 22C11– N-terminal, B- 6E10, and C- C-terminal). The levels of APP increased in the presence of X-XOD alone or together with the inhibitors, especially in the presence of the CTSB inhibitor (CA-074 Me). Moreover X-XOD treated cells accumulated APP in a different pattern. This increase and accumulation were not equally observed with the three antibodies probably due to the fact that each antibody recognizes entire APP but different APP fragments (sAPP, CTFs, etc.). These results were similar to that observed previously in SK-N-MC. With 6E10 and C-terminal antibodies we observed better the accumulation of APP pattern and their changes with the modulation of the proteases as expected. The 22C11 antibody had more background.

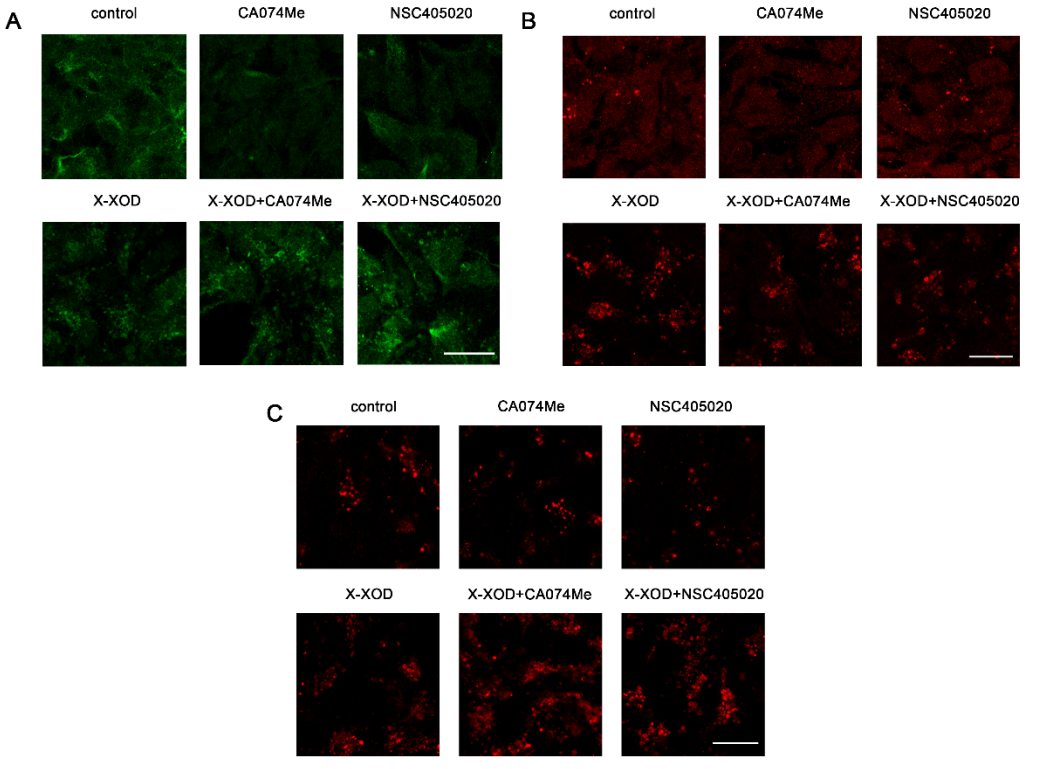

Figure 78. CA-074 Me or NSC405020 accumulate APP induced by OS. NPCs cells treated with X-XOD, in the presence or absence of CA-074 Me or of NSC405020, for 24 h were examined by confocal microscopy. The representative panel shows immunofluorescence images for (A) 22C11, (B) 6E10 and (C) Ct antibodies. Original magnification: 63×. Scale bar: 10 μm. No staining was observed when the primary antibodies were omitted.

We conclude that CTSB and MMP-14 modulate the APP processing although in different ways. The inhibition of CTSB in combination with OS, increase the APP levels whereas the inhibition of MMP-14 in combination with OS, impairs the increase of APP levels and the formation of the APP85 observed in X-XOD treated cells, as it had been observed previously in SK-N-MC. The inhibitors by themselves does not have also any effect on APP processing.

4.2.3. Effect of the inhibitors on lysosomal pathway changes in iPSCs derived cells

To analyze the lysosomal pathway LAMP2 was measured by Western blot (Figure 79). There was a slight increase of the lysosomal marker LAMP2 in cells treated with X-XOD, but lower than the observed in SK-N-MC (higher in X-XOD treated cells in the presence of the inhibitor CA-074 Me). However, the inhibitor NSC405020 did not decrease the levels of

LAMP2 in comparison to their controls, as it had been observed in SK-N-MC (Figures 25 and 41). Surprisingly, X-XOD had no effect on LAMP2 levels in neurons (Figure 79B).

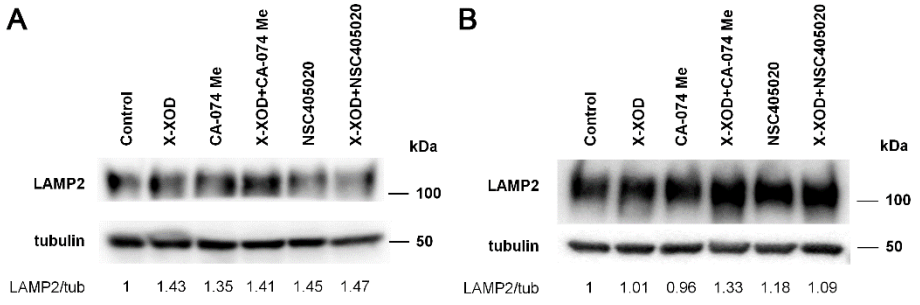

Figure 79. **CA-074 Me or NSC405020 increases LAMP2 levels induced by OS.** NPCs (A) and neurons (B) were treated with X-XOD in the presence or absence of CA-074 Me or of NSC405020. After incubation for 24 h, cell cultures were examined by Western blot using the anti-LAMP2 (lysosomes) and anti-CTSB (hydrolase of the lysosomes). Tubulin blot is shown as loading control (n=1).

In contrast, the lysosomal marker CD63 showed the expected results, similar to the ones obtained in SK-N-MC (Figure 80). There was an increase of protein levels in X-XOD treated cells, higher in combination with CA-074 Me, and lower in combination with NSC405020.

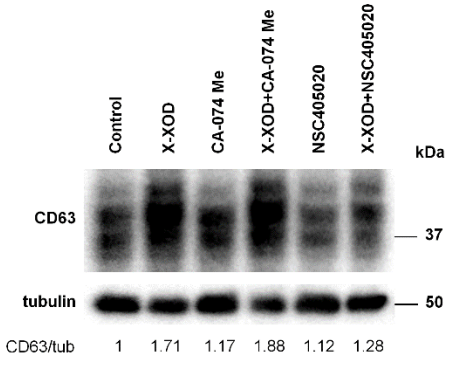

Figure 80. CA-074 Me increase CD63 levels whereas NSC405020 impairs the increase induced by OS. NPCs were treated with X-XOD in the presence or absence of CA-074 Me or of NSC405020. After incubation for 24 h, Western blotting was performed using CD63 antibody. Tubulin blot is shown as loading control. In the upper panel the band corresponds to CD63 and in the lower to α-tubulin (n=2).

The lysosomal burden was measured using the acidotropic probe LysoTracker®. The acidic vesicles increased (in number or in size) in the presence of X-XOD, even more in combination with CTSB and MMP-14 inhibitors (Figure 81). Moreover, the effect on

lysosomal burden of NSC405020 in NPCs was higher than the obtained in our SK-N-MC model.

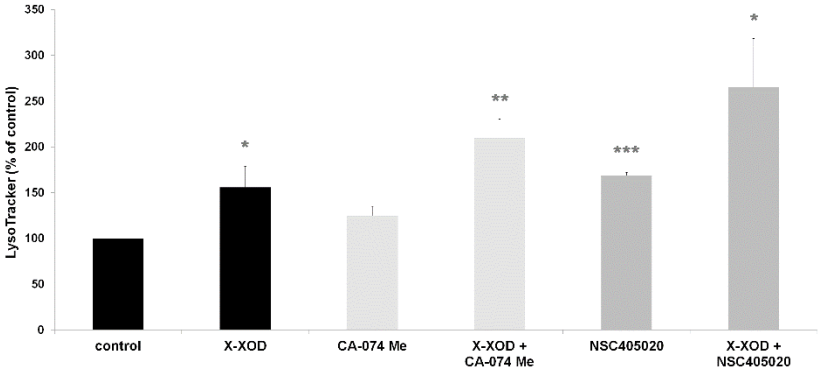

Figure 81. **CA-074 Me and NSC405020 increase the lysosomal burden induced by OS.** NPCs were treated with X-XOD in the presence or absence of CA-074 Me or of NSC405020. After incubation for 24 h, lysosomal quantity was analyzed by fluorometric measurement of LysoTracker. The graph shows the mean (±SEM) fluorescence values expressed as a percentage of the control value. ∗p<0.05, ∗∗p<0.01 and ∗∗∗p<0.01 (t-test, n=4).

To analyze the intracellular location pattern of some endolysosomal markers, immunofluorescence assays were performed. As it is observed in Figure 82 (A-LTR, B-LAMP2 and C-CD63) an increase in the presence of X-XOD was observed, as well as in the combination with both inhibitors, especially in the presence of CTSB inhibitor (CA-074 Me). These correlates with the results obtained in Western blot with anti-CD63 antibody and with the ones previously described in SK-N-MC.

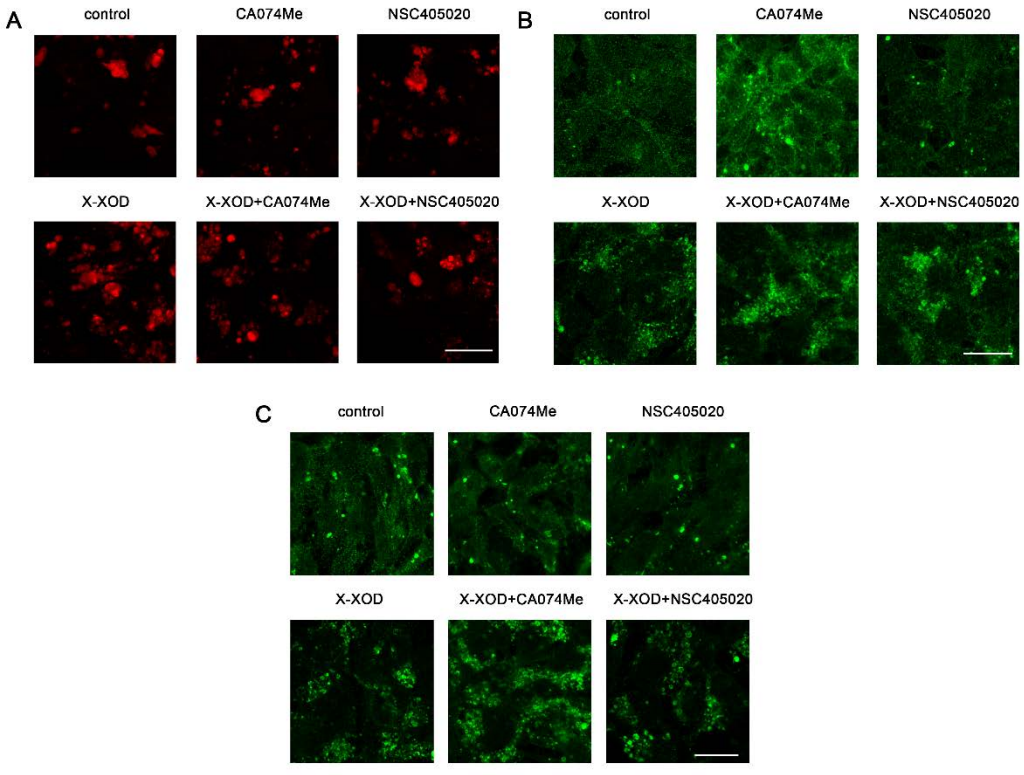

Figure 82. CA-074 Me and NSC405020 increase the accumulation of lysosomes induced by OS. NPCs cells treated with X-XOD, in the presence or absence of CA-074 Me or of NSC405020, for 24 h were examined by confocal microscopy. The representative panel shows immunofluorescence images for (A) LysoTracker probe, (B) anti-LAMP2 and (C) anti-CD63 antibodies. Original magnification: 63×. Scale bar: 10 μm. No staining was observed when the primary antibodies were omitted.

Taken these results together, it suggests that both inhibitors, CA-074 Me and NSC405020, produces changes on the lysosomal system induced by OS, indicating the role of CTSB and MMP-14 in the lysosomal pathway. Moreover, a parallel effect is observed on the APP processing, in which both inhibitors respectively alters the APP levels or the APP85.

DISCUSSION

1. Involvement of OS in APP processing and in lysosomal function

1.1. APP processing induced by OS

Numerous risk factors have been associated with the onset of AD, being one of them the aging-associated OS (Nunomura et al. 2001; Bonda et al., 2010). In addition to altering APP metabolism, OS affects protein degradation pathways including the proteasomal and lysosomal systems (Kiffin et al., 2006). Delving into this topic, we had previously reported the involvement of the ubiquitin-proteasome and the lysosome protein degradation systems in the regulation of APP metabolism/processing by the X-XOD free radical generating system (Recuero et al., 2013).

In this work, we aimed to identify proteases responsible for the connection between the alterations of the lysosomal system and those on APP proteolysis in the presence of OS. To do that, we focused on two bands recognized by APP specific antibodies whose quantity increased significantly in the presence of OS: one of 85 kDa recognized by the N-terminal specific antibody 22C11 and another one of about 56 kDa recognized by the oligomer specific A11 antibody.

Since A11 antibody is able to recognize oligomeric structures derived from several proteins, we assessed that the peptide of 56 kDa was indeed composed of Aβ oligomers, since it was immunoprecipitated by the Aβ specific antibody 6E10. This moiety probably corresponds to the previously described as Aβ*56, a dodecamer of Aβ peptide (Lesne et al., 2006). Aβ peptides are produced during the sequential proteolytic processing of APP via canonical and non-canonical secretases (Andrew et al., 2016). Their capacity to aggregate can lead to the formation of neurotoxic oligomers and to the accumulation of insoluble deposits in AD brains (Viola et al., 2015), which constitutes one of the hallmarks of the disease. It is widely accepted that Aβ oligomers are more potent neurotoxins than amyloid fibrils (Liu et al., 2015), and several have been isolated and studied in detail (Murakami et al., 2014). Recently, large oligomeric assembly states of Aβ have been associated with both aging and AD (Baker-Nigh et al., 2015).

APP85 has been recognized as an sAPP fragment, it was stained only by anti APP N-terminal antibodies and contained APP but not Aβ nor C-terminal sequences of APP. Most probably comes from a cleavage at the same site than the non-canonical η secretase that

results in shedding of an 80–95 kDa soluble fragment (sAPPη) and leaves a novel membrane-bound CTF, CTFη. This cleaveage is claimed to contribute to the production of Aβ and to the induction of synaptic dysfunction (Willem et al., 2015). Moreover, this new secretase cleavage of APP exceded β-secretase cleavage by almost 10-fold in human neurons, and accumulation of ηCTFs was also observed in dystrophic neurites surrounding amyloid plaques in the brains of AD patients (Willem et al., 2015).

Recent studies have revealed the complexity of the proteolytic processing of APP, with new secretases and the corresponding proteolytic fragments being identified (Andrew et al., 2016; Muller et al., 2017). These fragments include APP metabolites that accumulate in the brains of AD patients and may contribute to the synaptic dysfunction observed in the disease. Among these non-canonical proteases, our results suggested that cathepsin B, proposed as an alternative β secretase, and matrix metalloproteinase 14, similar to η secretase, were especially interesting for us as the potential responsible for the generation of the 56 and 85 kDa bands, respectively.

1.2. Lysosomal dysfunction induced by OS

OS contributes to neuronal damage and has been associated with neuronal cell death in several neurodegenerative diseases. The link between lysosome dysfunction and neurodegeneration has been evidenced by numerous research groups and is still under intense investigation because of its great potential as pharmacological target (Appelqvist et al., 2013; Whyte et al., 2017). Neurons are especially vulnerable to lysosome dysfunction and rely deeply on functional autophagic and endocytic pathways because these postmitotic cells are otherwise unable to dilute debris and undigested material through cellular divisions. Abnormalities of the lysosomal system in AD include very early-appearing endosome enlargement, accumulation of autophagic vesicles, increased lysosome biogenesis and lysosomal proteolysis deficits (Nixon et al., 2011). Interestingly, it has also been shown that in AD and Down's syndrome these activated or enlarged endosomes containing soluble Aβ appear prior to the deposition of amyloid plaques (Cataldo et al., 2004).

In addition, the lysosomal pathway is altered similarly to what APPen in LSDs, a group of disorders that are caused by dysfunction of lysosomal hydrolases or in a lesser extent by defective lysosomal membrane proteins (Filocamo et al., 2011). These abnormalities have also been reported in AD models and in our cell model of HSV-1 infection and OS (Santana

et al., 2013, Kristen et al., 2018), highlighting the implication of the lysosomal system in CNS pathologies and supporting the hypothesis that lysosomal dysfunction can cause the neurodegeneration induced by HSV-1 and OS.

The subcellular fractionation of the SK-N-MC cells revealed the presence of APP, the 56 kDa oligomer in the cell fraction enriched in endo-lysosomal vesicles, whereas the APP85 is equally present in both fractions (Cyt and L/LE). Moreover, the results also showed that the candidate proteases CTSB and MMP-14 were mainly localized in the endo-lysosome enriched fraction, as reported by other authors (Ishidoh et al., 2002, Mori et al., 2016). This observation reinforced the idea of its involvement in the formation and/or degradation of amyloid oligomers and in the formation of APP85, respectively.

2. Effect of the selected proteases on APP processing and on lysosomal pathway

2.1. Effect of CTSB on APP processing and on lysosomal pathway changes

Changes in the concentration, activity and localization of the endo-lysosomal cathepsins are habitually seen in aging neurons, and are thought to be of age-related neuropathological significance (Nakanishi et al., 2003; Cermak et al., 2016). Interestingly, CTSB, a cysteine protease that has been associated with AD since it can be found together with Aβ peptides in the extracellular amyloid plaques of AD brains (Cataldo et al., 1990). Furthermore, it has a potential role in the formation and in the clearance of Aβ peptides since it is claimed to have APP β-secretase activity and Aβ degradative activity (Hook et al., 2005; Mueller-Steiner et al., 2006).

In nice agreement with these data, the results of this tesis support the involvement of CTSB in the regulation of amyloid oligomer levels. Western blotting with the A11 antibody (which recognizes oligomeric structures) showed both X-XOD, that inhibits CTSB, and CA-074 Me to affect the levels of soluble amyloid oligomers, revealing a significantly increased large molecular weight soluble amyloid oligomer (~56 kDa). This oligomer is formed by Aβ since it was recognized by the 6E10 monoclonal antibody (which attaches to Aβ) and was not recognized by the APP C-terminal specific antibody. Thus, the 56 kDa band induced by OS in our model coud be the Aβ*56 described previously (Lesne et al 2006; Cheng et al., 2011).

Our results suggested also that the modulation of APP metabolism/processing by X-XOD induced OS or by the CTSB inhibitor CA-074 Me occurs via different mechanisms. For

example, although both treatments increased the 56 kDa oligomers, the levels of full lenght APP were increased by X-XOD but not by the CTSB inhibitor. Moreover CTSB did not affect APP85. In our aim to further characterize the APP metabolism modulation, we then studied the role of CTSB in the changes of amyloid oligomer and APP levels induced by X-XOD combining both treatments. If X-XOD modulates oligomer levels via the same mechanism as CA-074 Me, a higher increase in oligomer levels after the combination of both treatments would be expected. Nonetheless, we observed no effect on the oligomer levels, which reinforced our above mentioned conclusion that the modulation of APP metabolism/processing by both treatments takes place via different mechanism. However, we found a marked increase in intracellular APP and extracellular sAPPα levels when cells were treated with X-XOD in the presence of CA-074 Me.

In the light of these results, we propose that the modulation of APP metabolism by mild OS is partly mediated by CTSB, but that most probably involve additional mechanisms. These mechanisms could include its involvement on the ubiquitin proteasome pathway (Recuero et al., 2013), or its general effect on the lysosomal function (Santana et al., 2013; Kristen et al., 2018) that we reported previously. Although the mechanisms underlying the relations among Aβ aggregation, free radical damage and cell death remain unclear, it is interesting a recent report by Taneo and colleagues (Taneo et al., 2015) which shows that the induction of inflammatory response by Aβ oligomers is dependent on CTSB and reactive oxygen species (ROS). This work suggests that CTSB could serve as a therapeutic target for the treatment of AD, and support previous studies in cellular and animal models of the disease (Hook et al., 2005; Cho et al., 2013).

Our results in CTSB inhibited, or deficient cells, revealed an increase of lysosomal vesicles induced by OS observed with LysoTracker probe and of lysosomal markers observed by Western blot, and an enlargement of this vesicles observed by immunocytochemistry, but a decrease of degradation capacity as it is shown in the CTSB activity assays.

However, the fluorimetric measurement of LysoTracker with the CTSB deficiency resulted in lower levels than the results obtained with the CTSB inhibitor. The lysosomal burden appears to increase less in X-XOD treated deficient cells (clone 14), that changes 2 fold, than in SK-N-MC cells treated with the inhibitor CA-074 Me, that changes 3.2 fold. This might be due to the bigger effect that cause the CA-074 Me inhibitor on CTSB activity (the

remaining CTSB activity in the cells treated with the inhibitor is a 5% or less), whereas gene silencing in clone 14 is not complete and leaves a residual CTSB activity nearby 20%.

Our results about the increase of lysosomal burden and proteins are in concordance with the effect described when lacking CTSB expression increased the lysosomal levels via the increase in levels of the gene encoding TFEB. CTSB cleaves the calcium channel MCOLN1/TRPML1 in the lysosomes, maintaining suppression of the transcription factor TFEB and reducing expression of lysosomal and autophagy-related proteins. CTSB reduces the bioavailability of lysosomes and autophagosomes, and might have a physiological consequence in AD pathogenesis. This response controls the number of lysosomes and autophagosomes in the cell (Man et al., 2016).

Moreover, it is noteworthy that Cermak and colleagues (Cermak et al., 2016) have recently reported CTSB and CTSL (major regulators of lysosomal function) to possibly play an important role in the degradation of the key AD proteins, Aβ peptides and C-terminal fragments of the APP, and in degradation of β-secretase (BACE1). And revealed a significant reduction of the degradation capacity of lysosomes and substantially enlarged and increased lysosomal number upon CTSB inhibition.

2.2. Role of MMP-14 on the APP processing and on the lysosomal pathway

The abilities of several MMPs to degrade APP leading to aggregation of Aβ, as well as the increased expression of MMPs in postmortem brain tissue of AD patients, indicates that MMPs play an important role in the pathogenesis of AD (Wang et al., 2014). Their activities are determined through the induction of transcription by inflammatory mediators, through posttranslational modification by free radicals or cytokines and through inhibitory proteins such as tissue inhibitors of metalloproteinases (TIMPs) (Wang et al., 2014).

There is no much known about the MMP-14 in relation to the APP processing and the lysosomal pathway, therefore we wondered if this metalloproteinase would have any effect on it, once confirmed that it was transcriptionally altered by the induction of OS in our neuroblastoma cell model and its similarity with the MMP-24.

The study of MMP-14 activity is not conclusive, just indicative of its regulation in our cell model, due to the substrate inespecifity, that is not only recognized and cleavage by MMP-14 but also by MMP-11, but it is the better tool that we had to analyze it. In the MMP-14

deficient cells, although MMP-14 was silenced at a 90% (in terms of mRNA) its activity did not decrease in accordance with that reduction; in fact, it only decreased a 30%. Furthermore, the MMP-14 inhibitor (NSC405020) does not decrease activity probably because the mechanism of this inhibitor does not affect directly the catalytic pocket, it affects MMP-14 optimal conformation, due to interactions of the hemopexin domain, or there could be also a compensative effect of MMP-11. For dilucidate this, new activity assays with a specific subtrate of MMP-11 could be used, given that the MMP-11 is also highly expressed in our cell model.

Regarding the APP processing, the inhibition or silencing of MMP-14 causes a significant decrease or even makes disappear the APP85 induced by OS. This effect is similar to that described for MMP-24, as responsable for an APP fragment of a very approximate molecular weight (Willem et al., 2015). Moreover, the levels of APP are not altered, therefore the alteration is not due to less amount of APP able to process.

The mechanism of action of MMP-14 on the APP processing may be direct with APP acting as a substrate of MMP-14, or indirect through the effect that produces MMP-14 on others MMPs, given that MMP-14 is very upstream in the activation cascade of other MMPs, and it would be a mediator in the APP processing (Murphy et al., 2008; Buache et al., 2014).

The role of MMP-14 in Aβ degradation was analyzed comparing GM6001 and TIMP-2, and similar effects among them were observed (Liao et al., 2010). In contrast, we compared GM6001 and NSC405020 in our cell model, and at least in the results related to APP processing and lysosomal pathway were not similar. Although we are comparing at different levels of the APP processing this could be probably due to the specifity of the inhibitors, GM6001 and TIMP-2 are not specific only for MMP-14 while NSC405020 is specific only for MMP-14.

Regarding the lysosomal pattway, we observed in our cell model that lacking MMP-14 decreases the lysosomal burden and the lysosomal markers, but no effect on lysosome size was observed in comparison to the enlargement observed by the OS induction. However. it has been described that MMP-14 KO mice displayed significant increase in total endocytic and autophagic organelles. The size of lysosomes was also significantly larger in MMP-14 silenced mammary epithelial cells, which suggests that MMP-14 might be involved in regulating vesicle formation either in fusion or in division (Mori et al., 2016).

Analyses of other mechanisms in AD as autophagy, accumulation or aggregation of Aβ are needed in cells treated with the inhibitor NSC405020 and MMP-14 deficient cells. In this way, it would be of great interest to confirm the effect of MMP-14 on the whole system and not only on APP processing, being a possible therapeutic target.

2.3. Interaction of CTSB and MMP-14

Cathepsins participate in ECM degradation and remodelling and thus influence important cellular processes such as cell transformation and differentiation, motility, adhesion, invasion, angiogenesis, and metastasis. Also, cathepsins are involved in cell signalling and are capable of activating specific cell receptors and growth factors or liberating them from the ECM (Obermajer et al., 2008).

An effect of the CTSB inhibitor in MMP-14 activity was observed as well as an effect of the MMP-14 inhibitor in CTSB activity, in the neuroblastoma cell line and in the iPSC derived cells, suggesting a cross-link between these two proteases. Several studies have shown the ability of CTSB to degrade extracellular matrix (ECM) either intracellularly, extracellularly, or both by initiating a proteolytic cascade that involves urokinase plasminogen activator (uPA), plasminogen/plasmin, and MMPs. In vivo zymography showed the intralysosomal degradation of ECM components associated with active CTSB (Porter et al., 2013) demonstrating that phagocytic challenge promotes increased ECM degradation by mechanisms involving activation of proteases of at least three classes (cysteine proteases, serine proteases, and MMPs).

The relation between CTSB and MMPs has been also described in cancer research. CTSB has previously been shown to activate pro-urokinase plasminogen activator (pro-uPA), a serine protease and member of the plasminogen cascade involved in ECM degradation, matrix metalloproteinase (MMP) activation, and tumor cell invasión.; Rao and colleagues have shown that downregulation of CTSB and MMP9 more effectively reduces invasion of prostate tumor cells in vitro and tumor growth in vivo than downregulation of either cathepsin B or MMP9, and also their collaborative effect (Nalla et al., 2010). While many protein levels were decreased, immunodetection corroborated increased levels of matrix metalloproteinase, MMP2. Re-expression of CTSL rescues MMP2 abundance. CTSL and to a much lesser extent CTSB are able to degrade MMP2 at acidic and neutral pH. Addition of active MMP2 to the MEF secretome degrades proteins whose levels were also decreased by

CTSB and CTSL double deficiency. These results suggest a degradative CTSL-MMP2 axis, resulting in increased MMP2 levels upon cathepsin deficiency with subsequent degradation of secreted proteins such as collagen α-1 (Tholen et al., 2014).

3. Role of the proteases CTSB and MMP-14 in cells infected with HSV-1

Oxidative stress and HSV-1 infection play critical roles in the pathogenesis of AD (Harris et al., 2015; Persson et al., 2014; Tonnies et al., 2017). Over the last years, our group has contributed to the growing number of experimental evidence supporting the damaging relationship of both factors. To study the molecular mechanisms involved in AD, we developed a neuronal cell model of mild OS and HSV-1 infection. We showed that HSV-1 induces the main AD-like neurodegenerative events, such as aberrant tau phosphorylation (Alvarez et al., 2012), autophagy impairment, altered trafficking and metabolism of APP protein and the accumulation of the β-amyloid peptide (Santana et al., 2012). Moreover, OS is able to enhance the neurodegenerative events associated with HSV-1 infection (Santana et al., 2013).

In the present work, we have observed that the Aβ aggregation induced by the inhibition of CTSB is enhanced by the HSV-1 infection, even more in the presence of X-XOD. The levels of amyloid oligomers increase in infected cells in the presence of CA-074 Me analyzed by Western blot. Moreover, the infection caused a slight decrease of APP levels induced by the X-XOD or by itself, which increase when combine with the inhibition of CTSB. This increase might be due to a synergetic effect of HSV-1 and CA-074 Me in the formation of amyloid oligomers or to a response against the infection, as it had been described by Tanzi and colleagues. They observed that the infection can seed and accelerate β-amyloid deposition and that Aβ oligomers bind herpesvirus surface glycoproteins, accelerating β-amyloid deposition and leading to protective viral entrapment

Regarding the lysosomal system, the infection of HSV-1 caused a significant decrease of the degradative activity and impairs the increase of the lysosomal markers induced by OS. However, the infection does not affect the lysosomal burden and had no additional effect when combine with the inhibition of CTSB.

As it has been demontrated by numerous groups, HSV-1 is responsible for some of the neurodegenerative events observed in AD. Surprisingly, modulation of MMP-14 caused a

significant decrease in the infection of HSV-1. As a first characterization step, the effect of MMP-14 inhibition and MMP-14 deficiency on HSV-1 infection was evaluated and showed a reduction of HSV-1 infection efficiency. In MMP-14 modulated cells a reduction of infection was observed; less viral proteins by Western blot as well as less infected cells by immunocytochemistry, suggesting that MMP-14 might affect the HSV-1 viral cycle. Further experiments need to be done in order to confirm this hypothesis but impairment of HSV-1 infection induced by MMP-14 deficiency could affect the neurodegenerative events induced by the virus. No similar effects were observed with the modulation of CTSB.

It has been described previously the effect of MMP-14 on other viral infections; extracellular matrix proteolysis by MT1-MMP contributed to Influenza-related tissue damage and mortality, and selective inhibition of MT1-MMP protected the tissue from infection-related structural and compositional tissue damage (Talmi-Frank et al., 2016). Moreover, it has been described the effect of related MMPs with HSV; an early increased MMP-9 expression was involved in the evolution of herpes simplex encephalitis by facilitating the development of cerebrovascular complications (Martinez-Torres et al., 2004).

It will be of great interest to study the involvement of MMP-14 in the mechanisms of entry and replication of the HSV-1 and especially the implication on the main neuropathological hallmarks observed in HSV-1 infected cells as the accumulation of intracellular Aβ (Santana et al., 2012; Wozniak et al., 2007), autophagic vesicles (Itzhaki et al., 2008; Santana et al., 2012) and hyperphosphorylated tau protein (Alvarez et al., 2012; Wozniak et al., 2009).

HSV-1 infection does not affect APP levels neither the lysosomal levels induced by OS in the presence of the inhibition of MMP-14.

4. Validation of findings in SAD patients derived iPSCs

The development of methods to generate iPSCs from adult tissues (Takahashi et al., 2007) was particularly important for diseases of the central nervous system, since it allows the potential to provide a virtually limitless supply of cell types resembling human brain cells which were previously unattainable.

AD typically begins with loss of episodic memory, but ultimately leads to additional cortical symptoms related to language, attention, and visuospatial orientation. Amyloid plaque

deposition, neuritic plaques, neurofibrillary tangles and neuronal loss are extensive in the cerebral cortex. Therefore, studies modeling AD with iPSCs often begin with the generation of forebrain neurons. Differentiation to forebrain neuronal fates is referred to as the "default" for neuronal differentiation strategies, as differentiation to the neural lineage in the absence of exogenous patterning factors typically leads to neurons expressing markers of cortical neuronal fates (Sullivan et al., 2017). The base protocols used for these differentiations include dual-SMAD inhibition in a monolayer culture (Chambers et al., 2009), an embryoid body or aggregate method (Eiraku et al., 2008) or more recently, the formation of cerebral organoids (Lancaster et al., 2013).

While much progress has been made in generating a number of cell types found in the brain, further work is required to truly recapitulate the full repertoire of cells found in the mature brain (Sullivan et al., 2017). iPSCs will allow screening to occur in a disease-relevant context with the potential to enable a more rapid transition from the bench to the clinic. The ability to culture cells from SAD and FAD backgrounds will further permit more tailored treatment strategies by delineating the differences between and within these disease sub-types.

In this thesis, AD-TREM2 iPSC lines obtained from AD patients expressing the TREM2 R47H variant (Martins et al., 2018) were differentiated and used to validate the SK-N-MC neuroblastoma cell model. The p.R47H variant of TREM2 is a widely supported AD risk factor, with an associated risk for AD comparable to that of APOE ε4, although TREM2 variants are more rare (13% and 0.3% allelic frequency in Caucasian populations, respectively; Jiang et al., 2013). TREM2 encodes the triggering receptor expressed on myeloid cells 2 protein and is upregulated in plaque-associated microglia. The TREM2 risk variant impairs protein function, limiting its ability to clear amyloid and cellular debris, suggesting that the link between this gene and pathology is an imbalance in cellular protection mechanisms (Guerreiro et al., 2013).

When compared with the SK-N-MC cells, these iPSC-derived neural cell lines (NPCs and neurons), showed a very similar response to OS and to the modulation of CTSB and MMP-14. However, it will be necessary to confirm some interesting results suggesting different behavior in iPSC derived and neuroblastoma cells. These include the higher decrease in CTSB activity provoked by OS in neurons, in comparison to NPCs or neuroblastoma cell

line, or the apparent cross-modulation between CTSB and MMP-14 observed in NPCs. We have initiated the study of this cross-talk in SK-N-MC cells, and the preliminary results confirm this interaction.

The differentiation of these cells was not technically as straight forward as expected; therefore it would be also very interesting to increase the number of iPSC lines of patients that carry this variant to work with. This would increase the percentage of success to differentiate into more brain cell types. Moreover, it would be necessary to increase the number of experiments with these iPSCs cells with the R47H variant to dilucidate the implication of TREM2 not only in APP processing and lysosomal pathway markers but also in other neuropathological hallmarks of the disease, as the accumulation of intracellular Aβ and hyperphosphorylated tau protein, the impairment of autophagy, etc.

On the one hand, this model would be useful to compare SAD patients with controls. In preliminar studies with iPSCs (non-differentiated cells) we observed some changes in CTSB activity, which seems to be lower in AD patients derived cells. LysoTracker measures were also different between AD patients and controls. More experiments in the differentiated cell lines, but also in the non-differentiated cells, have to be done to confirm these preliminary results.

On the other hand, these cell lines may be used to characterize the response of neuron-like cells to HSV-1 infection alone or combined with OS. We would evaluate if there are differences in the APP processing, lysosomal alterations and AD-like neurodegenerative events induced by HSV-1 and OS between control- and patient-derived cells.

CONCLUSIONS

The experimental work carried out in this thesis has made it possible to obtain the following conclusions:

1. OS produces an alteration on the processing of APP, increasing the levels of two APP derivatives: an amyloid oligomer of 56 kDa and an N-terminal fragment of APP of 85 kDa (APP85).

2. The inhibition of CTSB increases the levels of APP induced by OS confirming the role of CTSB in the processing of APP. Moreover, the lysosomal levels are increased, although the degradative activity of the lysosomal system is decreased, suggesting a relation between the effects of CTSB on APP processing and lysosomal pathway.

3. The inhibition of MMP-14 decreases the levels of APP85 induced by OS, confirming the role of MMP-14 in the processing of APP. Moreover, the lysosomal levels are decreased. suggesting a relation between the effects of MMP-14 on APP processing and lysosomal pathway.

4. In cells infected with HSV-1 there is an increase of Aβ oligomers when combined with the inhibion of CTSB whereas the levels of APP decrease. Moreover, the infection decreases the degradative activity of the lysosomal system.

5. The inhibition of MMP-14 decreases the viral infection, suggesting that MMP-14 has a fundamental role in the mechanism of infection by HSV-1.

6. There is an interaction between the CTSB and the MMP-14. Inhibition of one has effects on the levels and activity of the other, and the other way around.

7. In neurons and NPCs derived from iPSC of patients with sporadic AD, the same results as in the SK-N-MC neuroblastoma model are observed, confirming the utility of this model for the study of APP processing and lysosomal pathway.

CONCLUSIONES

El trabajo experimental realizado en esta tesis ha permitido obtener las siguientes conclusiones:

1. El EO produce una alteración el procesamiento de APP, aumentando los niveles de dos derivados de APP: un oligómero amiloide de 56 kDa y un fragmento N-terminal de 85 kDa (APP85).

2. La inhibición de CTSB aumenta los niveles de APP inducidos por el EO confirmando el papel de CTSB en el procesamiento de APP. Además, los niveles lisosomales aumentan, aunque disminuye la actividad degradativa de los lisosomas, lo que sugiere una relación entre los efectos de CTSB en el procesamiento de APP y la vía lisosomal.

3. La inhibición de MMP-14 disminuye los niveles de APP85 inducido por el EO confirmando el papel de MMP-14 en el procesamiento de APP. Además, los niveles lisosomales disminuyen, lo que sugiere una relación entre los efectos de MMP-14 en el procesamiento de APP y la vía lisosomal.

4. En células infectadas con HSV-1 hay un aumento de los oligómeros de Aβ cuando se combina con la inhibición de CTSB, aunque los niveles de APP disminuyen. Además, la infección disminuye la actividad degradativa del sistema lisosomal.

5. La inhibición de MMP-14 disminuye la infección viral, sugiriendo que la MMP-14 tiene un papel fundamental en el mecanismo de infección del HSV-1.

6. Existe una interacción entre la CTSB y la MMP-14. La inhibición de una tiene efecto sobre los niveles y actividad de la otra, y viceversa.

7. En neuronas y progenitores neurales derivados de iPSC de pacientes con EA esporádica se observan los mismos resultados que en el modelo de neuroblastoma SK-N-MC, confirmando la utilidad de este modelo para el estudio del procesamiento de APP y de la vía lisosomal.

REFERENCES

Aizenstein, H. J., R. D. Nebes, J. A. Saxton, J. C. Price, C. A. Mathis, N. D. Tsopelas, S. K. Ziolko, J. A. James, B. E. Snitz, P. R. Houck, W. Bi, A. D. Cohen, B. J. Lopresti, S. T. DeKosky, E. M. Halligan, and W. E. Klunk. 2008. 'Frequent amyloid deposition without significant cognitive impairment among the elderly', *Arch Neurol*, 65: 1509-17.

Almeida, C. G., R. H. Takahashi, and G. K. Gouras. 2006. 'Beta-amyloid accumulation impairs multivesicular body sorting by inhibiting the ubiquitin-proteasome system', *J Neurosci*, 26: 4277-88.

Alonso, R., D. Pisa, A. I. Marina, E. Morato, A. Rabano, and L. Carrasco. 2014. 'Fungal infection in patients with Alzheimer's disease', *J Alzheimers Dis*, 41: 301-11.

Alvarez, G., J. Aldudo, M. Alonso, S. Santana, and F. Valdivieso. 2012. 'Herpes simplex virus type 1 induces nuclear accumulation of hyperphosphorylated tau in neuronal cells', *J Neurosci Res*, 90: 1020-9.

Andersen, J. K. 2004. 'Oxidative stress in neurodegeneration: cause or consequence?', *Nat Med*, 10 Suppl: S18-25.

Andrew, R. J., K. A. Kellett, G. Thinakaran, and N. M. Hooper. 2016. 'A Greek Tragedy: The Growing Complexity of Alzheimer Amyloid Precursor Protein Proteolysis', *J Biol Chem*, 291: 19235-44.

Appelqvist, H., P. Waster, K. Kagedal, and K. Ollinger. 2013. 'The lysosome: from waste bag to potential therapeutic target', *J Mol Cell Biol*, 5: 214-26.

Avrahami, L., D. Farfara, M. Shaham-Kol, R. Vassar, D. Frenkel, and H. Eldar-Finkelman. 2013. 'Inhibition of glycogen synthase kinase-3 ameliorates beta-amyloid pathology and restores lysosomal acidification and mammalian target of rapamycin activity in the Alzheimer disease mouse model: *in vivo* and *in vitro* studies', *J Biol Chem*, 288: 1295-306.

Baker-Nigh, A., S. Vahedi, E. G. Davis, S. Weintraub, E. H. Bigio, W. L. Klein, and C. Geula. 2015. 'Neuronal amyloid-beta accumulation within cholinergic basal forebrain in aging and Alzheimer's disease', *Brain*, 138: 1722-37.

Benilova, I., E. Karran, and B. De Strooper. 2012. 'The toxic Abeta oligomer and Alzheimer's disease: an emperor in need of clothes', *Nat Neurosci*, 15: 349-57.

Benitez, B. A., B. Cooper, P. Pastor, S. C. Jin, E. Lorenzo, S. Cervantes, and C. Cruchaga. 2013. 'TREM2 is associated with the risk of Alzheimer's disease in Spanish population', *Neurobiol Aging*, 34: 1711 e15-7.

Billings, L. M., S. Oddo, K. N. Green, J. L. McGaugh, and F. M. LaFerla. 2005. 'Intraneuronal Abeta causes the onset of early Alzheimer's disease-related cognitive deficits in transgenic mice', *Neuron*, 45: 675-88.

Birnbaum, J. H., D. Wanner, A. F. Gietl, A. Saake, T. M. Kundig, C. Hock, R. M. Nitsch, and C. Tackenberg. 2018. 'Oxidative stress and altered mitochondrial protein expression in the absence of amyloid-beta and tau pathology in iPSC-derived neurons from sporadic Alzheimer's disease patients', *Stem Cell Res*, 27: 121-30.

Bjorkhem, I., M. Heverin, V. Leoni, S. Meaney, and U. Diczfalusy. 2006. 'Oxysterols and Alzheimer's disease', *Acta Neurol Scand Suppl*, 185: 43-9.

Bonda, D. J., X. Wang, G. Perry, A. Nunomura, M. Tabaton, X. Zhu, and M. A. Smith. 2010. 'Oxidative stress in Alzheimer disease: a possibility for prevention', *Neuropharmacology*, 59: 290-4.

Bowman, E. J., A. Siebers, and K. Altendorf. 1988. 'Bafilomycins: a class of inhibitors of membrane ATPases from microorganisms, animal cells, and plant cells', *Proc Natl Acad Sci U S A*, 85: 7972-6.

Bradshaw, M. J., and A. Venkatesan. 2016. 'Herpes Simplex Virus-1 Encephalitis in Adults: Pathophysiology, Diagnosis, and Management', *Neurotherapeutics*, 13: 493-508.

Braulke, T., and J. S. Bonifacino. 2009. 'Sorting of lysosomal proteins', *Biochim Biophys Acta*, 1793: 605-14.

Brinckerhoff, C. E., and L. M. Matrisian. 2002. 'Matrix metalloproteinases: a tail of a frog that became a prince', *Nat Rev Mol Cell Biol*, 3: 207-14.

Brown, W. J., J. Goodhouse, and M. G. Farquhar. 1986. 'Mannose-6-phosphate receptors for lysosomal enzymes cycle between the Golgi complex and endosomes', *J Cell Biol*, 103: 1235-47.

Brzdak, P., D. Nowak, G. Wiera, and J. W. Mozrzymas. 2017. 'Multifaceted Roles of Metzincins in CNS Physiology and Pathology: From Synaptic Plasticity and Cognition to Neurodegenerative Disorders', *Front Cell Neurosci*, 11: 178.

Buache, E., R. Thai, C. Wendling, F. Alpy, A. Page, M. P. Chenard, V. Dive, M. Ruff, A. Dejaegere, C. Tomasetto, and M. C. Rio. 2014. 'Functional relationship between matrix metalloproteinase-11 and matrix metalloproteinase-14', *Cancer Med*, 3: 1197-210.

Bucci, C., P. Thomsen, P. Nicoziani, J. McCarthy, and B. van Deurs. 2000. 'Rab7: a key to lysosome biogenesis', *Mol Biol Cell*, 11: 467-80.

Bunker, V. W. 1992. 'Free radicals, antioxidants and aging', *Med Lab Sci*, 49: 299-312.

Burgos, J. S., C. Ramirez, I. Sastre, M. J. Bullido, and F. Valdivieso. 2002. 'Involvement of apolipoprotein E in the hematogenous route of herpes simplex virus type 1 to the central nervous system', *J Virol*, 76: 12394-8.

Burgos, J. S., C. Ramirez, I. Sastre, M. J. Bullido, and F. Valdivieso. 2003. 'ApoE4 is more efficient than E3 in brain access by herpes simplex virus type 1', *Neuroreport*, 14: 1825-7

Burgos, J. S., C. Ramirez, I. Sastre, and F. Valdivieso. 2006. 'Effect of apolipoprotein E on the cerebral load of latent herpes simplex virus type 1 DNA', *J Virol*, 80: 5383-7.

Buttle, D. J., M. Murata, C. G. Knight, and A. J. Barrett. 1992. 'CA074 methyl ester: a proinhibitor for intracellular cathepsin B', *Arch Biochem Biophys*, 299: 377-80.

Cai, Z., B. Zhao, and A. Ratka. 2011. 'Oxidative stress and beta-amyloid protein in Alzheimer's disease', *Neuromolecular Med*, 13: 223-50.

Cappai, R., and K. J. Barnham. 2008. 'Delineating the mechanism of Alzheimer's disease A beta peptide neurotoxicity', *Neurochem Res*, 33: 526-32.

Carrascosa, A. L., J. F. Santaren, and E. Vinuela. 1982. 'Production and titration of African swine fever virus in porcine alveolar macrophages', *J Virol Methods*, 3: 303-10.

Caspersen, C., N. Wang, J. Yao, A. Sosunov, X. Chen, J. W. Lustbader, H. W. Xu, D. Stern, G. McKhann, and S. D. Yan. 2005. 'Mitochondrial Abeta: a potential focal point for neuronal metabolic dysfunction in Alzheimer's disease', *FASEB J*, 19: 2040-1.

Cataldo, A. M., J. L. Barnett, S. A. Berman, J. Li, S. Quarless, S. Bursztajn, C. Lippa, and R. A. Nixon. 1995. 'Gene expression and cellular content of cathepsin D in Alzheimer's disease brain: evidence for early up-regulation of the endosomal-lysosomal system', *Neuron*, 14: 671-80.

Cataldo, A. M., J. L. Barnett, D. M. Mann, and R. A. Nixon. 1996. 'Colocalization of lysosomal hydrolase and beta-amyloid in diffuse plaques of the cerebellum and striatum in Alzheimer's disease and Down's syndrome', *J Neuropathol Exp Neurol*, 55: 704-15.

Cataldo, A. M., P. A. Paskevich, E. Kominami, and R. A. Nixon. 1991. 'Lysosomal hydrolases of different classes are abnormally distributed in brains of patients with Alzheimer disease', *Proc Natl Acad Sci U S A*, 88: 10998-1002.

Cataldo, A. M., S. Petanceska, N. B. Terio, C. M. Peterhoff, R. Durham, M. Mercken, P. D. Mehta, J. Buxbaum, V. Haroutunian, and R. A. Nixon. 2004. 'Abeta localization in abnormal endosomes: association with earliest Abeta elevations in AD and Down syndrome', *Neurobiol Aging*, 25: 1263-72.

Cataldo, A. M., C. M. Peterhoff, J. C. Troncoso, T. Gomez-Isla, B. T. Hyman, and R. A. Nixon. 2000. 'Endocytic pathway abnormalities precede amyloid beta deposition in sporadic Alzheimer's disease and Down syndrome: differential effects of APOE genotype and presenilin mutations', *Am J Pathol*, 157: 277-86.

Cataldo, A. M., C. Y. Thayer, E. D. Bird, T. R. Wheelock, and R. A. Nixon. 1990. 'Lysosomal proteinase antigens are prominently localized within senile plaques of Alzheimer's disease: evidence for a neuronal origin', *Brain Res*, 513: 181-92.

Cermak, S., M. Kosicek, A. Mladenovic-Djordjevic, K. Smiljanic, S. Kanazir, and S. Hecimovic. 2016. 'Loss of Cathepsin B and L Leads to Lysosomal Dysfunction, NPC-Like Cholesterol Sequestration and Accumulation of the Key Alzheimer's Proteins', *PLoS One*, 11: e0167428.

Chambers, S. M., C. A. Fasano, E. P. Papapetrou, M. Tomishima, M. Sadelain, and L. Studer. 2009. 'Highly efficient neural conversion of human ES and iPS cells by dual inhibition of SMAD signaling', *Nat Biotechnol*, 27: 275-80.

Cheng, F., R. Cappai, G. D. Ciccotosto, G. Svensson, G. Multhaup, L. A. Fransson, and K. Mani. 2011. 'Suppression of amyloid beta A11 antibody immunoreactivity by vitamin C: possible role of heparan sulfate oligosaccharides derived from glypican-1 by ascorbate-induced, nitric oxide (NO)-catalyzed degradation', *J Biol Chem*, 286: 27559-72.

Cho, K., S. Y. Yoon, J. E. Choi, H. J. Kang, H. Y. Jang, and D. H. Kim. 2013. 'CA-074 Me, a cathepsin B inhibitor, decreases APP accumulation and protects primary rat cortical neurons treated with okadaic acid', *Neurosci Lett*, 548: 222-7.

Cline, E. N., M. A. Bicca, K. L. Viola, and W. L. Klein. 2018. 'The Amyloid-beta Oligomer Hypothesis: Beginning of the Third Decade', *J Alzheimers Dis*, 64: S567-S610.

Corder, E. H., A. M. Saunders, N. J. Risch, W. J. Strittmatter, D. E. Schmechel, P. C. Gaskell, Jr., J. B. Rimmler, P. A. Locke, P. M. Conneally, K. E. Schmader, and et al., 1994. 'Protective effect of apolipoprotein E type 2 allele for late onset Alzheimer disease', *Nat Genet*, 7: 180-4.

Corder, E. H., A. M. Saunders, W. J. Strittmatter, D. E. Schmechel, P. C. Gaskell, G. W. Small, A. D. Roses, J. L. Haines, and M. A. Pericak-Vance. 1993. 'Gene dose of apolipoprotein E type 4 allele and the risk of Alzheimer's disease in late onset families', *Science*, 261: 921-3.

Cruchaga, C., G. Haller, S. Chakraverty, K. Mayo, F. L. Vallania, R. D. Mitra, K. Faber, J. Williamson, T. Bird, R. Diaz-Arrastia, T. M. Foroud, B. F. Boeve, N. R. Graff-Radford, P. St Jean, M. Lawson, M. G. Ehm, R. Mayeux, A. M. Goate, and Nia-Load Ncrad Family Study Consortium. 2012. 'Rare variants in APP, PSEN1 and PSEN2 increase risk for AD in late-onset Alzheimer's disease families', *PLoS One*, 7: e31039.

Cruchaga, C., C. M. Karch, S. C. Jin, B. A. Benitez, Y. Cai, R. Guerreiro, O. Harari, J. Norton, J. Budde, S. Bertelsen, A. T. Jeng, B. Cooper, T. Skorupa, D. Carrell, D. Levitch, S. Hsu, J. Choi, M. Ryten, C. Sassi, J. Bras, R. J. Gibbs, D. G. Hernandez, M. K. Lupton, J. Powell, P. Forabosco, P. G. Ridge, C. D. Corcoran, J. T. Tschanz, M. C. Norton, R. G. Munger, C. Schmutz, M. Leary, F. Y. Demirci, M. N. Bamne, X. Wang, O. L. Lopez, M. Ganguli, C. Medway, J. Turton, J. Lord, A. Braae, I. Barber, K. Brown, U. K. Consortium Alzheimer's Research, P. Pastor, O. Lorenzo-Betancor, Z. Brkanac, E. Scott, E. Topol, K. Morgan, E. Rogaeva, A. Singleton, J. Hardy, M. I. Kamboh, P. S. George-Hyslop, N. Cairns, J. C. Morris, J. S. K. Kauwe, and A. M. Goate. 2014. 'Rare coding variants in the phospholipase D3 gene confer risk for Alzheimer's disease', *Nature*, 505: 550-54.

Cummings, J., G. Lee, A. Ritter, and K. Zhong. 2018. 'Alzheimer's disease drug development pipeline: 2018', *Alzheimers Dement (N Y)*, 4: 195-214.

Cuyvers, E., and K. Sleegers. 2016. 'Genetic variations underlying Alzheimer's disease: evidence from genome-wide association studies and beyond', *Lancet Neurol*, 15: 857-68.

Dalton, T. P., H. G. Shertzer, and A. Puga. 1999. 'Regulation of gene expression by reactive oxygen', *Annu Rev Pharmacol Toxicol*, 39: 67-101.

De Strooper, B., and W. Annaert. 2000. 'Proteolytic processing and cell biological functions of the amyloid precursor protein', *J Cell Sci*, 113 (Pt 11): 1857-70.

Eimer, W. A., D. K. Vijaya Kumar, N. K. Navalpur Shanmugam, A. S. Rodriguez, T. Mitchell, K. J. Washicosky, B. Gyorgy, X. O. Breakefield, R. E. Tanzi, and R. D.

Moir. 2018. 'Alzheimer's Disease-Associated beta-Amyloid Is Rapidly Seeded by Herpesviridae to Protect against Brain Infection', *Neuron*, 99: 56-63 e3.

Eiraku, M., K. Watanabe, M. Matsuo-Takasaki, M. Kawada, S. Yonemura, M. Matsumura, T. Wataya, A. Nishiyama, K. Muguruma, and Y. Sasai. 2008. 'Self-organized formation of polarized cortical tissues from ESCs and its active manipulation by extrinsic signals', *Cell Stem Cell*, 3: 519-32.

Eskelinen, E. L., Y. Tanaka, and P. Saftig. 2003. 'At the acidic edge: emerging functions for lysosomal membrane proteins', *Trends Cell Biol*, 13: 137-45.

Fields, B.N., D.M. Knipe, and P.M. Howley, Fields virology. 3rd ed. 1996, Philadelphia:

Lippincott - Raven Press.

Filocamo, M., and A. Morrone. 2011. 'Lysosomal storage disorders: molecular basis and laboratory testing', *Hum Genomics*, 5: 156-69.

Finkel, T., and N. J. Holbrook. 2000. 'Oxidants, oxidative stress and the biology of aging', *Nature*, 408: 239-47.

Frackowiak, J., A. Zoltowska, and H. M. Wisniewski. 1994. 'Non-fibrillar beta-amyloid protein is associated with smooth muscle cells of vessel walls in Alzheimer disease', *J Neuropathol Exp Neurol*, 53: 637-45.

Frost, J. L., B. Liu, J. U. Rahfeld, M. Kleinschmidt, B. O'Nuallain, K. X. Le, I. Lues, B. J. Caldarone, S. Schilling, H. U. Demuth, and C. A. Lemere. 2015. 'An anti-pyroglutamate-3 Abeta vaccine reduces plaques and improves cognition in APPswe/PS1DeltaE9 mice', *Neurobiol Aging*, 36: 3187-99.

Fulop, T., R. F. Itzhaki, B. J. Balin, J. Miklossy, and A. E. Barron. 2018. 'Role of Microbes in the Development of Alzheimer's Disease: State of the Art - An International Symposium Presented at the 2017 IAGG Congress in San Francisco', *Front Genet*, 9: 362.

Gabbita, S. P., M. A. Lovell, and W. R. Markesbery. 1998. 'Increased nuclear DNA oxidation in the brain in Alzheimer's disease', *J Neurochem*, 71: 2034-40.

Gamaley, I. A., and I. V. Klyubin. 1999. 'Roles of reactive oxygen species: signaling and regulation of cellular functions', *Int Rev Cytol*, 188: 203-55.

Gerard, H. C., U. Dreses-Werringloer, K. S. Wildt, S. Deka, C. Oszust, B. J. Balin, W. H. Frey, 2nd, E. Z. Bordayo, J. A. Whittum-Hudson, and A. P. Hudson. 2006. 'Chlamydophila (Chlamydia) pneumoniae in the Alzheimer's brain', *FEMS Immunol Med Microbiol*, 48: 355-66.

Ghosh, P., N. M. Dahms, and S. Kornfeld. 2003. 'Mannose 6-phosphate receptors: new twists in the tale', *Nat Rev Mol Cell Biol*, 4: 202-12.

Gibson, G. E., and H. M. Huang. 2005. 'Oxidative stress in Alzheimer's disease', *Neurobiol Aging*, 26: 575-8.

Giraldo, M., F. Lopera, A. L. Siniard, J. J. Corneveaux, I. Schrauwen, J. Carvajal, C. Munoz, M. Ramirez-Restrepo, C. Gaiteri, A. J. Myers, R. J. Caselli, K. S. Kosik, E. M. Reiman, and M. J. Huentelman. 2013. 'Variants in triggering receptor expressed on myeloid cells 2 are associated with both behavioral variant frontotemporal lobar degeneration and Alzheimer's disease', *Neurobiol Aging*, 34: 2077 e11-8.

Glabe, C. G. 2008. 'Structural classification of toxic amyloid oligomers', *J Biol Chem*, 283: 29639-43.

Gonzalez Murcia, J. D., C. Schmutz, C. Munger, A. Perkes, A. Gustin, M. Peterson, M. T. Ebbert, M. C. Norton, J. T. Tschanz, R. G. Munger, C. D. Corcoran, and J. S. Kauwe. 2013. 'Assessment of TREM2 rs75932628 association with Alzheimer's disease in a population-based sample: the Cache County Study', *Neurobiol Aging*, 34: 2889 e11-3.

Grimm, M. O., V. C. Zimmer, J. Lehmann, H. S. Grimm, and T. Hartmann. 2013. 'The impact of cholesterol, DHA, and sphingolipids on Alzheimer's disease', *Biomed Res Int*, 2013: 814390.

Guerreiro, R., A. Wojtas, J. Bras, M. Carrasquillo, E. Rogaeva, E. Majounie, C. Cruchaga, C. Sassi, J. S. Kauwe, S. Younkin, L. Hazrati, J. Collinge, J. Pocock, T. Lashley, J. Williams, J. C. Lambert, P. Amouyel, A. Goate, R. Rademakers, K. Morgan, J. Powell, P. St George-Hyslop, A. Singleton, J. Hardy, and Group Alzheimer Genetic Analysis. 2013. 'TREM2 variants in Alzheimer's disease', *N Engl J Med*, 368: 117-27.

Haas, J. G., and R. Lathe. 2018. 'Microbes and Alzheimer's Disease: New Findings Call for a Paradigm Change', *Trends Neurosci*, 41: 570-73.

Hardy, J. 2009. 'The amyloid hypothesis for Alzheimer's disease: a critical reappraisal', *J Neurochem*, 110: 1129-34.

Harris, S. A., and E. A. Harris. 2015. 'Herpes Simplex Virus Type 1 and Other Pathogens are Key Causative Factors in Sporadic Alzheimer's Disease', *J Alzheimers Dis*, 48: 319-53.

Harris, S. A., and E. A. Harris. 2018. 'Molecular Mechanisms for Herpes Simplex Virus Type 1 Pathogenesis in Alzheimer's Disease', *Front Aging Neurosci*, 10: 48.

Hernandez-Guillamon, M., S. Mawhirt, S. Blais, J. Montaner, T. A. Neubert, A. Rostagno, and J. Ghiso. 2015. 'Sequential Amyloid-beta Degradation by the Matrix Metalloproteases MMP-2 and MMP-9', *J Biol Chem*, 290: 15078-91.

Higashi, S., and K. Miyazaki. 2003. 'Novel processing of beta-amyloid precursor protein catalyzed by membrane type 1 matrix metalloproteinase releases a fragment lacking the inhibitor domain against gelatinase A', *Biochemistry*, 42: 6514-26.

Hook, G., J. Yu, T. Toneff, M. Kindy, and V. Hook. 2014. 'Brain pyroglutamate amyloid-beta is produced by cathepsin B and is reduced by the cysteine protease inhibitor E64d, representing a potential Alzheimer's disease therapeutic', *J Alzheimers Dis*, 41: 129-49.

Hook, V., T. Toneff, M. Bogyo, D. Greenbaum, K. F. Medzihradszky, J. Neveu, W. Lane, G. Hook, and T. Reisine. 2005. 'Inhibition of cathepsin B reduces beta-amyloid production in regulated secretory vesicles of neuronal chromaffin cells: evidence for cathepsin B as a candidate beta-secretase of Alzheimer's disease', *Biol Chem*, 386: 931-40.

Hossini, A. M., M. Megges, A. Prigione, B. Lichtner, M. R. Toliat, W. Wruck, F. Schroter, P. Nuernberg, H. Kroll, E. Makrantonaki, C. C. Zouboulis, and J. Adjaye. 2015. 'Induced pluripotent stem cell-derived neuronal cells from a sporadic Alzheimer's disease donor as a model for investigating AD-associated gene regulatory networks', *BMC Genomics*, 16: 84.

Hung, S. Y., W. P. Huang, H. C. Liou, and W. M. Fu. 2009. 'Autophagy protects neuron from Abeta-induced cytotoxicity', *Autophagy*, 5: 502-10.

Ishidoh, K., and E. Kominami. 2002. 'Processing and activation of lysosomal proteinases', *Biol Chem*, 383: 1827-31.

Israel, M. A., S. H. Yuan, C. Bardy, S. M. Reyna, Y. Mu, C. Herrera, M. P. Hefferan, S. Van Gorp, K. L. Nazor, F. S. Boscolo, C. T. Carson, L. C. Laurent, M. Marsala, F. H. Gage, A. M. Remes, E. H. Koo, and L. S. Goldstein. 2012. 'Probing sporadic and familial Alzheimer's disease using induced pluripotent stem cells', *Nature*, 482: 216-20.

Itzhaki, R. F. 2014. 'Herpes simplex virus type 1 and Alzheimer's disease: increasing evidence for a major role of the virus', *Front Aging Neurosci*, 6: 202.

Itzhaki, R. F. 2016. 'Herpes and Alzheimer's Disease: Subversion in the Central Nervous System and How It Might Be Halted', *J Alzheimers Dis*, 54: 1273-81.

Itzhaki, R. F., S. L. Cosby, and M. A. Wozniak. 2008. 'Herpes simplex virus type 1 and Alzheimer's disease: the autophagy connection', *J Neurovirol*, 14: 1-4.

Itzhaki, R. F., W. R. Lin, D. Shang, G. K. Wilcock, B. Faragher, and G. A. Jamieson. 1997. 'Herpes simplex virus type 1 in brain and risk of Alzheimer's disease', *Lancet*, 349: 241-4.

Jamieson, G. A., N. J. Maitland, G. K. Wilcock, J. Craske, and R. F. Itzhaki. 1991. 'Latent herpes simplex virus type 1 in normal and Alzheimer's disease brains', *J Med Virol*, 33: 224-7.

Jan, A., O. Gokce, R. Luthi-Carter, and H. A. Lashuel. 2008. 'The ratio of monomeric to aggregated forms of Abeta40 and Abeta42 is an important determinant of amyloid-beta aggregation, fibrillogenesis, and toxicity', *J Biol Chem*, 283: 28176-89.

Jiang, S., Y. Li, X. Zhang, G. Bu, H. Xu, and Y. W. Zhang. 2014. 'Trafficking regulation of proteins in Alzheimer's disease', *Mol Neurodegener*, 9: 6.

Jiang, T., J. T. Yu, X. C. Zhu, and L. Tan. 2013. 'TREM2 in Alzheimer's disease', *Mol Neurobiol*, 48: 180-5.

Jonsson, T., H. Stefansson, S. Steinberg, I. Jonsdottir, P. V. Jonsson, J. Snaedal, S. Bjornsson, J. Huttenlocher, A. I. Levey, J. J. Lah, D. Rujescu, H. Hampel, I.

Giegling, O. A. Andreassen, K. Engedal, I. Ulstein, S. Djurovic, C. Ibrahim-Verbaas, A. Hofman, M. A. Ikram, C. M. van Duijn, U. Thorsteinsdottir, A. Kong, and K. Stefansson. 2013. 'Variant of TREM2 associated with the risk of Alzheimer's disease', *N Engl J Med*, 368: 107-16.

Jorm, A. F., and D. Jolley. 1998. 'The incidence of dementia: a meta-analysis', *Neurology*, 51: 728-33.

Kang, J., H. G. Lemaire, A. Unterbeck, J. M. Salbaum, C. L. Masters, K. H. Grzeschik, G. Multhaup, K. Beyreuther, and B. Muller-Hill. 1987. 'The precursor of Alzheimer's disease amyloid A4 protein resembles a cell-surface receptor', *Nature*, 325: 733-6.

Karch, C. M., and A. M. Goate. 2015. 'Alzheimer's disease risk genes and mechanisms of disease pathogenesis', *Biol Psychiatry*, 77: 43-51.

Kaushik, S., and A. M. Cuervo. 2012. 'Chaperone-mediated autophagy: a unique way to enter the lysosome world', *Trends Cell Biol*, 22: 407-17.

Kawahara, M., and Y. Kuroda. 2000. 'Molecular mechanism of neurodegeneration induced by Alzheimer's beta-amyloid protein: channel formation and disruption of calcium homeostasis', *Brain Res Bull*, 53: 389-97.

Kayed, R., Y. Sokolov, B. Edmonds, T. M. McIntire, S. C. Milton, J. E. Hall, and C. G. Glabe. 2004. 'Permeabilization of lipid bilayers is a common conformation-dependent activity of soluble amyloid oligomers in protein misfolding diseases', *J Biol Chem*, 279: 46363-6.

Kennedy, P. G., J. Rovnak, H. Badani, and R. J. Cohrs. 2015. 'A comparison of herpes simplex virus type 1 and varicella-zoster virus latency and reactivation', *J Gen Virol*, 96: 1581-602.

Kiffin, R., U. Bandyopadhyay, and A. M. Cuervo. 2006. 'Oxidative stress and autophagy', *Antioxid Redox Signal*, 8: 152-62.

Kitaguchi, N., Y. Takahashi, Y. Tokushima, S. Shiojiri, and H. Ito. 1988. 'Novel precursor of Alzheimer's disease amyloid protein shows protease inhibitory activity', *Nature*, 331: 530-2.

Klionsky, D.J., K. Abdelmohsen, A. Abe, M.J. Abedin, H. Abeliovich, A. Acevedo Arozena, H. Adachi, C.M. Adams, P.D. Adams, K. Adeli, P.J. Adhihetty, S.G. Adler, G. Agam, R. Agarwal, M.K. Aghi, M. Agnello, P. Agostinis, P.V. Aguilar, J. Aguirre-Ghiso, E.M. Airoldi, S. Ait-Si-Ali, T. Akematsu, E.T. Akporiaye, M. Al-Rubeai, G.M. Albaiceta, C. Albanese, D. Albani, M.L. Albert, J. Aldudo, H. Algul, M. Alirezaei, I. Alloza, A. Almasan, M. Almonte-Beceril, E.S. Alnemri, C. Alonso, N. Altan-Bonnet, D.C. Altieri, S. Alvarez, L. Alvarez-Erviti, S. Alves, G. Amadoro, A. Amano, C. Amantini, S. Ambrosio, I. Amelio, A.O. Amer, M. Amessou, A. Amon, Z. An, F.A. Anania, S.U. Andersen, U.P. Andley, C.K. Andreadi, N. Andrieu-Abadie, A. Anel, D.K. Ann, S. Anoopkumar-Dukie, M. Antonioli, H. Aoki, N. Apostolova, S. Aquila, K. Aquilano, K. Araki, E. Arama, A. Aranda, J. Araya, A. Arcaro, E. Arias, H. Arimoto, A.R. Ariosa, J.L. Armstrong, T. Arnould, I. Arsov, K. Asanuma, V. Askanas, E. Asselin, R. Atarashi, S.S. Atherton, J.D. Atkin, L.D.

Attardi, P. Auberger, G. Auburger, L. Aurelian, R. Autelli, L. Avagliano, M.L. Avantaggiati, L. Avrahami, S. Awale, N. Azad, T. Bachetti, J.M. Backer, D.H. Bae, J.S. Bae, O.N. Bae, S.H. Bae, E.H. Baehrecke, S.H. Baek, S. Baghdiguian, A. Bagniewska- Zadworna et al., Guidelines for the use and interpretation of assays for monitoring autophagy (3rd edition). Autophagy, 2016. 12(1): p. 1-222.

Kondo, T., K. Imamura, M. Funayama, K. Tsukita, M. Miyake, A. Ohta, K. Woltjen, M. Nakagawa, T. Asada, T. Arai, S. Kawakatsu, Y. Izumi, R. Kaji, N. Iwata, and H. Inoue. 2017. 'iPSC-Based Compound Screening and In Vitro Trials Identify a Synergistic Anti-amyloid beta Combination for Alzheimer's Disease', *Cell Rep*, 21: 2304-12.

Koprowski, H., Y. M. Zheng, E. Heber-Katz, N. Fraser, L. Rorke, Z. F. Fu, C. Hanlon, and B. Dietzschold. 1993. '*In vivo* expression of inducible nitric oxide synthase in experimentally induced neurologic diseases', *Proc Natl Acad Sci U S A*, 90: 3024-7.

Kountouras, J., E. Gavalas, C. Zavos, C. Stergiopoulos, D. Chatzopoulos, N. Kapetanakis, and D. Gisakis. 2007. 'Alzheimer's disease and Helicobacter pylori infection: Defective immune regulation and apoptosis as proposed common links', *Med Hypotheses*, 68: 378-88.

Koyuncu, O. O., I. B. Hogue, and L. W. Enquist. 2013. 'Virus infections in the nervous system', *Cell Host Microbe*, 13: 379-93.

Kristen, H., S. Santana, I. Sastre, M. Recuero, M. J. Bullido, and J. Aldudo. 2015. 'Herpes simplex virus type 2 infection induces AD-like neurodegeneration markers in human neuroblastoma cells', *Neurobiol Aging*, 36: 2737-47.

Kristen, H., I. Sastre, T. Munoz-Galdeano, M. Recuero, J. Aldudo, and M. J. Bullido. 2018. 'The lysosome system is severely impaired in a cellular model of neurodegeneration induced by HSV-1 and oxidative stress', *Neurobiol Aging*, 68: 5-17.

Kuperstein, I., K. Broersen, I. Benilova, J. Rozenski, W. Jonckheere, M. Debulpaep, A. Vandersteen, I. Segers-Nolten, K. Van Der Werf, V. Subramaniam, D. Braeken, G. Callewaert, C. Bartic, R. D'Hooge, I. C. Martins, F. Rousseau, J. Schymkowitz, and B. De Strooper. 2010. 'Neurotoxicity of Alzheimer's disease Abeta peptides is induced by small changes in the Abeta42 to Abeta40 ratio', *EMBO J*, 29: 3408-20.

LaFerla, F. M., K. N. Green, and S. Oddo. 2007. 'Intracellular amyloid-beta in Alzheimer's disease', *Nat Rev Neurosci*, 8: 499-509.

Lai, A., S. S. Sisodia, and I. S. Trowbridge. 1995. 'Characterization of sorting signals in the beta-amyloid precursor protein cytoplasmic domain', *J Biol Chem*, 270: 3565-73.

Lambert, J. C., S. Heath, G. Even, D. Campion, K. Sleegers, M. Hiltunen, O. Combarros, D. Zelenika, M. J. Bullido, B. Tavernier, L. Letenneur, K. Bettens, C. Berr, F. Pasquier, N. Fievet, P. Barberger-Gateau, S. Engelborghs, P. De Deyn, I. Mateo, A. Franck, S. Helisalmi, E. Porcellini, O. Hanon, Investigators European Alzheimer's Disease Initiative, M. M. de Pancorbo, C. Lendon, C. Dufouil, C. Jaillard, T. Leveillard, V. Alvarez, P. Bosco, M. Mancuso, F. Panza, B. Nacmias, P. Bossu, P. Piccardi, G. Annoni, D. Seripa, D. Galimberti, D. Hannequin, F. Licastro, H.

Soininen, K. Ritchie, H. Blanche, J. F. Dartigues, C. Tzourio, I. Gut, C. Van Broeckhoven, A. Alperovitch, M. Lathrop, and P. Amouyel. 2009. 'Genome-wide association study identifies variants at CLU and CR1 associated with Alzheimer's disease', *Nat Genet*, 41: 1094-9.

Lambert, J. C., C. A. Ibrahim-Verbaas, D. Harold, A. C. Naj, R. Sims, C. Bellenguez, A. L. DeStafano, J. C. Bis, G. W. Beecham, B. Grenier-Boley, G. Russo, T. A. Thorton-Wells, N. Jones, A. V. Smith, V. Chouraki, C. Thomas, M. A. Ikram, D. Zelenika, B. N. Vardarajan, Y. Kamatani, C. F. Lin, A. Gerrish, H. Schmidt, B. Kunkle, M. L. Dunstan, A. Ruiz, M. T. Bihoreau, S. H. Choi, C. Reitz, F. Pasquier, C. Cruchaga, D. Craig, N. Amin, C. Berr, O. L. Lopez, P. L. De Jager, V. Deramecourt, J. A. Johnston, D. Evans, S. Lovestone, L. Letenneur, F. J. Moron, D. C. Rubinsztein, G. Eiriksdottir, K. Sleegers, A. M. Goate, N. Fievet, M. W. Huentelman, M. Gill, K. Brown, M. I. Kamboh, L. Keller, P. Barberger-Gateau, B. McGuiness, E. B. Larson, R. Green, A. J. Myers, C. Dufouil, S. Todd, D. Wallon, S. Love, E. Rogaeva, J. Gallacher, P. St George-Hyslop, J. Clarimon, A. Lleo, A. Bayer, D. W. Tsuang, L. Yu, M. Tsolaki, P. Bossu, G. Spalletta, P. Proitsi, J. Collinge, S. Sorbi, F. Sanchez-Garcia, N. C. Fox, J. Hardy, M. C. Deniz Naranjo, P. Bosco, R. Clarke, C. Brayne, D. Galimberti, M. Mancuso, F. Matthews, Initiative European Alzheimer's Disease, Genetic, Disease Environmental Risk in Alzheimer's, Consortium Alzheimer's Disease Genetic, Heart Cohorts for, Epidemiology Aging Research in Genomic, S. Moebus, P. Mecocci, M. Del Zompo, W. Maier, H. Hampel, A. Pilotto, M. Bullido, F. Panza, P. Caffarra, B. Nacmias, J. R. Gilbert, M. Mayhaus, L. Lannefelt, H. Hakonarson, S. Pichler, M. M. Carrasquillo, M. Ingelsson, D. Beekly, V. Alvarez, F. Zou, O. Valladares, S. G. Younkin, E. Coto, K. L. Hamilton-Nelson, W. Gu, C. Razquin, P. Pastor, I. Mateo, M. J. Owen, K. M. Faber, P. V. Jonsson, O. Combarros, M. C. O'Donovan, L. B. Cantwell, H. Soininen, D. Blacker, S. Mead, T. H. Mosley, Jr., D. A. Bennett, T. B. Harris, L. Fratiglioni, C. Holmes, R. F. de Bruijn, P. Passmore, T. J. Montine, K. Bettens, J. I. Rotter, A. Brice, K. Morgan, T. M. Foroud, W. A. Kukull, D. Hannequin, J. F. Powell, M. A. Nalls, K. Ritchie, K. L. Lunetta, J. S. Kauwe, E. Boerwinkle, M. Riemenschneider, M. Boada, M. Hiltuenen, E. R. Martin, R. Schmidt, D. Rujescu, L. S. Wang, J. F. Dartigues, R. Mayeux, C. Tzourio, A. Hofman, M. M. Nothen, C. Graff, B. M. Psaty, L. Jones, J. L. Haines, P. A. Holmans, M. Lathrop, M. A. Pericak-Vance, L. J. Launer, L. A. Farrer, C. M. van Duijn, C. Van Broeckhoven, V. Moskvina, S. Seshadri, J. Williams, G. D. Schellenberg, and P. Amouyel. 2013. 'Meta-analysis of 74,046 individuals identifies 11 new susceptibility loci for Alzheimer's disease', *Nat Genet*, 45: 1452-8.

Lambert, J. C., D. Zelenika, M. Hiltunen, V. Chouraki, O. Combarros, M. J. Bullido, G. Tognoni, N. Fievet, A. Boland, B. Arosio, E. Coto, M. Del Zompo, I. Mateo, A. Frank-Garcia, S. Helisalmi, E. Porcellini, A. Pilotto, P. Forti, R. Ferri, M. Delepine, E. Scarpini, G. Siciliano, V. Solfrizzi, S. Sorbi, G. Spalletta, G. Ravaglia, F. Valdivieso, V. Alvarez, P. Bosco, M. Mancuso, F. Panza, B. Nacmias, P. Bossu, P. Piccardi, G. Annoni, D. Seripa, D. Galimberti, F. Licastro, M. Lathrop, H. Soininen, and P. Amouyel. 2011. 'Evidence of the association of BIN1 and PICALM with the AD risk in contrasting European populations', *Neurobiol Aging*, 32: 756 e11-5.

Lancaster, M. A., M. Renner, C. A. Martin, D. Wenzel, L. S. Bicknell, M. E. Hurles, T. Homfray, J. M. Penninger, A. P. Jackson, and J. A. Knoblich. 2013. 'Cerebral organoids model human brain development and microcephaly', *Nature*, 501: 373-9.

Lauritzen, I., R. Pardossi-Piquard, C. Bauer, E. Brigham, J. D. Abraham, S. Ranaldi, P. Fraser, P. St-George-Hyslop, O. Le Thuc, V. Espin, L. Chami, J. Dunys, and F. Checler. 2012. 'The beta-secretase-derived C-terminal fragment of betaAPP, C99, but not Abeta, is a key contributor to early intraneuronal lesions in triple-transgenic mouse hippocampus', *J Neurosci*, 32: 16243-1655a.

LeBlanc, A. C., R. Xue, and P. Gambetti. 1996. 'Amyloid precursor protein metabolism in primary cell cultures of neurons, astrocytes, and microglia', *J Neurochem*, 66: 2300-10.

Lee, J. H., W. H. Yu, A. Kumar, S. Lee, P. S. Mohan, C. M. Peterhoff, D. M. Wolfe, M. Martinez-Vicente, A. C. Massey, G. Sovak, Y. Uchiyama, D. Westaway, A. M. Cuervo, and R. A. Nixon. 2010. 'Lysosomal proteolysis and autophagy require presenilin 1 and are disrupted by Alzheimer-related PS1 mutations', *Cell*, 141: 1146-58.

Lesne, S., M. T. Koh, L. Kotilinek, R. Kayed, C. G. Glabe, A. Yang, M. Gallagher, and K. H. Ashe. 2006. 'A specific amyloid-beta protein assembly in the brain impairs memory', *Nature*, 440: 352-7.

Letenneur, L., K. Peres, H. Fleury, I. Garrigue, P. Barberger-Gateau, C. Helmer, J. M. Orgogozo, S. Gauthier, and J. F. Dartigues. 2008. 'Seropositivity to herpes simplex virus antibodies and risk of Alzheimer's disease: a population-based cohort study', *PLoS One*, 3: e3637.

Lewis, J., D. W. Dickson, W. L. Lin, L. Chisholm, A. Corral, G. Jones, S. H. Yen, N. Sahara, L. Skipper, D. Yager, C. Eckman, J. Hardy, M. Hutton, and E. McGowan. 2001. 'Enhanced neurofibrillary degeneration in transgenic mice expressing mutant tau and APP', *Science*, 293: 1487-91.

Li, W. W., J. Li, and J. K. Bao. 2012. 'Microautophagy: lesser-known self-eating', *Cell Mol Life Sci*, 69: 1125-36.

Li, X. J., Z. W. Du, E. D. Zarnowska, M. Pankratz, L. O. Hansen, R. A. Pearce, and S. C. Zhang. 2005. 'Specification of motoneurons from human embryonic stem cells', *Nat Biotechnol*, 23: 215-21.

Liao, M. C., and W. E. Van Nostrand. 2010. 'Degradation of soluble and fibrillar amyloid beta-protein by matrix metalloproteinase (MT1-MMP) *in vitro*', *Biochemistry*, 49: 1127-36.

Licastro, F., I. Carbone, M. Ianni, and E. Porcellini. 2011. 'Gene signature in Alzheimer's disease and environmental factors: the virus chronicle', *J Alzheimers Dis*, 27: 809-17.

Lin, T. K., G. Hughes, A. Muratovska, F. H. Blaikie, P. S. Brookes, V. Darley-Usmar, R. A. Smith, and M. P. Murphy. 2002. 'Specific modification of mitochondrial protein

thiols in response to oxidative stress: a proteomics approach', *J Biol Chem*, 277: 17048-56.

Liu, P., M. N. Reed, L. A. Kotilinek, M. K. Grant, C. L. Forster, W. Qiang, S. L. Shapiro, J. H. Reichl, A. C. Chiang, J. L. Jankowsky, C. M. Wilmot, J. P. Cleary, K. R. Zahs, and K. H. Ashe. 2015. 'Quaternary Structure Defines a Large Class of Amyloid-beta Oligomers Neutralized by Sequestration', *Cell Rep*, 11: 1760-71.

Lorenzen, A., J. Samosh, K. Vandewark, P. H. Anborgh, C. Seah, A. C. Magalhaes, S. P. Cregan, S. S. Ferguson, and S. H. Pasternak. 2010. 'Rapid and direct transport of cell surface APP to the lysosome defines a novel selective pathway', *Mol Brain*, 3: 11.

Lovheim, H., J. Gilthorpe, R. Adolfsson, L. G. Nilsson, and F. Elgh. 2015. 'Reactivated herpes simplex infection increases the risk of Alzheimer's disease', *Alzheimers Dement*, 11: 593-9.

Lubke, T., P. Lobel, and D. E. Sleat. 2009. 'Proteomics of the lysosome', *Biochim Biophys Acta*, 1793: 625-35.

Mach, L., J. S. Mort, and J. Glossl. 1994. 'Noncovalent complexes between the lysosomal proteinase cathepsin B and its propeptide account for stable, extracellular, high molecular mass forms of the enzyme', *J Biol Chem*, 269: 13036-40.

Malnar, M., S. Hecimovic, N. Mattsson, and H. Zetterberg. 2014. 'Bidirectional links between Alzheimer's disease and Niemann-Pick type C disease', *Neurobiol Dis*, 72 Pt A: 37-47.

Man, S. M., and T. D. Kanneganti. 2016. 'Regulation of lysosomal dynamics and autophagy by CTSB/cathepsin B', *Autophagy*, 12: 2504-05.

Markesbery, W. R., and J. M. Carney. 1999. 'Oxidative alterations in Alzheimer's disease', *Brain Pathol*, 9: 133-46.

Marques, C. P., M. C. Cheeran, J. M. Palmquist, S. Hu, and J. R. Lokensgard. 2008. 'Microglia are the major cellular source of inducible nitric oxide synthase during experimental herpes encephalitis', *J Neurovirol*, 14: 229-38.

Marquez-Sterling, N. R., A. C. Lo, S. S. Sisodia, and E. H. Koo. 1997. 'Trafficking of cell-surface beta-amyloid precursor protein: evidence that a sorting intermediate participates in synaptic vesicle recycling', *J Neurosci*, 17: 140-51.

Martinez-Torres, F. J., S. Wagner, J. Haas, R. Kehm, J. Sellner, W. Hacke, and U. Meyding-Lamade. 2004. 'Increased presence of matrix metalloproteinases 2 and 9 in short- and long-term experimental herpes simplex virus encephalitis', *Neurosci Lett*, 368: 274-8.

Martins, S., H. Yigit, M. Bohndorf, N. Graffmann, A. R. Fiszl, W. Wruck, K. Sleegers, C. Van Broeckhoven, and J. Adjaye. 2018a. 'Lymphoblast-derived integration-free iPSC line AD-TREM2-1 from a 67year-old Alzheimer's disease patient expressing the TREM2 p.R47H variant', *Stem Cell Res*, 29: 60-63.

Martins, S., H. Yigit, M. Bohndorf, N. Graffmann, A. R. Fiszl, W. Wruck, K. Sleegers, C. Van Broeckhoven, and J. Adjaye. 2018. 'Lymphoblast-derived integration-free iPSC line AD-TREM2-3 from a 74year-old Alzheimer's disease patient expressing the TREM2 p.R47H variant', *Stem Cell Res*, 30: 141-44.

Masters, C. L., R. Bateman, K. Blennow, C. C. Rowe, R. A. Sperling, and J. L. Cummings. 2015. 'Alzheimer's disease', *Nat Rev Dis Primers*, 1: 15056.

Maxfield, F. R., and T. E. McGraw. 2004. 'Endocytic recycling', *Nat Rev Mol Cell Biol*, 5: 121-32.

Meyding-Lamade, U., J. Haas, W. Lamade, K. Stingele, R. Kehm, A. Fath, K. Heinrich, B. Storch Hagenlocher, and B. Wildemann. 1998. 'Herpes simplex virus encephalitis: long-term comparative study of viral load and the expression of immunologic nitric oxide synthase in mouse brain tissue', *Neurosci Lett*, 244: 9-12.

Miklossy, J. 2011. 'Emerging roles of pathogens in Alzheimer disease', *Expert Rev Mol Med*, 13: e30.

Milatovic, D., Y. Zhang, S. J. Olson, K. S. Montine, L. J. Roberts, 2nd, J. D. Morrow, T. J. Montine, T. S. Dermody, and T. Valyi-Nagy. 2002. 'Herpes simplex virus type 1 encephalitis is associated with elevated levels of F2-isoprostanes and F4-neuroprostanes', *J Neurovirol*, 8: 295-305.

Moir, R. D., R. Lathe, and R. E. Tanzi. 2018. 'The antimicrobial protection hypothesis of Alzheimer's disease', *Alzheimers Dement*.

Mori, H., R. Bhat, A. Bruni-Cardoso, E. I. Chen, D. M. Jorgens, K. Coutinho, K. Louie, B. B. Bowen, J. L. Inman, V. Tecca, S. J. Lee, S. Becker-Weimann, T. Northen, M. Seiki, A. D. Borowsky, M. Auer, and M. J. Bissell. 2016. 'New insight into the role of MMP14 in metabolic balance', *PeerJ*, 4: e2142.

Mueller-Steiner, S., Y. Zhou, H. Arai, E. D. Roberson, B. Sun, J. Chen, X. Wang, G. Yu, L. Esposito, L. Mucke, and L. Gan. 2006. 'Antiamyloidogenic and neuroprotective functions of cathepsin B: implications for Alzheimer's disease', *Neuron*, 51: 703-14.

Muller, U. C., T. Deller, and M. Korte. 2017. 'Not just amyloid: physiological functions of the amyloid precursor protein family', *Nat Rev Neurosci*, 18: 281-98.

Murakami, K. 2014. 'Conformation-specific antibodies to target amyloid beta oligomers and their application to immunotherapy for Alzheimer's disease', *Biosci Biotechnol Biochem*, 78: 1293-305.

Muratore, C. R., P. Srikanth, D. G. Callahan, and T. L. Young-Pearse. 2014. 'Comparison and optimization of hiPSC forebrain cortical differentiation protocols', *PLoS One*, 9: e105807.

Murphy, G., and H. Nagase. 2008. 'Progress in matrix metalloproteinase research', *Mol Aspects Med*, 29: 290-308.

Naj, A. C., G. D. Schellenberg, and Consortium Alzheimer's Disease Genetics. 2017. 'Genomic variants, genes, and pathways of Alzheimer's disease: An overview', *Am J Med Genet B Neuropsychiatr Genet*, 174: 5-26.

Nakamura, S., and T. Yoshimori. 2017. 'New insights into autophagosome-lysosome fusion', *J Cell Sci*, 130: 1209-16.

Nakanishi, H. 2003. 'Neuronal and microglial cathepsins in aging and age-related diseases', *Aging Res Rev*, 2: 367-81.

Nalla, A. K., B. Gorantla, C. S. Gondi, S. S. Lakka, and J. S. Rao. 2010. 'Targeting MMP-9, uPAR, and cathepsin B inhibits invasion, migration and activates apoptosis in prostate cancer cells', *Cancer Gene Ther*, 17: 599-613.

Nhan, H. S., K. Chiang, and E. H. Koo. 2015. 'The multifaceted nature of amyloid precursor protein and its proteolytic fragments: friends and foes', *Acta Neuropathol*, 129: 1-19.

Nicoll, M. P., J. T. Proenca, and S. Efstathiou. 2012. 'The molecular basis of herpes simplex virus latency', *FEMS Microbiol Rev*, 36: 684-705.

Nixon, R. A. 2005. 'Endosome function and dysfunction in Alzheimer's disease and other neurodegenerative diseases', *Neurobiol Aging*, 26: 373-82.

Nixon, R. A. 2006. 'Autophagy in neurodegenerative disease: friend, foe or turncoat?', *Trends Neurosci*, 29: 528-35.

Nixon, R. A., and A. M. Cataldo. 1995. 'The endosomal-lysosomal system of neurons: new roles', *Trends Neurosci*, 18: 489-96.

Nixon, R. A., and D. S. Yang. 2011. 'Autophagy failure in Alzheimer's disease--locating the primary defect', *Neurobiol Dis*, 43: 38-45.

Nixon, R. A., D. S. Yang, and J. H. Lee. 2008. 'Neurodegenerative lysosomal disorders: a continuum from development to late age', *Autophagy*, 4: 590-9.

Nunomura, A., R. J. Castellani, X. Zhu, P. I. Moreira, G. Perry, and M. A. Smith. 2006. 'Involvement of oxidative stress in Alzheimer disease', *J Neuropathol Exp Neurol*, 65: 631-41.

Nunomura, A., G. Perry, G. Aliev, K. Hirai, A. Takeda, E. K. Balraj, P. K. Jones, H. Ghanbari, T. Wataya, S. Shimohama, S. Chiba, C. S. Atwood, R. B. Petersen, and M. A. Smith. 2001. 'Oxidative damage is the earliest event in Alzheimer disease', *J Neuropathol Exp Neurol*, 60: 759-67.

Nunomura, A., G. Perry, M. A. Pappolla, R. Wade, K. Hirai, S. Chiba, and M. A. Smith. 1999. 'RNA oxidation is a prominent feature of vulnerable neurons in Alzheimer's disease', *J Neurosci*, 19: 1959-64.

Obermajer, N., Z. Jevnikar, B. Doljak, and J. Kos. 2008. 'Role of cysteine cathepsins in matrix degradation and cell signalling', *Connect Tissue Res*, 49: 193-6.

Ochalek, A., B. Mihalik, H. X. Avci, A. Chandrasekaran, A. Teglasi, I. Bock, M. L. Giudice, Z. Tancos, K. Molnar, L. Laszlo, J. E. Nielsen, B. Holst, K. Freude, P. Hyttel, J. Kobolak, and A. Dinnyes. 2017. 'Neurons derived from sporadic Alzheimer's disease iPSCs reveal elevated TAU hyperphosphorylation, increased amyloid levels, and GSK3B activation', *Alzheimers Res Ther*, 9: 90.

Oddo, S., A. Caccamo, J. D. Shepherd, M. P. Murphy, T. E. Golde, R. Kayed, R. Metherate, M. P. Mattson, Y. Akbari, and F. M. LaFerla. 2003. 'Triple-transgenic model of Alzheimer's disease with plaques and tangles: intracellular Abeta and synaptic dysfunction', *Neuron*, 39: 409-21.

Ohkuma, S., and B. Poole. 1978. 'Fluorescence probe measurement of the intralysosomal pH in living cells and the perturbation of pH by various agents', *Proc Natl Acad Sci U S A*, 75: 3327-31.

Owen, D. J., C. M. Crump, and S. C. Graham. 2015. 'Tegument Assembly and Secondary Envelopment of Alphaherpesviruses', *Viruses*, 7: 5084-114.

Palu, G., M. A. Biasolo, G. Sartor, L. Masotti, E. Papini, M. Floreani, and P. Palatini. 1994. 'Effects of herpes simplex virus type 1 infection on the plasma membrane and related functions of HeLa S3 cells', *J Gen Virol*, 75 (Pt 12): 3337-44.

Pappolla, M. A., R. A. Omar, K. S. Kim, and N. K. Robakis. 1992. 'Immunohistochemical evidence of oxidative [corrected] stress in Alzheimer's disease', *Am J Pathol*, 140: 621-8.

Peric, A., and W. Annaert. 2015. 'Early etiology of Alzheimer's disease: tipping the balance toward autophagy or endosomal dysfunction?', *Acta Neuropathol*, 129: 363-81.

Persson, T., B. O. Popescu, and A. Cedazo-Minguez. 2014. 'Oxidative stress in Alzheimer's disease: why did antioxidant therapy fail?', *Oxid Med Cell Longev*, 2014: 427318.

Piper, R. C., and D. J. Katzmann. 2007. 'Biogenesis and function of multivesicular bodies', *Annu Rev Cell Dev Biol*, 23: 519-47.

Pisa, D., R. Alonso, A. Juarranz, A. Rabano, and L. Carrasco. 2015. 'Direct visualization of fungal infection in brains from patients with Alzheimer's disease', *J Alzheimers Dis*, 43: 613-24.

Platt, F. M., B. Boland, and A. C. van der Spoel. 2012. 'The cell biology of disease: lysosomal storage disorders: the cellular impact of lysosomal dysfunction', *J Cell Biol*, 199: 723-34.

Porcellini, E., I. Carbone, M. Ianni, and F. Licastro. 2010. 'Alzheimer's disease gene signature says: beware of brain viral infections', *Immun Aging*, 7: 16.

Portelius, E., T. Lashley, A. Westerlund, R. Persson, N. C. Fox, K. Blennow, T. Revesz, and H. Zetterberg. 2015. 'Brain amyloid-beta fragment signatures in pathological aging and Alzheimer's disease by hybrid immunoprecipitation mass spectrometry', *Neurodegener Dis*, 15: 50-7.

Porter, K., Y. Lin, and P. B. Liton. 2013. 'Cathepsin B is up-regulated and mediates extracellular matrix degradation in trabecular meshwork cells following phagocytic challenge', *PLoS One*, 8: e68668.

Porter, K., J. Nallathambi, Y. Lin, and P. B. Liton. 2013. 'Lysosomal basification and decreased autophagic flux in oxidatively stressed trabecular meshwork cells: implications for glaucoma pathogenesis', *Autophagy*, 9: 581-94.

Pottier, C., D. Wallon, S. Rousseau, A. Rovelet-Lecrux, A. C. Richard, A. Rollin-Sillaire, T. Frebourg, D. Campion, and D. Hannequin. 2013. 'TREM2 R47H variant as a risk factor for early-onset Alzheimer's disease', *J Alzheimers Dis*, 35: 45-9.

Py, N. A., A. E. Bonnet, A. Bernard, Y. Marchalant, E. Charrat, F. Checler, M. Khrestchatisky, K. Baranger, and S. Rivera. 2014. 'Differential spatio-temporal regulation of MMPs in the 5xFAD mouse model of Alzheimer's disease: evidence for a pro-amyloidogenic role of MT1-MMP', *Front Aging Neurosci*, 6: 247.

Ratnikov, B. I., P. Cieplak, K. Gramatikoff, J. Pierce, A. Eroshkin, Y. Igarashi, M. Kazanov, Q. Sun, A. Godzik, A. Osterman, B. Stec, A. Strongin, and J. W. Smith. 2014. 'Basis for substrate recognition and distinction by matrix metalloproteinases', *Proc Natl Acad Sci U S A*, 111: E4148-55.

Readhead, B., J. V. Haure-Mirande, C. C. Funk, M. A. Richards, P. Shannon, V. Haroutunian, M. Sano, W. S. Liang, N. D. Beckmann, N. D. Price, E. M. Reiman, E. E. Schadt, M. E. Ehrlich, S. Gandy, and J. T. Dudley. 2018. 'Multiscale Analysis of Independent Alzheimer's Cohorts Finds Disruption of Molecular, Genetic, and Clinical Networks by Human Herpesvirus', *Neuron*, 99: 64-82 e7.

Recuero, M., V. A. Munive, I. Sastre, J. Aldudo, F. Valdivieso, and M. J. Bullido. 2013. 'A free radical-generating system regulates AbetaPP metabolism/processing: involvement of the ubiquitin/proteasome and autophagy/lysosome pathways', *J Alzheimers Dis*, 34: 637-47.

Recuero, M., T. Munoz, J. Aldudo, M. Subias, M. J. Bullido, and F. Valdivieso. 2010. 'A free radical-generating system regulates APP metabolism/processing', *FEBS Lett*, 584: 4611-8.

Recuero, M., M. C. Vicente, A. Martinez-Garcia, M. C. Ramos, P. Carmona-Saez, I. Sastre, J. Aldudo, E. Vilella, A. Frank, M. J. Bullido, and F. Valdivieso. 2009. 'A free radical-generating system induces the cholesterol biosynthesis pathway: a role in Alzheimer's disease', *Aging Cell*, 8: 128-39.

Remacle, A. G., V. S. Golubkov, S. A. Shiryaev, R. Dahl, J. L. Stebbins, A. V. Chernov, A. V. Cheltsov, M. Pellecchia, and A. Y. Strongin. 2012. 'Novel MT1-MMP small-molecule inhibitors based on insights into hemopexin domain function in tumor growth', *Cancer Res*, 72: 2339-49.

Roberts, R. 2005. 'Lysosomal cysteine proteases: structure, function and inhibition of cathepsins', *Drug News Perspect*, 18: 605-14.

Rogaeva, E. 2002. 'The solved and unsolved mysteries of the genetics of early-onset Alzheimer's disease', *Neuromolecular Med*, 2: 1-10.

Rohrer, J., and R. Kornfeld. 2001. 'Lysosomal hydrolase mannose 6-phosphate uncovering enzyme resides in the trans-Golgi network', *Mol Biol Cell*, 12: 1623-31.

Roussos, P., P. Katsel, P. Fam, W. Tan, D. P. Purohit, and V. Haroutunian. 2015. 'The triggering receptor expressed on myeloid cells 2 (TREM2) is associated with enhanced inflammation, neuropathological lesions and increased risk for Alzheimer's dementia', *Alzheimers Dement*, 11: 1163-70.

Rowe, A. M., A. J. St Leger, S. Jeon, D. K. Dhaliwal, J. E. Knickelbein, and R. L. Hendricks. 2013. 'Herpes keratitis', *Prog Retin Eye Res*, 32: 88-101.

Ruiz, A., O. Dols-Icardo, M. J. Bullido, P. Pastor, E. Rodriguez-Rodriguez, A. Lopez de Munain, M. M. de Pancorbo, J. Perez-Tur, V. Alvarez, A. Antonell, J. Lopez-Arrieta, I. Hernandez, L. Tarraga, M. Boada, A. Lleo, R. Blesa, A. Frank-Garcia, I. Sastre, C. Razquin, S. Ortega-Cubero, E. Lorenzo, P. Sanchez-Juan, O. Combarros, F. Moreno, A. Gorostidi, X. Elcoroaristizabal, M. Baquero, E. Coto, R. Sanchez-Valle, J. Clarimon, and consortium dementia genetic Spanish. 2014. 'Assessing the role of the TREM2 p.R47H variant as a risk factor for Alzheimer's disease and frontotemporal dementia', *Neurobiol Aging*, 35: 444 e1-4.

Saftig, P., and J. Klumperman. 2009. 'Lysosome biogenesis and lysosomal membrane proteins: trafficking meets function', *Nat Rev Mol Cell Biol*, 10: 623-35.

Santana, S., M. J. Bullido, M. Recuero, F. Valdivieso, and J. Aldudo. 2012. 'Herpes simplex virus type I induces an incomplete autophagic response in human neuroblastoma cells', *J Alzheimers Dis*, 30: 815-31.

Santana, S., M. Recuero, M. J. Bullido, F. Valdivieso, and J. Aldudo. 2012. 'Herpes simplex virus type I induces the accumulation of intracellular beta-amyloid in autophagic compartments and the inhibition of the non-amyloidogenic pathway in human neuroblastoma cells', *Neurobiol Aging*, 33: 430 e19-33.

Santana, S., I. Sastre, M. Recuero, M. J. Bullido, and J. Aldudo. 2013. 'Oxidative stress enhances neurodegeneration markers induced by herpes simplex virus type 1 infection in human neuroblastoma cells', *PLoS One*, 8: e75842.

Schmechel, D. E., D. Goldgaber, D. S. Burkhart, J. R. Gilbert, D. C. Gajdusek, and A. D. Roses. 1988. 'Cellular localization of messenger RNA encoding amyloid-beta-protein in normal tissue and in Alzheimer disease', *Alzheimer Dis Assoc Disord*, 2: 96-111.

Schmid, C. D., L. N. Sautkulis, P. E. Danielson, J. Cooper, K. W. Hasel, B. S. Hilbush, J. G. Sutcliffe, and M. J. Carson. 2002. 'Heterogeneous expression of the triggering receptor expressed on myeloid cells-2 on adult murine microglia', *J Neurochem*, 83: 1309-20.

Selkoe, D. J., and J. Hardy. 2016. 'The amyloid hypothesis of Alzheimer's disease at 25 years', *EMBO Mol Med*, 8: 595-608.

Sela-Passwell, N., G. Rosenblum, T. Shoham, and I. Sagi. 2010. 'Structural and functional bases for allosteric control of MMP activities: can it pave the path for selective inhibition?', *Biochim Biophys Acta*, 1803: 29-38.

Shearman, M. S., C. I. Ragan, and L. L. Iversen. 1994. 'Inhibition of PC12 cell redox activity is a specific, early indicator of the mechanism of beta-amyloid-mediated cell death', *Proc Natl Acad Sci U S A*, 91: 1470-4.

Shulman, R. G., D. L. Rothman, K. L. Behar, and F. Hyder. 2004. 'Energetic basis of brain activity: implications for neuroimaging', *Trends Neurosci*, 27: 489-95.

Siest, G., T. Pillot, A. Regis-Bailly, B. Leininger-Muller, J. Steinmetz, M. M. Galteau, and S. Visvikis. 1995. 'Apolipoprotein E: an important gene and protein to follow in laboratory medicine', *Clin Chem*, 41: 1068-86.

Siintola, E., S. Partanen, P. Stromme, A. Haapanen, M. Haltia, J. Maehlen, A. E. Lehesjoki, and J. Tyynela. 2006. 'Cathepsin D deficiency underlies congenital human neuronal ceroid-lipofuscinosis', *Brain*, 129: 1438-45.

Sims, R., S. J. van der Lee, A. C. Naj, C. Bellenguez, N. Badarinarayan, J. Jakobsdottir, B. W. Kunkle, A. Boland, R. Raybould, J. C. Bis, E. R. Martin, B. Grenier-Boley, S. Heilmann-Heimbach, V. Chouraki, A. B. Kuzma, K. Sleegers, M. Vronskaya, A. Ruiz, R. R. Graham, R. Olaso, P. Hoffmann, M. L. Grove, B. N. Vardarajan, M. Hiltunen, M. M. Nothen, C. C. White, K. L. Hamilton-Nelson, J. Epelbaum, W. Maier, S. H. Choi, G. W. Beecham, C. Dulary, S. Herms, A. V. Smith, C. C. Funk, C. Derbois, A. J. Forstner, S. Ahmad, H. Li, D. Bacq, D. Harold, C. L. Satizabal, O. Valladares, A. Squassina, R. Thomas, J. A. Brody, L. Qu, P. Sanchez-Juan, T. Morgan, F. J. Wolters, Y. Zhao, F. S. Garcia, N. Denning, M. Fornage, J. Malamon, M. C. D. Naranjo, E. Majounie, T. H. Mosley, B. Dombroski, D. Wallon, M. K. Lupton, J. Dupuis, P. Whitehead, L. Fratiglioni, C. Medway, X. Jian, S. Mukherjee, L. Keller, K. Brown, H. Lin, L. B. Cantwell, F. Panza, B. McGuinness, S. Moreno-Grau, J. D. Burgess, V. Solfrizzi, P. Proitsi, H. H. Adams, M. Allen, D. Seripa, P. Pastor, L. A. Cupples, N. D. Price, D. Hannequin, A. Frank-Garcia, D. Levy, P. Chakrabarty, P. Caffarra, I. Giegling, A. S. Beiser, V. Giedraitis, H. Hampel, M. E. Garcia, X. Wang, L. Lannfelt, P. Mecocci, G. Eiriksdottir, P. K. Crane, F. Pasquier, V. Boccardi, I. Henandez, R. C. Barber, M. Scherer, L. Tarraga, P. M. Adams, M. Leber, Y. Chen, M. S. Albert, S. Riedel-Heller, V. Emilsson, D. Beekly, A. Braae, R. Schmidt, D. Blacker, C. Masullo, H. Schmidt, R. S. Doody, G. Spalletta, W. T. Longstreth, Jr., T. J. Fairchild, P. Bossu, O. L. Lopez, M. P. Frosch, E. Sacchinelli, B. Ghetti, Q. Yang, R. M. Huebinger, F. Jessen, S. Li, M. I. Kamboh, J. Morris, O. Sotolongo-Grau, M. J. Katz, C. Corcoran, M. Dunstan, A. Braddel, C. Thomas, A. Meggy, R. Marshall, A. Gerrish, J. Chapman, M. Aguilar, S. Taylor, M. Hill, M. D. Fairen, A. Hodges, B. Vellas, H. Soininen, I. Kloszewska, M. Daniilidou, J. Uphill, Y. Patel, J. T. Hughes, J. Lord, J. Turton, A. M. Hartmann, R. Cecchetti, C. Fenoglio, M. Serpente, M. Arcaro, C. Caltagirone, M. D. Orfei, A. Ciaramella, S. Pichler, M. Mayhaus, W. Gu, A. Lleo, J. Fortea, R. Blesa, I. S. Barber, K. Brookes, C. Cupidi, R. G. Maletta, D. Carrell, S. Sorbi, S. Moebus, M. Urbano, A. Pilotto, J. Kornhuber, P. Bosco, S. Todd, D. Craig, J. Johnston, M. Gill, B. Lawlor, A. Lynch, N. C. Fox, J. Hardy, Aruk Consortium, R. L. Albin, L. G. Apostolova, S. E. Arnold, S. Asthana, C. S. Atwood, C. T. Baldwin, L. L. Barnes, S. Barral, T. G. Beach, J. T. Becker, E. H. Bigio, T. D. Bird, B. F. Boeve, J. D. Bowen, A. Boxer, J. R. Burke, J. M. Burns, J. D. Buxbaum, N. J. Cairns, C. Cao, C. S. Carlson, C. M. Carlsson, R. M. Carney, M. M. Carrasquillo, S. L. Carroll, C. C. Diaz, H. C. Chui, D. G. Clark, D. H. Cribbs, E. A. Crocco, C. DeCarli, M. Dick, R. Duara, D. A. Evans, K. M. Faber, K. B. Fallon, D. W. Fardo, M. R. Farlow, S. Ferris, T. M. Foroud, D. R. Galasko, M. Gearing, D. H. Geschwind, J. R. Gilbert, N. R. Graff-Radford, R. C. Green, J. H. Growdon, R. L. Hamilton, L. E. Harrell, L. S. Honig, M. J. Huentelman, C. M. Hulette, B. T. Hyman, G. P. Jarvik, E. Abner, L. W. Jin, G. Jun, A. Karydas, J. A. Kaye, R. Kim, N. W. Kowall, J. H. Kramer, F. M. LaFerla, J. J. Lah, J. B. Leverenz, A. I. Levey, G. Li, A. P. Lieberman, K. L. Lunetta, C. G.

Lyketsos, D. C. Marson, F. Martiniuk, D. C. Mash, E. Masliah, W. C. McCormick, S. M. McCurry, A. N. McDavid, A. C. McKee, M. Mesulam, B. L. Miller, C. A. Miller, J. W. Miller, J. C. Morris, J. R. Murrell, A. J. Myers, S. O'Bryant, J. M. Olichney, V. S. Pankratz, J. E. Parisi, H. L. Paulson, W. Perry, E. Peskind, A. Pierce, W. W. Poon, H. Potter, J. F. Quinn, A. Raj, M. Raskind, B. Reisberg, C. Reitz, J. M. Ringman, E. D. Roberson, E. Rogaeva, H. J. Rosen, R. N. Rosenberg, M. A. Sager, A. J. Saykin, J. A. Schneider, L. S. Schneider, W. W. Seeley, A. G. Smith, J. A. Sonnen, S. Spina, R. A. Stern, R. H. Swerdlow, R. E. Tanzi, T. A. Thornton-Wells, J. Q. Trojanowski, J. C. Troncoso, V. M. Van Deerlin, L. J. Van Eldik, H. V. Vinters, J. P. Vonsattel, S. Weintraub, K. A. Welsh-Bohmer, K. C. Wilhelmsen, J. Williamson, T. S. Wingo, R. L. Woltjer, C. B. Wright, C. E. Yu, L. Yu, F. Garzia, F. Golamaully, G. Septier, S. Engelborghs, R. Vandenberghe, P. P. De Deyn, C. M. Fernadez, Y. A. Benito, H. Thonberg, C. Forsell, L. Lilius, A. Kinhult-Stahlbom, L. Kilander, R. Brundin, L. Concari, S. Helisalmi, A. M. Koivisto, A. Haapasalo, V. Dermecourt, N. Fievet, O. Hanon, C. Dufouil, A. Brice, K. Ritchie, B. Dubois, J. J. Himali, C. D. Keene, J. Tschanz, A. L. Fitzpatrick, W. A. Kukull, M. Norton, T. Aspelund, E. B. Larson, R. Munger, J. I. Rotter, R. B. Lipton, M. J. Bullido, A. Hofman, T. J. Montine, E. Coto, E. Boerwinkle, R. C. Petersen, V. Alvarez, F. Rivadeneira, E. M. Reiman, M. Gallo, C. J. O'Donnell, J. S. Reisch, A. C. Bruni, D. R. Royall, M. Dichgans, M. Sano, D. Galimberti, P. St George-Hyslop, E. Scarpini, D. W. Tsuang, M. Mancuso, U. Bonuccelli, A. R. Winslow, A. Daniele, C. K. Wu, Charge Adgc Eadi Gerad/Perades, O. Peters, B. Nacmias, M. Riemenschneider, R. Heun, C. Brayne, D. C. Rubinsztein, J. Bras, R. Guerreiro, A. Al-Chalabi, C. E. Shaw, J. Collinge, D. Mann, M. Tsolaki, J. Clarimon, R. Sussams, S. Lovestone, M. C. O'Donovan, M. J. Owen, T. W. Behrens, S. Mead, A. M. Goate, A. G. Uitterlinden, C. Holmes, C. Cruchaga, M. Ingelsson, D. A. Bennett, J. Powell, T. E. Golde, C. Graff, P. L. De Jager, K. Morgan, N. Ertekin-Taner, O. Combarros, B. M. Psaty, P. Passmore, S. G. Younkin, C. Berr, V. Gudnason, D. Rujescu, D. W. Dickson, J. F. Dartigues, A. L. DeStefano, S. Ortega-Cubero, H. Hakonarson, D. Campion, M. Boada, J. K. Kauwe, L. A. Farrer, C. Van Broeckhoven, M. A. Ikram, L. Jones, J. L. Haines, C. Tzourio, L. J. Launer, V. Escott-Price, R. Mayeux, J. F. Deleuze, N. Amin, P. A. Holmans, M. A. Pericak-Vance, P. Amouyel, C. M. van Duijn, A. Ramirez, L. S. Wang, J. C. Lambert, S. Seshadri, J. Williams, and G. D. Schellenberg. 2017. 'Rare coding variants in PLCG2, ABI3, and TREM2 implicate microglial-mediated innate immunity in Alzheimer's disease', *Nat Genet*, 49: 1373-84.

Smith, M. A., C. A. Rottkamp, A. Nunomura, A. K. Raina, and G. Perry. 2000. 'Oxidative stress in Alzheimer's disease', *Biochim Biophys Acta*, 1502: 139-44.

Snyder, E. M., Y. Nong, C. G. Almeida, S. Paul, T. Moran, E. Y. Choi, A. C. Nairn, M. W. Salter, P. J. Lombroso, G. K. Gouras, and P. Greengard. 2005. 'Regulation of NMDA receptor trafficking by amyloid-beta', *Nat Neurosci*, 8: 1051-8.

Soldano, A., and B. A. Hassan. 2014. 'Beyond pathology: APP, brain development and Alzheimer's disease', *Curr Opin Neurobiol*, 27: 61-7.

Sotthibundhu, A., A. M. Sykes, B. Fox, C. K. Underwood, W. Thangnipon, and E. J. Coulson. 2008. 'Beta-amyloid(1-42) induces neuronal death through the p75 neurotrophin receptor', *J Neurosci*, 28: 3941-6.

Srikanth, P., and T. L. Young-Pearse. 2014. 'Stem cells on the brain: modeling neurodevelopmental and neurodegenerative diseases using human induced pluripotent stem cells', *J Neurogenet*, 28: 5-29.

Steiner, I., P. G. Kennedy, and A. R. Pachner. 2007. 'The neurotropic herpes viruses: herpes simplex and varicella-zoster', *Lancet Neurol*, 6: 1015-28.

Steinman, R. M., I. S. Mellman, W. A. Muller, and Z. A. Cohn. 1983. 'Endocytosis and the recycling of plasma membrane', *J Cell Biol*, 96: 1-27.

Sullivan, S. E., and T. L. Young-Pearse. 2017. 'Induced pluripotent stem cells as a discovery tool for Alzheimers disease', *Brain Res*, 1656: 98-106.

Swerdlow, R. H., J. M. Burns, and S. M. Khan. 2014. 'The Alzheimer's disease mitochondrial cascade hypothesis: progress and perspectives', *Biochim Biophys Acta*, 1842: 1219-31.

Takahashi, K., K. Tanabe, M. Ohnuki, M. Narita, T. Ichisaka, K. Tomoda, and S. Yamanaka. 2007. 'Induction of pluripotent stem cells from adult human fibroblasts by defined factors', *Cell*, 131: 861-72.

Takahashi, K., and S. Yamanaka. 2006. 'Induction of pluripotent stem cells from mouse embryonic and adult fibroblast cultures by defined factors', *Cell*, 126: 663-76.

Takashima, A., K. Noguchi, K. Sato, T. Hoshino, and K. Imahori. 1993. 'Tau protein kinase I is essential for amyloid beta-protein-induced neurotoxicity', *Proc Natl Acad Sci U S A*, 90: 7789-93.

Takazawa, T., G. F. Croft, M. W. Amoroso, L. Studer, H. Wichterle, and A. B. Macdermott. 2012. 'Maturation of spinal motor neurons derived from human embryonic stem cells', *PLoS One*, 7: e40154.

Talmi-Frank, D., Z. Altboum, I. Solomonov, Y. Udi, D. A. Jaitin, M. Klepfish, E. David, A. Zhuravlev, H. Keren-Shaul, D. R. Winter, I. Gat-Viks, M. Mandelboim, T. Ziv, I. Amit, and I. Sagi. 2016. 'Extracellular Matrix Proteolysis by MT1-MMP Contributes to Influenza-Related Tissue Damage and Mortality', *Cell Host Microbe*, 20: 458-70.

Tanaka, S., S. Nakamura, K. Ueda, M. Kameyama, S. Shiojiri, Y. Takahashi, N. Kitaguchi, and H. Ito. 1988. 'Three types of amyloid protein precursor mRNA in human brain: their differential expression in Alzheimer's disease', *Biochem Biophys Res Commun*, 157: 472-9.

Taneo, J., T. Adachi, A. Yoshida, K. Takayasu, K. Takahara, and K. Inaba. 2015. 'Amyloid beta oligomers induce interleukin-1beta production in primary microglia in a cathepsin B- and reactive oxygen species-dependent manner', *Biochem Biophys Res Commun*, 458: 561-7.

Tanzi, R. E., D. M. Kovacs, T. W. Kim, R. D. Moir, S. Y. Guenette, and W. Wasco. 1996. 'The gene defects responsible for familial Alzheimer's disease', *Neurobiol Dis*, 3: 159-68.

Tholen, S., M. L. Biniossek, M. Gansz, T. D. Ahrens, M. Schlimpert, J. N. Kizhakkedathu, T. Reinheckel, and O. Schilling. 2014. 'Double deficiency of cathepsins B and L results in massive secretome alterations and suggests a degradative cathepsin-MMP axis', *Cell Mol Life Sci*, 71: 899-916.

Toei, M., R. Saum, and M. Forgac. 2010. 'Regulation and isoform function of the V-ATPases', *Biochemistry*, 49: 4715-23.

Tomic, J. L., A. Pensalfini, E. Head, and C. G. Glabe. 2009. 'Soluble fibrillar oligomer levels are elevated in Alzheimer's disease brain and correlate with cognitive dysfunction', *Neurobiol Dis*, 35: 352-8.

Tonnies, E., and E. Trushina. 2017. 'Oxidative Stress, Synaptic Dysfunction, and Alzheimer's Disease', *J Alzheimers Dis*, 57: 1105-21.

Torres, M., S. Jimenez, R. Sanchez-Varo, V. Navarro, L. Trujillo-Estrada, E. Sanchez-Mejias, I. Carmona, J. C. Davila, M. Vizuete, A. Gutierrez, and J. Vitorica. 2012. 'Defective lysosomal proteolysis and axonal transport are early pathogenic events that worsen with age leading to increased APP metabolism and synaptic Abeta in transgenic APP/PS1 hippocampus', *Mol Neurodegener*, 7: 59.

Turk, V., V. Stoka, O. Vasiljeva, M. Renko, T. Sun, B. Turk, and D. Turk. 2012. 'Cysteine cathepsins: from structure, function and regulation to new frontiers', *Biochim Biophys Acta*, 1824: 68-88.

Valyi-Nagy, T., and T. S. Dermody. 2005. 'Role of oxidative damage in the pathogenesis of viral infections of the nervous system', *Histol Histopathol*, 20: 957-67.

Valyi-Nagy, T., S. J. Olson, K. Valyi-Nagy, T. J. Montine, and T. S. Dermody. 2000. 'Herpes simplex virus type 1 latency in the murine nervous system is associated with oxidative damage to neurons', *Virology*, 278: 309-21.

Vina, J., and A. Lloret. 2010. 'Why women have more Alzheimer's disease than men: gender and mitochondrial toxicity of amyloid-beta peptide', *J Alzheimers Dis*, 20 Suppl 2: S527-33.

Viola, K. L., and W. L. Klein. 2015. 'Amyloid beta oligomers in Alzheimer's disease pathogenesis, treatment, and diagnosis', *Acta Neuropathol*, 129: 183-206.

Wang, X. X., M. S. Tan, J. T. Yu, and L. Tan. 2014. 'Matrix metalloproteinases and their multiple roles in Alzheimer's disease', *Biomed Res Int*, 2014: 908636.

Whyte, L. S., A. A. Lau, K. M. Hemsley, J. J. Hopwood, and T. J. Sargeant. 2017. 'Endo-lysosomal and autophagic dysfunction: a driving factor in Alzheimer's disease?', *J Neurochem*, 140: 703-17.

Willem, M., S. Tahirovic, M. A. Busche, S. V. Ovsepian, M. Chafai, S. Kootar, D. Hornburg, L. D. Evans, S. Moore, A. Daria, H. Hampel, V. Muller, C. Giudici, B. Nuscher, A. Wenninger-Weinzierl, E. Kremmer, M. T. Heneka, D. R. Thal, V. Giedraitis, L. Lannfelt, U. Muller, F. J. Livesey, F. Meissner, J. Herms, A. Konnerth, H. Marie, and C. Haass. 2015. 'eta-Secretase processing of APP inhibits neuronal activity in the hippocampus', *Nature*, 526: 443-7.

Williams, W. M., and Y. W. Chung. 2006. 'Evidence for an age-related attenuation of cerebral microvascular antioxidant response to oxidative stress', *Life Sci*, 79: 1638-44.

Wolfe, D. M., J. H. Lee, A. Kumar, S. Lee, S. J. Orenstein, and R. A. Nixon. 2013. 'Autophagy failure in Alzheimer's disease and the role of defective lysosomal acidification', *Eur J Neurosci*, 37: 1949-61.

Wozniak, M. A., R. F. Itzhaki, S. J. Shipley, and C. B. Dobson. 2007. 'Herpes simplex virus infection causes cellular beta-amyloid accumulation and secretase upregulation', *Neurosci Lett*, 429: 95-100.

Wozniak, M. A., A. P. Mee, and R. F. Itzhaki. 2009. 'Herpes simplex virus type 1 DNA is located within Alzheimer's disease amyloid plaques', *J Pathol*, 217: 131-8.

Yagi, T., D. Ito, Y. Okada, W. Akamatsu, Y. Nihei, T. Yoshizaki, S. Yamanaka, H. Okano, and N. Suzuki. 2011. 'Modeling familial Alzheimer's disease with induced pluripotent stem cells', *Hum Mol Genet*, 20: 4530-9.

Yamamoto, A., Y. Tagawa, T. Yoshimori, Y. Moriyama, R. Masaki, and Y. Tashiro. 1998. 'Bafilomycin A1 prevents maturation of autophagic vacuoles by inhibiting fusion between autophagosomes and lysosomes in rat hepatoma cell line, H-4-II-E cells', *Cell Struct Funct*, 23: 33-42.

Yamamoto, N., E. Matsubara, S. Maeda, H. Minagawa, A. Takashima, W. Maruyama, M. Michikawa, and K. Yanagisawa. 2007. 'A ganglioside-induced toxic soluble Abeta assembly. Its enhanced formation from Abeta bearing the Arctic mutation', *J Biol Chem*, 282: 2646-55.

Yatin, S. M., M. Aksenova, M. Aksenov, W. R. Markesbery, T. Aulick, and D. A. Butterfield. 1998. 'Temporal relations among amyloid beta-peptide-induced free-radical oxidative stress, neuronal toxicity, and neuronal defensive responses', *J Mol Neurosci*, 11: 183-97.

Yin, Z., C. Pascual, and D. J. Klionsky. 2016. 'Autophagy: machinery and regulation', *Microb Cell*, 3: 588-96.

Yoshimori, T., A. Yamamoto, Y. Moriyama, M. Futai, and Y. Tashiro. 1991. 'Bafilomycin A1, a specific inhibitor of vacuolar-type H(+)-ATPase, inhibits acidification and protein degradation in lysosomes of cultured cells', *J Biol Chem*, 266: 17707-12.

Yu, W. H., A. M. Cuervo, A. Kumar, C. M. Peterhoff, S. D. Schmidt, J. H. Lee, P. S. Mohan, M. Mercken, M. R. Farmery, L. O. Tjernberg, Y. Jiang, K. Duff, Y. Uchiyama, J. Naslund, P. M. Mathews, A. M. Cataldo, and R. A. Nixon. 2005. 'Macroautophagy--a novel Beta-amyloid peptide-generating pathway activated in Alzheimer's disease', *J Cell Biol*, 171: 87-98.

Yu, W. H., A. Kumar, C. Peterhoff, L. Shapiro Kulnane, Y. Uchiyama, B. T. Lamb, A. M. Cuervo, and R. A. Nixon. 2004. 'Autophagic vacuoles are enriched in amyloid precursor protein-secretase activities: implications for beta-amyloid peptide over-production and localization in Alzheimer's disease', *Int J Biochem Cell Biol*, 36: 2531-40.

Zemlan, F. P., O. J. Thienhaus, and H. B. Bosmann. 1989. 'Superoxide dismutase activity in Alzheimer's disease: possible mechanism for paired helical filament formation', *Brain Res*, 476: 160-2.

Zeng, H., M. Guo, K. Martins-Taylor, X. Wang, Z. Zhang, J. W. Park, S. Zhan, M. S. Kronenberg, A. Lichtler, H. X. Liu, F. P. Chen, L. Yue, X. J. Li, and R. H. Xu. 2010. 'Specification of region-specific neurons including forebrain glutamatergic neurons from human induced pluripotent stem cells', *PLoS One*, 5: e11853.

Zhang, Y. W., R. Thompson, H. Zhang, and H. Xu. 2011. 'APP processing in Alzheimer's disease', *Mol Brain*, 4: 3.

Zhang, Z., M. Song, X. Liu, S. Su Kang, D. M. Duong, N. T. Seyfried, X. Cao, L. Cheng, Y. E. Sun, S. Ping Yu, J. Jia, A. I. Levey, and K. Ye. 2015. 'Delta-secretase cleaves amyloid precursor protein and regulates the pathogenesis in Alzheimer's disease', *Nat Commun*, 6: 8762.

Zheng, H., and E. H. Koo. 2006. 'The amyloid precursor protein: beyond amyloid', *Mol Neurodegener*, 1: 5.

Zheng, W. H., S. Bastianetto, F. Mennicken, W. Ma, and S. Kar. 2002. 'Amyloid beta peptide induces tau phosphorylation and loss of cholinergic neurons in rat primary septal cultures', *Neuroscience*, 115: 201-11.

ANNEX I

Effect of HSV- 1 in CTSB deficient cells

Effect of HSV-1 on CTSB enzymatic activity

In CTSB deficient cells, the HSV-1 infection in the presence of X-XOD caused a reduction of activity by up to 95% ($p<0.001$) in comparison to untreated non-deficient cells (Figure 83), similar to the results obtained above in the presence of the inhibitor CA-074 Me in SK-N-MC cells (Figure 51). The pattern of the treatments was similar in both cell lines, with lower CTSB activity in the CTSB deficient cells.

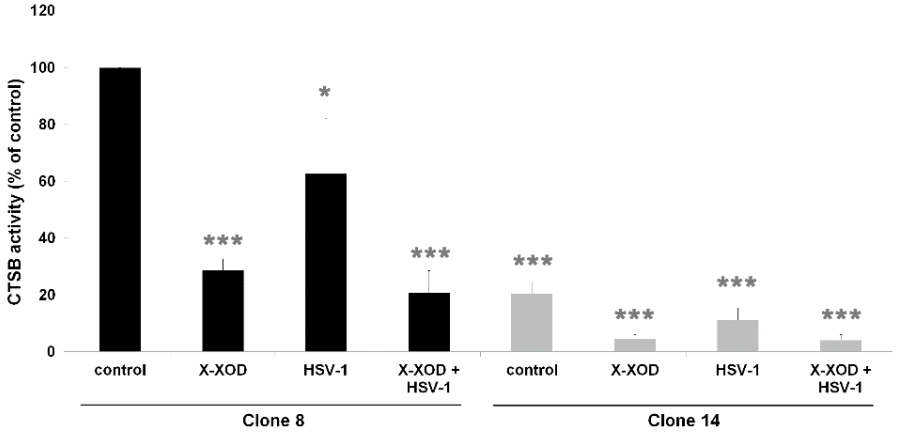

Figure 83. HSV-1 reduces CTSB activity in CTSB deficient cells. CTSB deficient cells were infected with HSV-1 and treated with X-XOD. After incubation for 24 h, CTSB activity was analyzed. Proteolysis of the fluorogenic substrate z-RR-AMC was used to monitor CTSB activity. The graph shows the mean (±SEM) fluorescence values expressed as a percentage of the control value. $*p<0.05$, $**p<0.01$ and $***p<0.01$ (t-test, n=4).

Effect of HSV-1 on APP processing

In CTSB deficient cells, the effect of HSV-1 in deficient cells on APP proteolysis was examined in cell lysates by Western blotting using the antibody 22C11 (Figure 84). We observed a significant increase of APP in X-XOD treated cells in comparison to non-deficient cells that is impaired in infected cells. The levels of APP in infected cells decreased as described above for CA-074 Me treated cells.

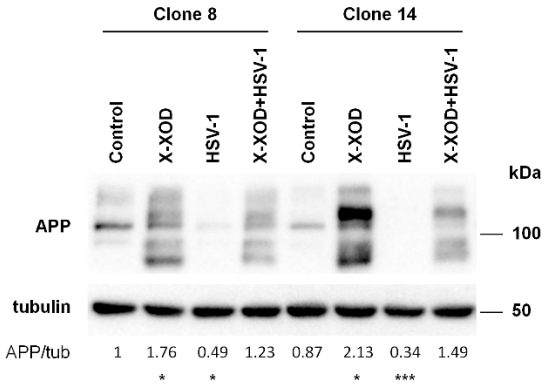

Figure 84. **HSV-1 decrease the levels of APP and APP fragments.** CTSB deficient cells were infected with HSV-1 and treated with X-XOD. After incubation for 24 h, cell cultures were examined by Western blot using the anti-N-terminal APP antibody (22C11). Tubulin blot is shown as loading control. A representative experiment is shown. In the upper panel, the bands correspond to APP and APP fragments, and in the lower panel to α-tubulin. The data show the mean (± SEM) densitometry values (normalized by α-tubulin). Values for control were set at 1. ∗p<0.05, ∗∗p<0.01 and ∗∗∗p<0.01 (t-test, n=4).

As shown in Figure 85, the immunofluorescence assay of these CTSB deficient cells with specific antibodies for APP, 22C11 for the N-terminal (A) and Ct for the C-terminal (B), revealed a decrease of the levels of immunofluorescence in HSV-1 infected cells, especially in the presence of X-XOD, in comparison to control cells. The levels of APP are higher in CTSB deficient cells in comparison to non-deficient cells.

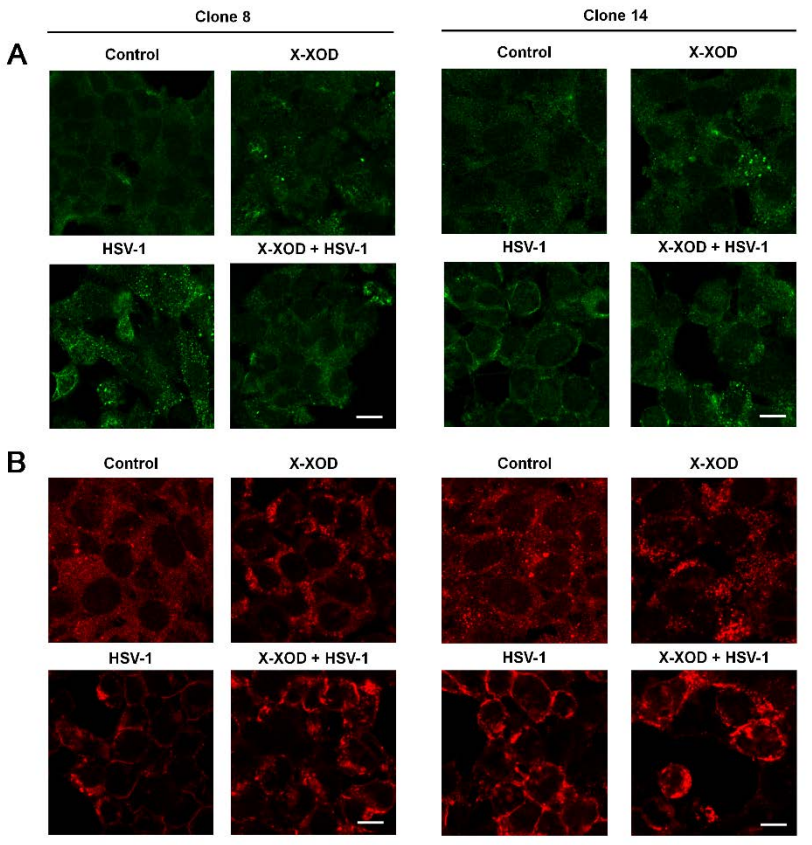

Figure 85. HSV-1 levels increases APP levels in CTSB deficient cells induced by OS. CTSB deficient cells were infected with HSV-1 and treated with X-XOD for 24 h, and were examined by confocal microscopy. The representative panel shows immunofluorescence images for (A) 22C11 (N-terminal) and (B) anti-C-terminal antibodies. Original magnification: 63×. Scale bar: 10 μm. No staining was observed when the primary antibodies were omitted.

Effect of HSV-1 on lysosomal pathway changes

In CTSB deficient cells, the HSV-1 infection in the absence or presence of X-XOD induced higher levels of lysosomal proteins than in non-deficient X-XOD treated cells (Figure 86). Moreover, HSV-1 infected cells decrease their levels of lysosomal proteins in comparison to not infected cells.

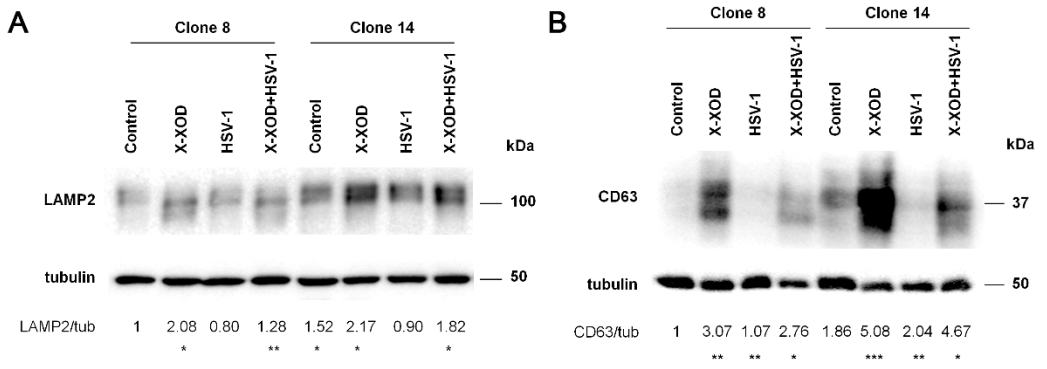

Figure 86. **HSV-1 decreases the lysosomal levels induced by OS.** CTSB deficient cells were infected with HSV-1 and treated with X-XOD. After incubation for 24 h, cell cultures were examined by Western blot using anti-LAMP2 and anti-CD63 antibodies. Tubulin blot is shown as loading control. A representative experiment is shown. In the upper panel, the bands correspond to LAMP2 or CD63, and in the lower panel to α-tubulin. The data show the mean (± SEM) densitometry values (normalized by α-tubulin). Values for control were set at 1. ∗p<0.05, ∗∗p<0.01 and ∗∗∗p<0.01 (t-test, n=4).

The lysosomal burden was measured also as described for CTSB inhibition. LysoTracker levels of control deficient cells decreases in comparison to untreated non-deficient cells. There was no effect of the HSV-1 infection in X-XOD treated cells on the lysosomal burden, neither in CTSB deficient cells nor in non-deficient. However, a significant increase of the burden in HSV-1 infected cells, in comparison to untreated of non-deficient cells, was observed (Figure 87).

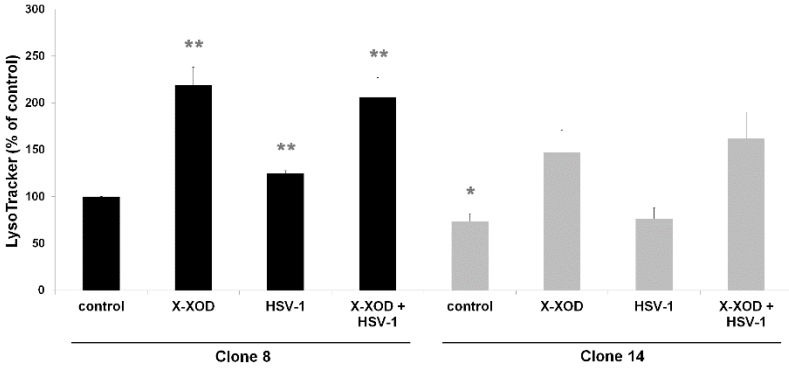

Figure 87. **HSV-1 does not affect the lysosomal burden in CTSB deficient cells.** CTSB deficient cells were infected with HSV-1 and treated with X-XOD. After incubation for 24 h, lysosomal quantity was analyzed by fluorometric measurement of LysoTracker. The graph shows the mean (±SEM) fluorescence values expressed as a percentage of the control value. ∗p<0.05, ∗∗p<0.01 and ∗∗∗p<0.01 (t-test, n=4)

As shown in Figure 88, the immunofluorescence assay of these infected cells with specific antibodies of lysosomal pathway, LysoTracker probe (A) and CD63 antibody (B), revealed a decrease in the levels of immunofluorescence of HSV-1 infected cells in the presence or absence of X-XOD, in comparison to X-XOD or control treated cells, respectively. Showing higher fluorescence of these lysosomal markers in HSV-1 infected CTSB deficient cells in comparison to non-deficient.

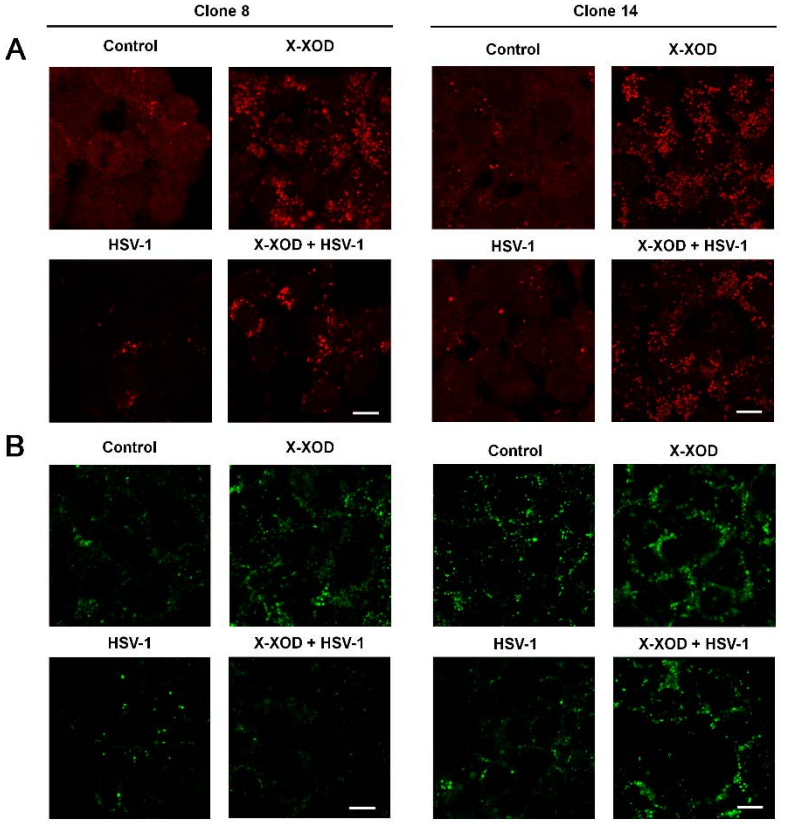

Figure 88. HSV-1 increases the lysosomal markers in CTSB deficient cells. CTSB deficient cells were infected with HSV-1 and treated with X-XOD for 24 h and were examined by confocal microscopy. The representative panel shows immunofluorescence images for (A) LysoTracker probe and (B) anti-CD63 antibody. Original magnification: 63×. Scale bar: 10 μm. No staining was observed when the primary antibodies were omitted.

Effect of HSV-1 in MMP-14 deficient cells

Effect of HSV-1 on MMP-14 enzyme levels

In MMP-14 deficient cells, HSV-1 infected cells showed similar MMP-14 activity to non-deficient cells (Figure 89), being lower in the presence of OS. The Western blot showed a significant decrease of MMP-14 levels in infected cells, approximately a 72% reduction in deficient cells in comparison to control non-deficient cells, and a reduction of 50% in comparison to infected non-deficient cells. Moreover, no reduction on MMP-14 levels was observed in deficient infected cells in comparison to untreated deficient cells.

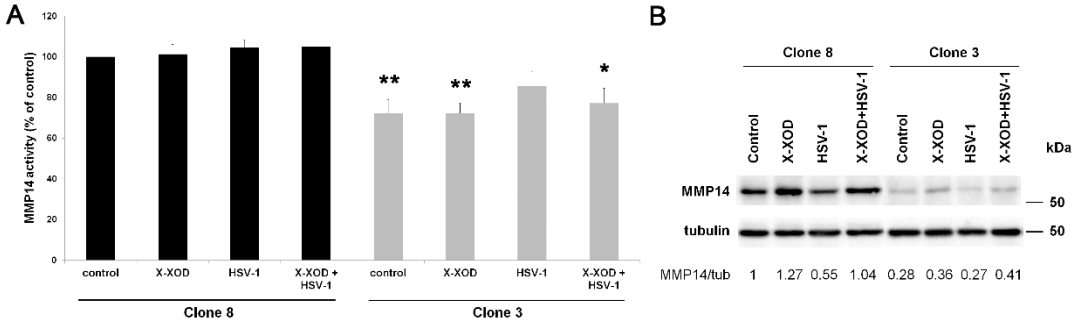

Figure 89. HSV-1 does not affect MMP-14 activity/levels in MMP-14 deficient cells. MMP-14 deficient cells were infected with HSV-1 and treated with X-XOD. After incubation for 24 h, (A) MMP-14 activity was analyzed. Proteolysis of the fluorogenic substrate MCA-PLA-C(OMeBz)-WAR(Dpa)-NH_2 was used to monitor MMP-14 activity. The graph shows the mean (±SEM) fluorescence values expressed as a percentage of the control value. ∗p<0.05, ∗∗p<0.01 and ∗∗∗p<0.01 (t-test, n=4) and (B) Western blot was analyzed with anti-MMP-14 antibody. Tubulin blot is shown as loading control. The data show the mean (± SEM) densitometry values (normalized by α-tubulin). Values for control were set at 1 (n=4).

As shown in Figure 90, the immunofluorescence assay of these infected cells with MMP-14 antibody revealed a reduction of MMP-14 immunofluorescence and a different pattern in HSV-1 infected cells in MMP-14 deficient cells, in comparison to non-deficient cells. Reinforcing the idea of an interaction between MMP-14 and HSV-1.

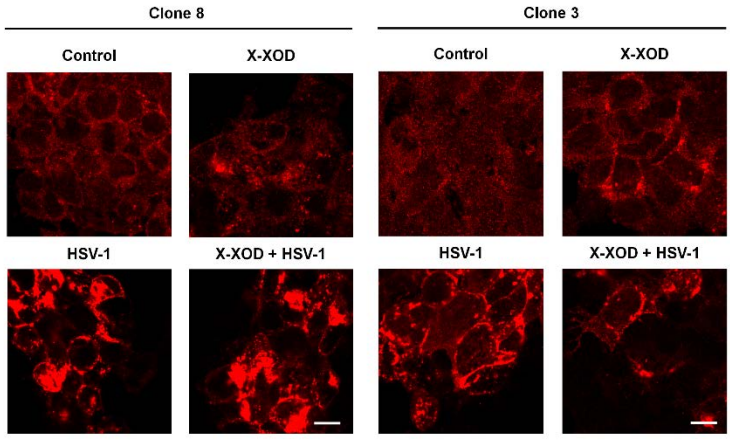

Figure 90. HSV-1 accumulates MMP-14 in a different pattern in MMP-14 deficient cells. MMP-14 deficient cells were infected with HSV-1 and treated with X-XOD for 24 h, and were examined by confocal microscopy. The representative panel shows immunofluorescence images for anti-MMP-14 antibody. Original magnification: 63×. Scale bar: 10 μm. No staining was observed when the primary antibodies was omitted.

Effect of HSV-1 on APP processing

In MMP-14 deficient cells, the effect of HSV-1 infection on APP proteolysis was examined in cell lysates by Western blotting using the antibody 22C11 (Figure 91). We observed in infected deficient cells a significant decrease of APP together with APP85.

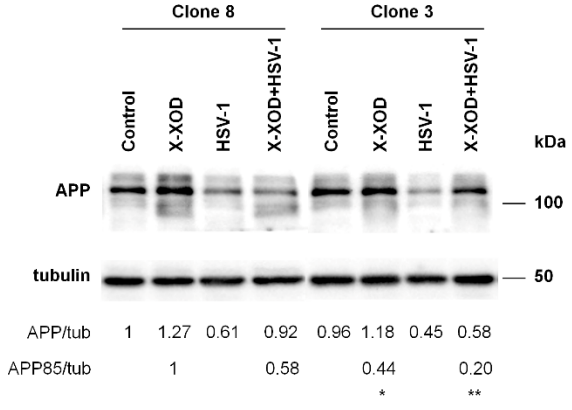

Figure 91. **HSV-1 decreases the levels of APP and APP fragment in MMP-14 deficient cells induced by OS.** MMP-14 deficient cells were infected with HSV-1 and treated with X-XOD. After incubation for 24 h, cell cultures were examined by Western blot using the anti-N-terminal APP antibody (22C11). Tubulin blot is shown as loading control. A representative experiment is shown. In the upper panel, the bands correspond to APP and APP fragments, and in the lower panel to α-tubulin. The data show the mean (± SEM) densitometry values (normalized by α-tubulin). Values for control were set at 1. ∗p<0.05, ∗∗p<0.01 and ∗∗∗p<0.01 (t-test, n=4).

The immunofluorescence assay of these infected MMP-14 deficient cells with the 22C11 antibody revealed a decrease of the levels of APP (Figure 92), which correlated with the results obtained by Western blot. The same condense pattern of reorganization previously described was observed in HSV-1 infected cells.

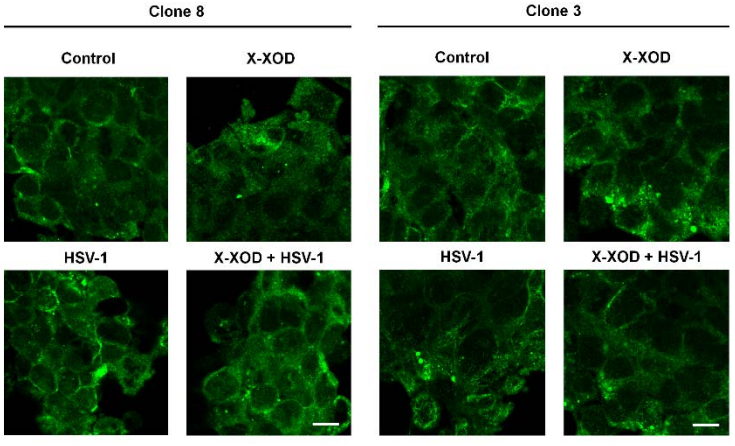

Figure 92. HSV-1 decreases APP levels in MMP-14 deficient cells. MMP-14 deficient cells were infected with HSV-1 and treated with X-XOD, in the presence or absence of NSC405020, for 24 h and were examined by confocal microscopy. The representative panel shows immunofluorescence images for anti-MMP-14 antibody. Original magnification: 63×. Scale bar: 10 μm. No staining was observed when the primary antibodies was omitted.

Effect of HSV-1 on lysosomal pathway changes

In MMP-14 deficient cells the lysosomal markers were measured by Western blot using the specific antibodies for LAMP2 and CD63 (Figure 93). The levels of lysosomal proteins decreased in infected deficient cells in comparison to infected non-deficient cells.

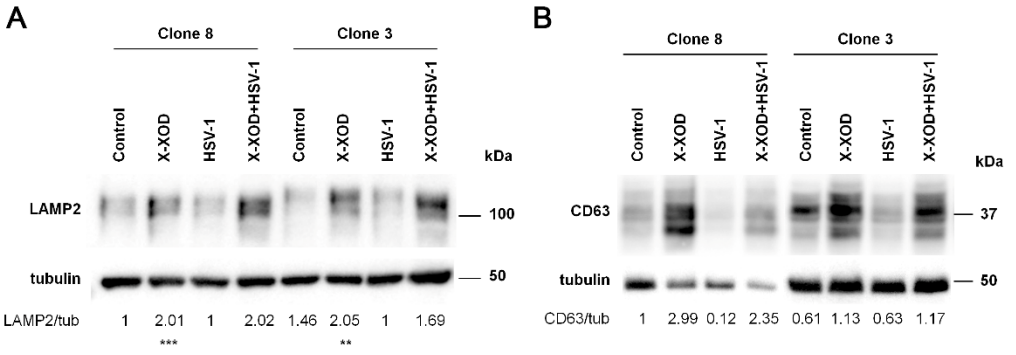

Figure 93. **HSV-1 decreases the lysosomal levels in MMP-14 deficient cells induced by OS.** MMP-14 deficient cells were infected with HSV-1 and treated with X-XOD. After incubation for 24 h, cell cultures were examined by Western blot using anti-LAMP2 and anti-CD63 antibody. Tubulin blot is shown as loading control. A representative experiment is shown. In the upper panel, the bands correspond to LAMP2 or CD63 and in the lower panel to α-tubulin. The data show the mean (± SEM) densitometry values (normalized by α-tubulin). Values for control were set at 1. ∗p<0.05, ∗∗p<0.01 and ∗∗∗p<0.01 (t-test, n=4).

The lysosomal burden was measured in MMP-14 deficient cells. LysoTracker levels of infected deficient cells decreased significantly in comparison to non-deficient cells (p=0.00157). Moreover, there was a general decrease of lysosomal burden in the deficient cell line in comparison to each treatment of non-deficient cells (Figure 94).

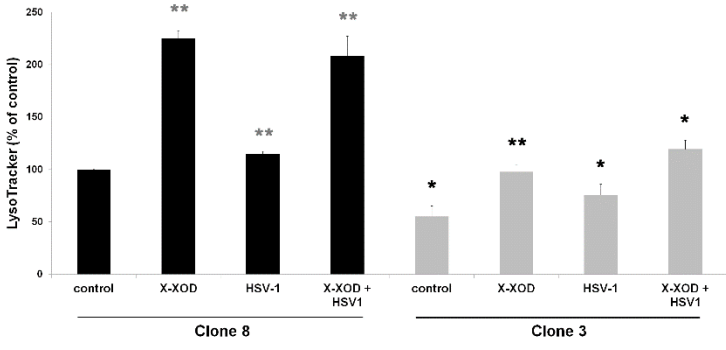

Figure 94. HSV-1 decreases the lysosomal burden in MMP-14 deficient cells. MMP-14 deficient cells were infected with HSV-1 and treated with X-XOD. After incubation for 24 h, lysosomal quantity was analyzed by fluorometric measurement of LysoTracker. The graph shows the mean (±SEM) fluorescence values expressed as a percentage of the control value. ∗p<0.05, ∗∗p<0.01 and ∗∗∗p<0.01 (t-test, n=4)